A study of the bonding of aluminium alloys to mild steel prepared by an overcasting process

A thesis submitted for the degree of

Doctor of Philosophy

By

Alireza Valizadeh

Department of Mechanical, Aerospace and Civil Engineering

Brunel Centre for Advanced Solidification Technology (BCAST), Brunel University London

2020

In the name of Allah, the entirely merciful, the especially merciful.

‘’Bring me blocks of iron, when he had filled up the space between the two steep mountain-sides, He said, "Blow (with your bellows)" Then, when he had made it (red) as fire, he said: "Bring me molten Lead, that I may pour over it. So, Gog and Magog were unable to pass over it, nor were they able (to effect) in it any penetration’’.

Surat Al-Kahf: 95

Holy Quran

Abstract

Fabrication of aluminium/steel bimetallic components has been extremely useful in automobile and aerospace industries for the development of lightweight structural and functional applications. This research investigates the possibility of using overcasting of liquid aluminium to solid steel to bond aluminium to steel. Specifically, the bonding of steel to aluminium-tin based alloy can enable the use of steel as a reinforcement in soft aluminium-tin bearings to improve their life expectancy. This project is concerned with the understanding of the effect of overcasting processing conditions (eg. cooling rate and melt holding time) and alloy composition on resultant bond microstructure, kinetics of interaction layer and mechanical properties of aluminium/steel joint.

Two cooling rates of 0.63 K/s and 5 K/s were used during overcasting process with sand and steel moulds, respectively. Steel substrates coated with Zn, Ni and Ni-Zn layers of thickness ranging from 2 µm to 12 µm were used for this study. A range of aluminium alloy compositions were studied. They include pure Al, binary Al- (1-12.2 wt%) Si, Al-20wt%Sn-7wt%Si and Al-Si-Mg alloys.

The microstructure of overcast sample was characterised using a combination of scanning electron microscopy (SEM), X-ray Diffraction (XRD) and Transmission Electron Microscopy (TEM). The bond strength of overcast sample was determined using tensile testing method.

This research studied the effect of zinc coating in a very systematic way on the Al/steel joints. Different cooling rates and holding times used to study the behaviour of microstructure and strength of joints between overcast aluminium and steel substrates with and without coatings of zinc, gallium-zinc, nickel and nickel-zinc. Interaction between pure aluminium and steel in different processing conditions were studied. No interaction was found between pure aluminium and zinc coated steel overcast at a high cooling rate of 5 K/s (750/500 ºC). However, an interaction was detected in samples prepared at a lower cooling rate of 0.63 K/s (750/500 ºC). to provide a metallurgical bond between Al and steel. After this experiment, all samples were made inside sand mould in the same cooling rate of 0.63 K/s (750/500 ºC). Intermetallic compound (IMC) interaction layer was found between aluminium and steel with finger-like features of the IMC were directed towards steel. $Al_{13}Fe_4$ phase was detected within

the IMC next to the aluminium and Al_5Fe_2 phase was detected within IMC layer adjacent to steel. The kinetics of formation of Al_5Fe_2 IMC was demonstrated to be controlled by a mass diffusion process. It is confirmed that growth of IMC layer followed a parabolic law. TEM studies confirmed the presence of $Al_{13}Fe_4$ with the IMC next to aluminium and Al_6Fe_2 within IMC next to steel. From all bond strength tests, the fractures were found to propagate alongside the IMC and perpendicular to the direction of the force.

Interaction of pure aluminium/gallium-zinc coated steel was similar to the pure aluminium/zinc coated steel and no difference in the joint microstructure was detected.

Interaction between pure aluminium and uncoated steel joint occurred after holding at750 ºC for 1 minute. The joint microstructure consisted of isolated islands of IMC discontinuous layer located between the aluminium and steel regions. These islands didn't touch each other during their growth.

Interaction between pure aluminium and nickel coated steel, resulted in the formation of $Al_{13}Fe_4$ and Al_5Fe_2 IMC layers between aluminium and steel. However, the kinetics of formation of the IMC layer was slower than the interaction of pure aluminium with zinc coated steel. The reason can be lower melting temperature of zinc coating compared with nickel coating, 420 ºC vs. 1455 ºC. As the low melting point coating of zinc melts faster in overcasting process, interaction layer forms quickly in the bond between aluminium and zinc coated steel.

Interaction between pure aluminium/NiZn coated steel gave very similar interaction between pure aluminium and zinc coated steel, however the kinetics of interaction was slower in NiZn coated steel because the nickel coating reduced the kinetics of interaction between steel and aluminium. Similar IMC layers were formed on NiZn coated steel that were found previously in zinc coated steel.

Measurement of bonding strength revealed that generally the bond strength increased by increasing holding time from 0 to 10 minutes. However, uncoated steel showed very small or zero bond strength in bimetallic joints with different aluminium alloys. All of the measured bond strengths are related to the formation of IMC layers. Under processing conditions with no IMC, no bond was formed. However, increasing holding time gave rise to increased IMC thickness and stronger bond strength. For example,

at high cooling rate of 5 K/s, IMC did not have enough time to form in pure aluminium/Zn coated steel joint, so no bond formed in the joint. Generally, it was found that different coatings on the steel substrate can change the kinetics of interaction between aluminium and steel, even though IMC phases remained unchanged for all the coatings used in this study.

Two types of cracks were detected in the bimetallic joints. The first type was found between $Al_{13}Fe_4$ phase and aluminium. The second type was found alongside the Al_5Fe_2 phase. The first type of crack was formed because of the difference in diffusion rates of elements between the IMC and the aluminium, while the second type of crack was formed because of the difference in thermal expansion coefficients.

Kirkendal effect led to the formation of pores within the Al_5Fe_2 layer in the samples prepared after holding the aluminium melt at 750 ºC for 30 minutes and more. They formed feasibly because the rate of diffusion of one element was higher than the other element. Addition of silicon to aluminium reduced the kinetics of formation of IMC layer by reducing the atomic diffusion rate. Therefore, lowering of atomic diffusion and reaction kinetics can be the reasons of reduction in thickness of IMC layers after addition of silicon in the aluminium melt.

Thickness of the interaction layer in Al-20Sn-7Si/nickel coated and zinc coated steel joints was increased by increasing holding time. The interaction layer thickness in Al-20Sn-7Si/zinc coated steel sample was higher than those in the Al-20Sn-7Si/nickel coated steel. Bond strength of Al-20Sn-7Si/zinc coated steel after holding for 5 minutes in 750 ºC was measured to be 30 MPa, the maximum bond strength of the bimetal joints.

Kinetics of interaction layers was compared in all of the processing conditions using parabolic law. The Al/Zn coated steel joint had the highest rate of formation of IMC, and Al-7Si/Ni coated steel joint had the lowest rate of formation of IMC. Thanks to the high activation energy of pure aluminium and low melting temperature of zinc coat, the Al/Zn coated steel joint accelerated the interaction between aluminium and steel while the low activation of Al-7Si and high melting temperature of the nickel coat reduced the kinetics of interaction in the Al-7Si/Ni coated steel joint.

Finally, it was concluded that careful control of processing conditions and material composition is required to achieve improvement in the strength of the bimetal joint without excessive degradation of the strengths of the primary materials.
Keywords: overcasting, aluminium, joining, microstructure, mechanical properties

Preface

This thesis is a description of work that I performed in the Brunel Centre for Advanced Solidification Technology, Brunel University London from 1st July 2015 to 31st October 2019. To the best of my knowledge, this work is original, except where suitable references are made to previous work. Neither this, nor any substantially similar dissertation has been submitted to any other institution nor is it the result of my own work. The content of the dissertation does not exceed 60,000 words.

Related publications and awards

Peer reviewed conference papers

A.Valizadeh, I.T.H.Chang, I.Stone, Bonding of Aluminium to Low Carbon Steel using an Overcasting Process, SP17 conference, Windsor, UK, 2017

Conference presentations

1. A.Valizadeh, I.Chang, I.Stone, The Effect of a Zinc Coating on the Bonding of Aluminium to Low Carbon Steel, Euromat 2017, 17-22 September 2017, Thessaloniki, Greece

2. A.Valizadeh, I.Chang, Using overcasting as a bonding process to join dissimilar materials, The International Conference of Welding and Related Technologies — Present and Future, E.O.Paton Electric Welding Institute of the National Academy of Sciences of Ukraine, 5-6 December 2018, Kiev, Ukraine

Award

Frank Fitzgerald Medal and Travel Award, IOM3, 2018

Acknowledgement

I would like to express my sincere gratitude and grateful admiration to my supervisors Prof. Isaac Chang, Dr Ian Stone and Prof. Zhongyun Fan for their continuous guidance, utmost effort, encouragement and interest through the work that contributed in its completeness.

I am extremely thankful to my parents and my family for being the source of my inspiration, throughout the difficult times of this study.

I owe my deepest gratitude to The Worshipful Company of Tin Plate Workers Alias Wire Workers of the City of London for the financial support to conduct this research work. I am especially grateful to the support and encouragement provided by members of the education, enterprise and charities committee including Bev Page, William Boyd, Robert Spencer, Christine Purdy and Lindsay Millington during my PhD project.

I would like to show my gratitude to Prof. Hari Babu, Dr Kawther Al-Helal, Prof. Dmitry Eskin and Dr Yan Huang for their support in conducting the research work, preparing this thesis and for many inspiring discussions.

I would like to thank Director of Brunel Centre for Advanced Solidification Technology (BCAST), Prof. Zhongjun Fan for the provision of casting and characterisation facilities to carry out this project. I like to extend my appreciation to Tata Steel Company for the supply of nickel coated steel and nickel-zinc coated steel plates for this work.

I wish to express my thanks to my colleagues in BCAST for their support and letting me feel part of the team whenever we worked together. Also, my deepest respect goes to technicians in BCAST laboratories who helped me to perform the related experiments. Finally, I would like to thank the technicians and director of Experimental Techniques Centre (ETC), Prof. Ian Boyd for the provision of advanced characterisation facilities in Brunel to study the microstructure of overcast samples.

Table of contents

Abbreviations

at.%	Atomic percent
CTE	Coefficient of linear Thermal Expansion
FIB	focused ion beam
Gal	Gallium
Ni	Nickel coated steel
NiZn	Nickel-Zinc coated steel
OM	Optical microscope
OPS	Optical Emission Spectroscope
RT	Room Temperature
SEM	Scanning electron microscope
TEM	Transmission electron microscope
Uncoated	Uncoated steel
Wt.%	Weight percent
XRD	X-ray diffraction
Zn	Zinc coated steel

List of acronyms

º	degree
ºC	degree Celsius
min	minute
kg	kilogram
s	second
t	time
T	temperature
K	degree Kelvin

Chapter 1 Introduction

1.1 Background and motivations

The project follows on from a Technology Strategy Board (now Innovate UK) funded collaborative R&D programme to develop high-tin aluminium (Hi-TINAL) bearing alloys, with the potential to replace lead-bronze in aeroengine fuel pump and whitemetals in turbomachinery and oil & gas applications [1].

Enforced by recent implementation of the REACH (Registration, Evaluation, Authorisation and Restriction of Chemicals) legislation, the bearing industries are replacing hazardous Pb (lead) containing bearing materials by environment friendly bearing alloys. Moreover, the market needs for higher performance capability requires an alternative to Sn based whitemetals in industrial bearings. For example, large aeroengine fuel pump bearings based on Pb-bronzes are manufactured through a multi-material, multi-stage route, and it is expected that high-Sn Al alloy bearings machined from cast billets will significantly reduce manufacturing costs and increase service intervals, as well as remove Pb and the use of other hazardous chemicals [1].

The newly developed alloys were shown to have bearing properties that were superior to both Pb-bronze and whitemetals [2]. However, the high-tin aluminium alloys suffered from cavitation erosion when subject to severe cavitation (likely in the case of fuel pumps for large aeroengines) [2]. This cavitation occurs in a localised region of the bearings [1]. Hence, the application of local reinforcement of steel to this high-tin aluminium alloy bearings can offer a potential solution to mitigate the cavitation issue without compromising the bearing performance and its overall weight. It is also typical for large bearings for turbomachinery in oil and gas sectors to be supported by a steel backing. The present project therefore focuses on the application of casting technique to fabricate aluminium (eg. pure aluminium, binary Al-Si and commercial high-tin aluminium alloy and 6060 alloy) onto and around steel (referred as overcasting).

A schematic diagram of a bearing component is presented at Figure 1-1, showing (A) the bearing and (B) the location where turbulence of fuel causes cavitation erosion. A local reinforcing steel in area of the dashed area may prohibit cavitation

erosion and strengthen the bearing. Reinforcing locally with a different material requires bonding between these two sides.

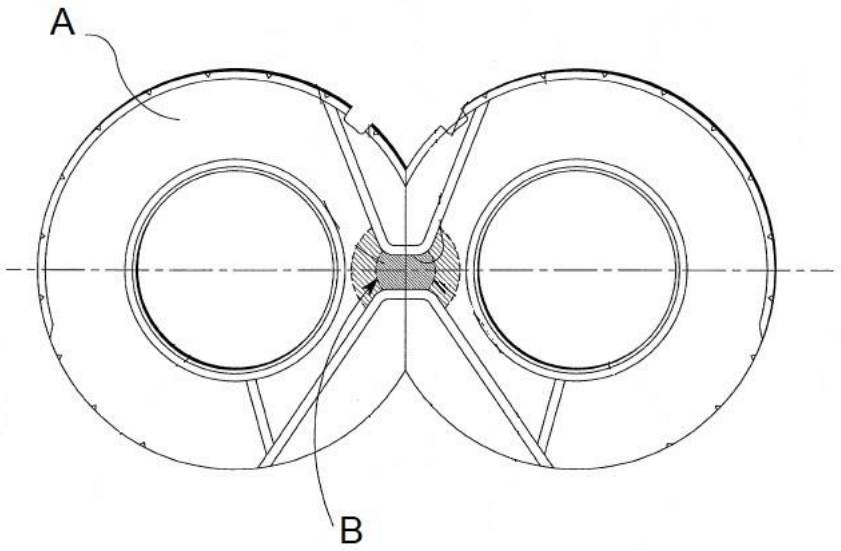

Figure 1-1-Schematic diagram of bearing of an aeroengine fuel pump. (A) demonstrates the bearing and (B) demonstrates the position that is vulnerable to corrosion erosion [3].

The first question is in the selection of material. The selected reinforcing plate steel should bond properly to the aluminium-tin bearing alloy and be compatible in terms of thermal expansion coefficient. The second question concerns with the possibility of making a metallurgical bond between the bearing alloy and the steel reinforcing. The functionality of the bearing depends on its integrity, so it is impossible to use a loose reinforcing plate (steel) in the bearing and it is necessary to make a metallurgical bond between the Aluminium-Tin bearing and the steel reinforcing [1]. So far, many studies have been focussed on the development of aluminium-tin based bearing alloys [1, 4] and techniques to bond aluminium to steel, aluminium to aluminium or other materials such as iron [5, 6], steel, stainless steel [7], low carbon steel [8, 9] and other materials using brazing and resistance welding. Despite all these, no research found about aluminium-tin alloys bonding to other metals.

Overcasting can offer a novel joining technique but the bonding parameters have not been optimised for the fabrication of aluminium and steel bimetallic components. Casting is the root of the production of most of the metallic materials, by bonding during casting instead of a separate bonding process, it is possible to remove bonding step

by mixing it with the casting process. The advantage of this method is not only the low price of production but also the fast speed production by removing one step of the production line.

Aims and Objectives

The main aim of this research project is to develop a low-cost processing method to bond aluminium-tin casting alloy to steel insert with sufficient strength and metallurgical integrity. This is achieved by studying the microstructural development of overcast samples and their bond strength, as a function of processing conditions (eg. cooling rate, melt holding time), melt composition (eg. pure aluminium, Al-Si binary alloy, commercial high-tin aluminium based bearing alloy and Al6060) and coatings (eg. Zn, Ni, NiZn) of steel insert. The microstructure and property of the overcast samples are studied using a combination of optical microscopy (OM), scanning electron microscopy (SEM), transmission electron microscopy (TEM), energy dispersive spectroscopy (EDS), X-Ray diffractometry (XRD) and tensile test to establish the optimum overcasting conditions to control the formation of interaction layer with a good metallurgical bond between aluminium casting and steel insert,

1.2 Layout of thesis

The research project is concerned with the study of the bonding of aluminium alloys onto mild steel prepared by overcasting method. The current thesis is divided into six chapters.

Chapter 1 is an introduction to the thesis.

Chapter 2 presents the background and the current state of the research in the field. It includes the fabrication, microstructure and properties of dissimilar joints of aluminium and steel including the characteristics of aluminium casting alloys and steel insert. Overcasting process is described in details as it is the main method employed in the current research to fabricate dissimilar joint between aluminium and steel.

In chapter 3, the characteristics of the raw materials, the production process of aluminium and steel dissimilar joints and the techniques of characterisation are introduced.

In chapter 4, the effects of different cooling rates (eg. from 0.63 K/s to 5 K/s), coatings on steel insert (eg. Zn-, Ni-, Ni/Zn) and holding times on formation kinetics of the intermetallic phase within the interaction layer and strength of the bond between aluminium casting and steel insert were introduced. The overcast samples were examined using a combination of OM, SEM and TEM. Bond strengths were measured and fracture surfaces were examined. Finally, imperfections in the bond were presented.

In chapter 5, the effect of casting alloy composition (eg. Al- (1-12.2 wt%) Si, Al-20wt%Sn-7wt%Si and Al6060 on the interaction between the molten alloy with zinc or nickel coated steel inserts and its resultant bond strength is described.

In chapter 6 the experimental results are discussed in terms of the role of processing conditions and alloy composition on: (1) the kinetics of formation of the intermetallic phase within the interaction layer between aluminium cast and steel insert; (2) the bond strength; and (3) imperfections in the joint.

In chapter 7, the findings of the project are summarised and the suggestions for future work are presented.

Chapter 2 Literature review

2.1 Introduction

This chapter contains a detailed review of the past and current literature on research topics related to this PhD study presented in this thesis. The physical properties of materials such as aluminium and steel used in this research are first summarised, and this is followed by a review of the principles of bonding processes and specific joining techniques that are currently using in industries for dissimilar bonding of aluminium to steel. These joining techniques based on the base metal physical state can be divided into solid-solid processes such as diffusion bonding, solid-liquid processes such as overcasting or semi liquid- semi liquid processes such as bonding by semi continuous casting. Both advantages and limitations of these processes will be discussed and compared with a particular emphasis on overcasting as a bonding process that was used in this research. A review on the microstructural development in the interface between aluminium and steel in these dissimilar joints prepared by conventional bonding methods and contribution of microstructural development to mechanical bond strength was described. The role of different interlayers in bonding aluminium to steel was studied and effects of the presence of different solute elements in aluminium alloys on the dissimilar joint and evolution of interaction layer were discussed regarding phases found in Al-Fe binary system. The thermodynamic consideration of the phases present in the interaction layer between Al and steel using phase diagram will be presented. This includes the effects of solute elements of aluminium alloy and coating of steel (interlayer) on the growth kinetics of the interaction layer and the formation of different intermetallic phases. Finally, defects and failure of aluminium/steel joints are reviewed.

2.2 Importance of bonding aluminium to steel

The need for lighter and higher performance products has many industrial sectors such as automotive and aerospace to continuously seek innovative approaches using knowledge from various discipline fields including engineering design, material science, and manufacturing in a combined way to reduce the mass of a whole product structure.

Industrial studies and scientific research revealed that generally innovative hybrid products can only be used if the properties of materials are adapted to the requirements and the function of each component [10]. The increasing demand for joints of dissimilar materials has led to development of new joining techniques or improvement of exciting joining processes [10].

Aluminium is famous as lightweight metal and is used in light weight structures by transportation industries to increase energy efficiency and reduced emission of greenhouse gases [11]. However, the monolithic material cannot always meet the complex requirements of lightweight applications in different industries, for example in some cases tensile strength of the component should be higher or wear properties should be higher than the wear properties of aluminium. So, hybrid design and manufacturing such as aluminium/steel can meet the requirements to enhance the properties of final products [12]. However, joining these materials is always a challenge for engineers. There are a certain number of joining processes of successful bonding of aluminium to other materials such as steel, stainless steel, titanium and etc.

2.3 Bonding processes

Based on the needs and applications, there are different types of classification of bonding processes. One type of the classification is based on the base metal state. In majority of bonding processes, both the base metals are in solid state in the outset of the joining operation. This includes Tungsten Inert Gas welding, laser beam welding and electron beam welding processes. In some specific bonding processes, such as Semi Continuous Casting, the two sides of the bond are in liquid state [13]. However, in overcasting, one base metal is in the solid-state while the other base metal is in the liquid state [13]. Figure 2-1 shows the classification of the bonding processes based on the base metal state.

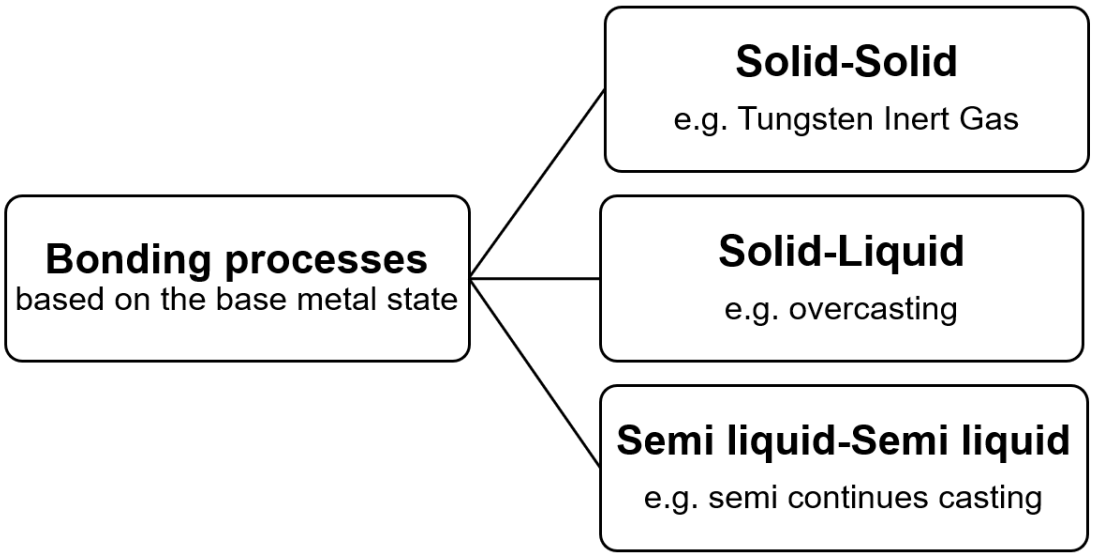

Figure 2-1-Classification of bonding processes based on the base metal state.

In most of the commercial bonding processes both base metals are in solid state. Here two examples of electron beam welding and weld-brazing are presented.

Electron Beam welding is using electron beam in a vacuumed chamber for welding a broad range of materials including dissimilar materials. High energy density and accurately controllable beam size and location are the main advantages of the process [14]. For example, Dinda used Electron Beam Welding to weld DP600-steel to Al 5754-alloy by different beam oscillations and found 1 mm diameter of beam oscillations being optimum. Non-optimum oscillations deteriorated quality of the joint by higher porosities and increased size of intermetallic phases [15].

Brazing is using a filler material to join different materials while the filler metal has a lower melting point than the base metals. In brazing, the base metals should be hot enough, so that filler metal melts, flows and wets the surface of the joint [16]. Filliard studied the effects of different process parameters on bonding AA6016-T4 aluminium and DX56D+Z140M steel sheets by using weld-brazing, a mix of brazing and laser welding. They noticed that power of the laser can change the cooling rate and thermal cycle to change the properties of the joint [17].

Several methods have been reported as the bonding processes to join dissimilar materials. Different bonding processes such as TIG [18], Laser Beading Welding [19], Explosive Welding [20, 21], Electron Beam Welding [22], [23], Resistance Welding [24, 25], MIG [26] are used to join aluminium and steel. In some cases, the need for specialised applications led to using hybrid welding processes [27-29] such as laser-MIG [30]. Although there are successful applications of the above-mentioned bonding processes, there are two main restrictions in using them: the high cost of manufacturing and limitations in bonding more complicated geometries of joints. Thanks to low manufacturing cost and the ability to bond complicated geometries, overcasting [31], compound casting [32-34] bimetallic casting [35], insert casting [36] or hybrid casting [37] as a key enabling technology can be a reliable process needed for hybrid structures comprised of light metals such as aluminium and magnesium. A schematic diagram of a setup that Liu et al. used for overcasting is illustrated in Figure 2-2. In this assembly, a thermocouple measures the melt temperature while argon gas flow covers the atmosphere of the chamber. In overcasting, known also as hybrid casting and compound-casting, a region of fusion reaction can be formed between two dissimilar metals and a continuous metallic transition region bonds one base metal to another [38].

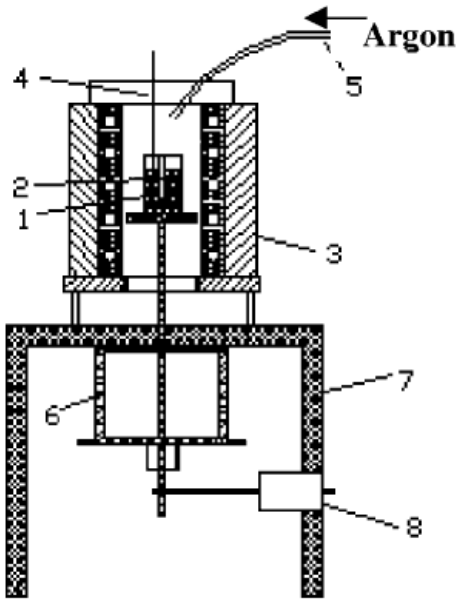

Figure 2-2- The schematic diagram of a setup for overcasting. (1) Liquid aluminium (2) steel (3) furnace (4) thermocouple (5) argon gas inlet (6) water tank (7) table (8) unite to move the crucible [6].

Bonding of aluminium alloys in industry is performing by different processes such as welding, soldering and brazing. Study of all of these bonding processes may help to achieve a better understanding of the problems involved in overcasting of aluminium. Among all of the bonding processes, it seems that brazing and welding have more similarities with overcasting than the other bonding processes. So, study the brazing and welding are more suitable to overcasting than the other bonding processes.

Generally, not all aluminium alloys can be brazed. For example, certain casting alloys containing high amounts of alloying ingredients and high-strength wrought aluminium alloys are not possible to braze. These alloying ingredients often prevent adequate wetting by filler metal due to their unique oxide film combination. These alloys also melt in temperatures below those of commercially available filler metals. [39]

In the selection of brazing filler metals, the following factors should be considered:

- Metallurgical compatibility with the base metals being joined
- Heating method and heating rate
- Service requirements of the brazed assemblies
- Brazing temperature required, e.g. heat treating the part during the brazing cycle
- Joint design considerations such as fit up, size of brazed components, length of joint
- Form of the filler metal
- Aesthetic requirements
- Safety considerations

Same factors should be considered when bonding using the compound casting process [39].

2.4 Controlling parameters for overcasting

No research studied or introduced effects of different controlling parameters of overcasting process. This literature review tries to understand influential parameters that possibly effect on bond properties in overcasting by referring to controlling parameters of overcasting process, controlling parameters of similar bonding processes such as brazing and welding used and introduced to apply on overcasting process.

There are generally three main parameters that can be applied to liquid metal, base metal and atmosphere that are possible to control the overcasting process. Figure 2-3 shows a chart that is demonstrating the overcasting parameters. Like any fusion bonding process [40], bonding temperature is the main factor controlling the bond properties. Low-temperature input stops the bond formation and high temperature can end up with an excessive amount of heat input or intermetallic phase that is brittle and finally will drop the bond strength. The heat input in the overcasting process is controlled by the casting temperature, heat transfer in the liquid metal and the primary temperature of the solid metal. The fluid dynamic of the molten metal may affect the formation of the bond. Also, the composition of liquid metal can affect bond properties. Researchers have shown the effects of silicon and copper on the interaction between solid steel and liquid aluminium [40-43].

In overcasting process, the solid metal may control the bond properties in different means. The composition of the solid metal can affect the formation of the bond between two materials[45]. For example, based on the research by Hwang et al. increasing the carbon concentration and the cementite phase in solid steel led to a smoother interface and decrease the thickness of the intermetallic layer formed between aluminium and steel [46]. Also, the topography of the solid/liquid interface can affect the formation of the interaction layer. Lan et al. noticed that increasing surface roughness of solid cast iron can enhance the bond strength to liquid aluminium [47]. The surface coat of solid metal is another factor that affects the formation of the intermetallic layer and the bond properties [48]. The effect of zinc-coating in ultrasonic spot welding of aluminium to steel studied by Haddadi et al. [49] and Jia et al. [ref] studied the effect of zinc coat on the laser welding of aluminium to zinc coated steel [50]. Similar to other bonding processes such as brazing [50, 12], the flux may also enhance the bond properties in the overcasting process. Pan et al. reported a successful application of ultrasonic waves to improve the bond between solid steel and liquid aluminium. By using ultrasound they could break the oxide layers on top of liquid aluminium and improve the wettability of the solid steel by molten aluminium [36]. Ultrasonic is another method that can be used to improve the bond between solid metal and overcast liquid metal.

The atmosphere can affect the bond properties in two different ways: change in pressure and using air, inert gas or vacuum. Using pressure to improve the bond properties has a long history. Bhegat used high pressure in squeeze casting to enhance the bond between stainless steel wire and liquid aluminium. He could improve the tensile strength and elongation by using squeeze casting [33]. Also, Liu studied aluminium-aluminium bimetal fabrication by using squeeze casting [52]. Change in the atmosphere by using inert gas and vacuum can also affect the bond properties. Hattori studied brazeability of aluminium in the vacuum-nitrogen atmosphere [53].

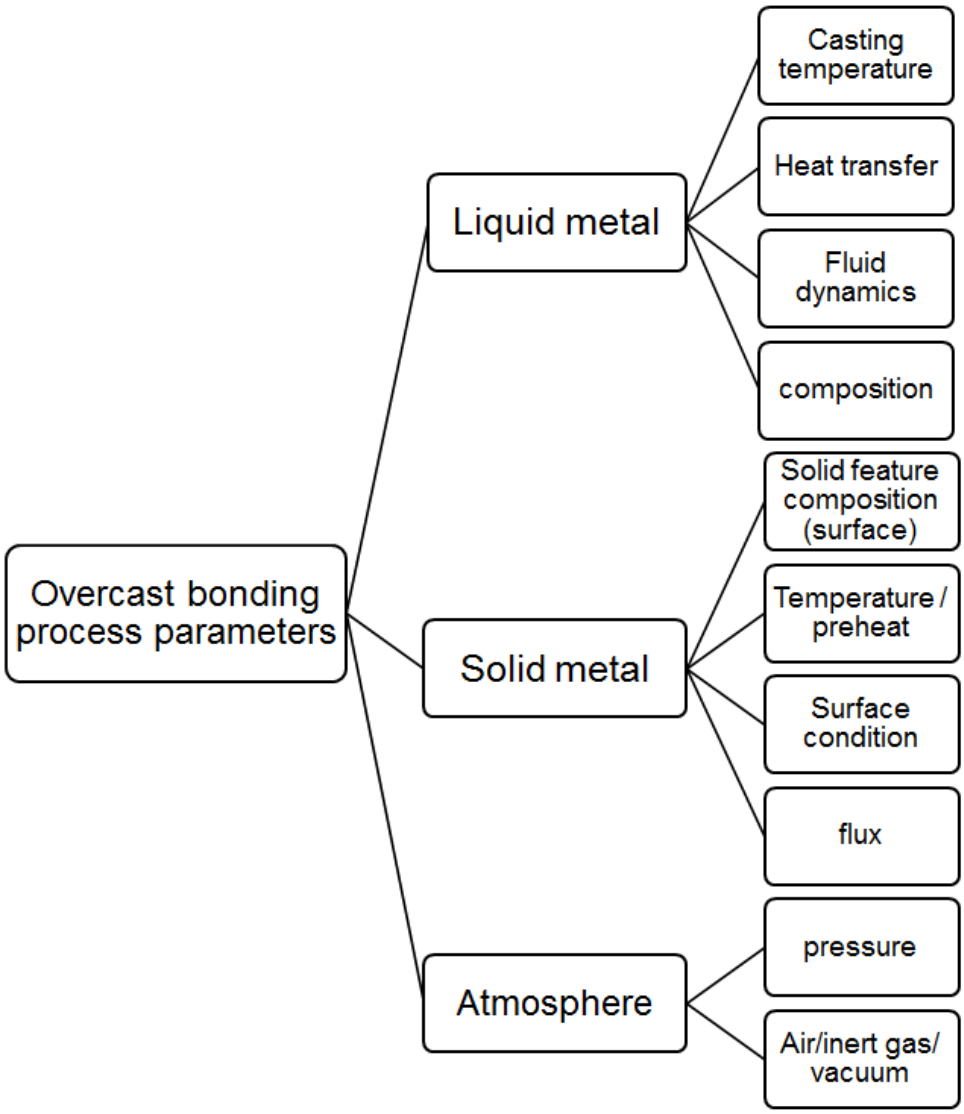

Figure 2-3- The chart of overcasting process parameters.

2.5 Overcasting of aluminium on top of steel

Because of the low manufacturing cost and high efficiency, overcasting has been used to bond different materials, such as aluminium and steel [53, 54], stainless steel and structural alloy steel [56], aluminium and cast iron [47], aluminium and copper [56, 57], magnesium and aluminium [59], cast iron and steel [60]. However, the application of using overcasting as a bonding method of aluminium to steel is very limited because of the presence of oxide films on the surface of molten aluminium and absorbed contaminants on the solid metal surface that leads to non-wetting of the solid metal with molten aluminium [61]. First known recorded attempts to bond aluminium to steel by overcasting date back to 1938 when researchers tried to patent bonding ferrous metals to non-ferrous just by casting on top of each other [62]. Then, Choe et al. [61] improved the bond strength between solid steel and overcast aluminium by using a zinc coat on top of steel. Also, Dezellus [49] used a push-out test to measure the bond strength of the steel/aluminium overcast parts and Bouayad et al. [50] studied the growth kinetics of the interaction layer between solid iron and molten aluminium. Viala et al. [63] used overcasting to bond aluminium into iron.

2.6 Effective materials characteristics on Al/Fe bimetallic joints

While using mild steels in compound casting process is restricted by their properties, some of them are used to improve wearing properties [64]. Different properties of elements including thermal expansion coefficient at 25 ºC reported in Table 2-1. The thermal expansion coefficient of stainless steel is 28% lower than that of aluminium; 16.0 vs 22.2 (10^{-6} m/ (m K) at 25ºC (Table 2-1). That means by cooling down from 500ºC to 25ºC there is a 3 -millimetre difference in each metre length, such that this property should be considered in the compound casting production process [65].

Table 2-1-Properties of different materials

	Aluminium	Steel	Zinc
Melting point, °C	660.32	1370-1400	419.53
Boiling point, °C	2470	-	907
Density, g/cm3	Liq 2.37 RT 2.70	8.0	Liq 6.57 RT 7.14
Crystal structure	FCC	BCC	HCP
Thermal expansion, (10-6 m/ (m K) 25 ºC	22.2	16.0	30.2
Atomic radius, pm	143	-	134
Heat of vaporization, kJ/mol	-	-	115

2.7 Intermetallic phases in the binary Al-Fe system

The interaction between the molten Al and iron is governed by the thermodynamic condition defined by the equilibrium phase diagram. Figure 2-4 shows a binary Fe-Al equilibrium phase diagram [66]. The system is characterised by an iron-based solid solution near the Fe rich region of the phase diagram and six non-stoichiometric intermetallic compounds of Fe_3Al, FeAl, $FeAl_2$, Fe_2Al_5, Fe_2Al_3 and $FeAl_3$ with increasing Al content. Detailed characteristics of the phases are described in Table 2-2. There have been several microstructural studies of the interface layer between aluminium and iron formed as a result of molten aluminium comes in contact with solid iron [47, 64, 65].

Researchers reported different morphologies of interaction between aluminium and steel of different processes such as welding and annealing, although in most of cases only Al_5Fe_2 and $Al_{13}Fe_4$ intermetallic phases formed in the bond between two metals [96– 98]. The research by Pochec et al. showed $Al_{13}Fe_4$, Al_5Fe_2, $FeAl_2$, and FeAl phases form by order during isothermal sintering of Fe and Al. Pochec also noticed that the sequence of formation of the phases is consistent with the Al-Fe phase diagram [71].

In the old literature, $FeAl_3$ was using until Black [72] in 1955 found that the true composition formula is $Al_{13}Fe_4$. Although only when Grin et al. [73] published a paper about structure refinement in 1994, the $Al_{13}Fe_4$ formula generally accepted in the literature. This research is using $Al_{13}Fe_4$ to refer to the intermetallic phase.

The initial studies of the interface layer had reported the formation of more than one intermetallic phase [48], while later researchers could only confirm the formation of $FeAl_3$ in the interface layer [63]. Such early findings were later explained more by other researchers who identified the major intermetallic phase as Fe_2Al_5 [67]. Although subsequent investigation principally supported the new findings, the formation of other minor phases was also reported. The last reports identified the interfacial reaction products as Fe_2Al_5 and $FeAl_3$ as the minor phase [74].

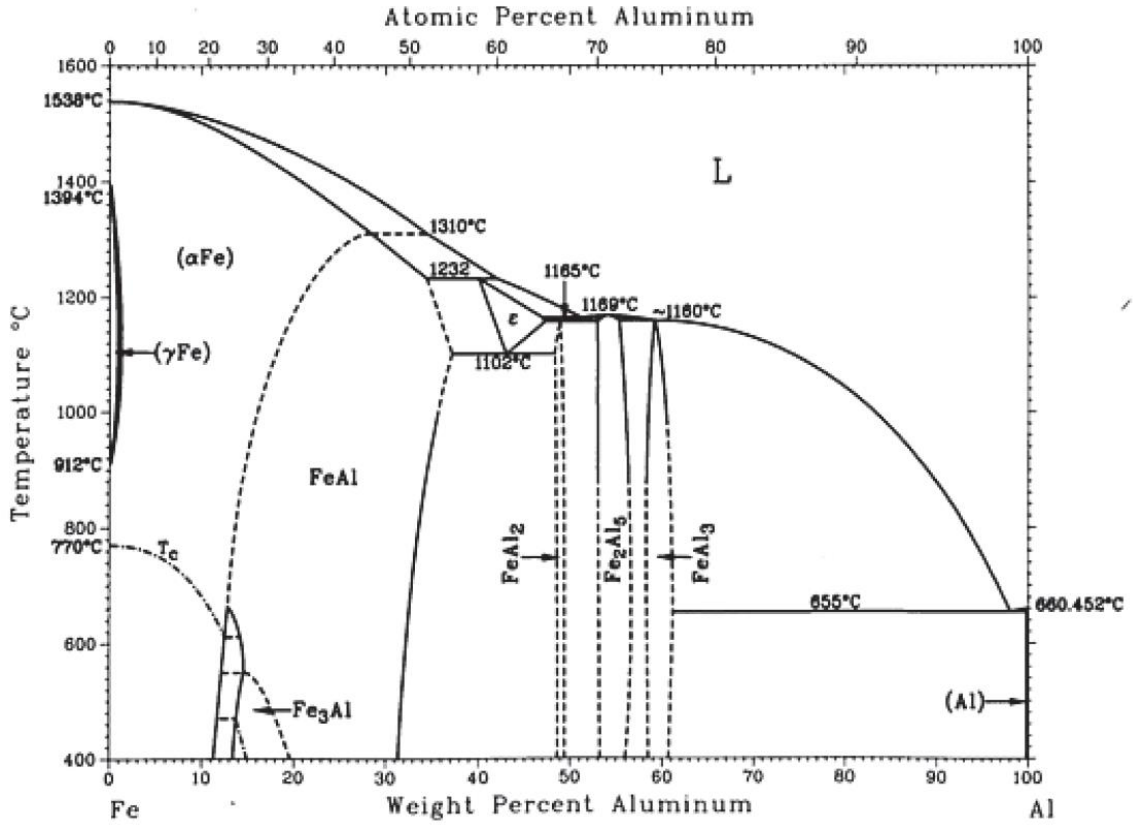

Figure 2-4- Al-Fe binary phase diagram [63].

Table 2-1-The atomic percent of the iron and aluminium in different Fe-Al IMC phases [14]

	Al (at %)	Fe (at %)
Fe_3Al	12-28	66-80
FeAl	Around 43	Around 53
$FeAl_2$	Around 51	Around 47
Fe_2Al_5	51-74	26-37
$FeAl_3$	Around 79	Around 19.5

The development of a suitable interfacial bond between the solid steel and liquid aluminium is a primary requirement for optimum performance of an aluminium/steel bimetal joint. The nature and the properties of the interface (thickness, continuity, chemistry, strength and adhesion) are determined by factors both intrinsic to the steel and aluminium (chemistry, crystallography, defect content), as well as extrinsic to them (e.g. test conditions such as time, temperature, pressure, atmosphere and other process variables). A moderate chemical interaction between solid steel and liquid aluminium improves wetting, assists liquid state fabrication of the joint and enhances the strength of the interface [75]. Table 2-2 shows some of the physical and mechanical properties of Al-Fe intermetallic phases.

Table 2-2- Crystal structure and properties of Fe-Al intermetallics (IMCs) [11,12, 13]

	Crystal structure	Stability range (at.%)	Density ($Mg\ mm^{-1}$)	Vickers Hardness	CTE K^{-1} (10^{-6} m/(m K))
Fe (solid solution)	BCC	0-45	7.8		16.0 (25 ºC)
ɣ-Fe	FCC	0-1.3	7.8		
FeAl	BCC (order)	23-55	5.58	470-667	16.07 (250 to 750 ºC)
Fe_3Al	Do3	23-34	6.72	330-368	
Fe_2Al_3	Cubic (complex)	58-65	-		
$FeAl_2$	Triclinic	66-66.9	-	1058-1070	14.17 (200 to 800 ºC)
Fe_2Al_5	Orthorhombic	70-73	4.11	1000-1158	
$Al_{13}Fe_4$	Monoclinic	74.5-76.5	3.9	772-1017	15.2 (27 to 627 ºC)
Al (solid solution)	FCC	99.998-100	2.69		22.2 (25ºc)

It is quite beneficial to have a thorough knowledge and understanding of the reaction products and kinetics to devise, design and control processing conditions to achieve bimetallic products with the required characteristics [75].

Development of an optimum bond between solid steel and liquid aluminium involves some degree of physical and/or chemical interaction between these two constituents. However, in aluminium/steel bimetal joints in elevated temperatures usually chemical interactions (like adsorption, solute segregation, interdiffusion, dissolution precipitation and compound formation) between the two materials dominate effect on the evolution of interface and chemical interactions are not so effective. The atomic percentage of composition of every Al-Fe intermetallic phase is demonstrated in Table 2-1. Partitioning of solutes between the different phases and thermodynamic shift in phase equilibria in the interface as a result of chemical interactions could result in the

formation of non-equilibrium phases during the evolution of the interface to a more stable configuration [75]. From a purely thermodynamic stand point, interfaces in composites are inherently unstable; as a result, morphological and structural transformations continue well beyond primary fabrication. A judicious control of processing conditions, aluminium and steel composition is usually required to achieve improvement in the strength of the bimetallic interface without excessive degradation of the strengths of the primary materials [75]. Besides chemical interactions between the liquid aluminium and solid steel, the thermoelastic compatibility between two materials also must be considered. A large mismatch of thermal expansion coefficient between the dissimilar materials of a joint can give rise to large thermoelastic clamping stresses during cooling from the fabrication temperature [75]. However, that do apply only on more complicated surfaces such as fibre and matrix that mechanical bond can form a joint. These stresses could give rise to interfacial cracking if the joint cannot accommodate stresses by plastic flow. Intriguing new concepts which employ interface modification through deposition of stress absorbing compliant layers are being explored in bimetallic joints for high temperature applications. The primary objective of these compliant layers is to reduce the thermal expansion coefficient mismatch that induces stresses [75].

Researchers used different bonding processes to join aluminium to steel. Song et al. [12] studied the intermetallic layer formed in the dissimilar aluminium alloy/stainless steel joint that was bonded by tungsten inert gas welding-brazing. An intermetallic layer with uniform thickness of less than 10 μm detected alongside the bond. Al_8Fe_2Si intermetallic phase was detected in the interface with Al-12Si filler metal in welded seam side and $(Al,Si)_{13}Fe_4$ layer in the steel side with hardness values of 1025 and 835 HV respectively. However, the interface with filler metal of Al-6Cu had a layer of $Al_{13}(Fe,Cu)_4$ with the hardness of 645 HV. The average of tensile strength for Al-12Si filler metal was measured 100-120 MPa while the fracture was propagated alongside the $(Al,Si)_{13}Fe_4$ intermetallic phase. The average of measured strength of the joint with Al-6Cu filler metal was 155-175 MPa that was more than half of the aluminium base metal strength [12]. SEM micrograph of the interaction layer of Al-12 wt% Si and milled steel produced by tungsten Inert Gas welding presented in Figure 2-5. TEM characterisations show formation of Al_8Fe_2Si at interaction layer I and $(Al,Si)_{13}Fe_4$ at layer II [12].

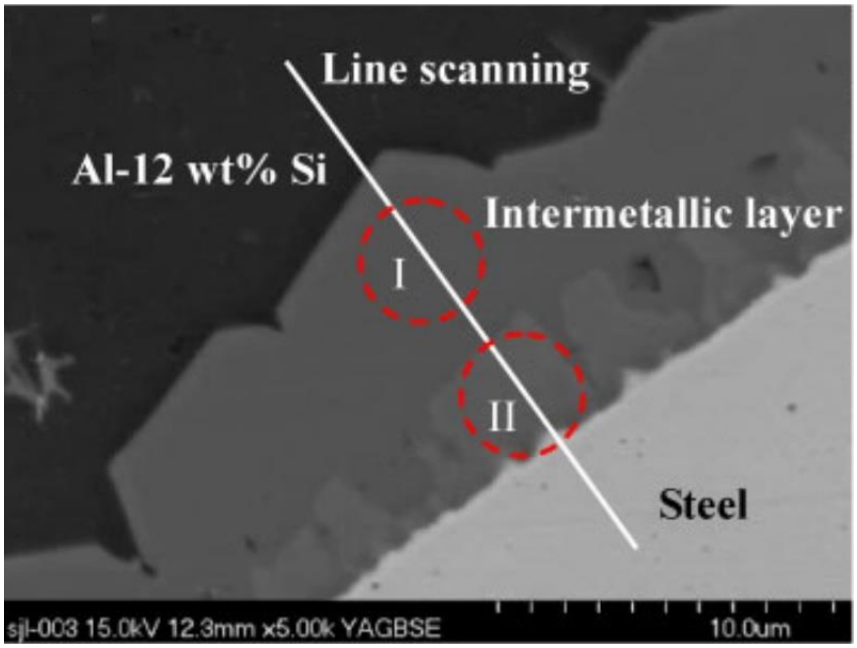

Figure 2-5-SEM micrograph of the interaction layer between Al-12 wt% Si and steel welded by Tungsten Inert Gas welding process [11].

Dong et al. [76] used tungsten inert gas welding to join galvanised steel to aluminium alloys by different filler wires of Al-5Si, Al-12Si, Al-6Cu, Al-10Si-4Cu, and Zn-15Al to introduce different amounts of Si, Cu and Zn to the filler wires. The studies showed that increasing Si of the filler metal increased the tensile strength of the joint and decreased the thickness of the interaction layer between steel and aluminium alloy. For Al-12Si filler, the thickness of the interaction layer was measured as 2 μm and the tensile strength was measured to be 136 MPa[reference]. The experiments proved that Al-Si-Cu filler wire could make a thinner interlayer than Al-Cu filler wire. The fracture was propagated in weld metal of the Al-Si-Cu filler wire however it propagated at intermetallic compound layer of the joint with Al-Cu filler wire. However, Zn-Al filler wire gave a thicker interfacial layer of intermetallic compound in weld that leaded to a weak joint [76].

2.8 Al-20wt%Sn-7wt%Si and Al6060 aluminium alloys

High tin aluminium alloys are famous for their good tribological and mechanical properties as a bearing that make the alloy suitable for bearing applications in cylinder

liners and combustion engine pistons. High tin aluminium alloys are potential alloys to replace lead-bronze bearings that not environmentally friendly. The tin content of the alloy spread over a continuous aluminium rich matrix while the aluminium rich matrix tolerates the structural integrity of the alloy, the segregated particles of tin act as solid lubricants [69, 4].

In the wrought aluminium-magnesium-silicon family of 6000 aluminium alloys, Al6060 is famous for its ability to be forged, extruded and rolled. The ultimate tensile strength of Al6060 alloy is between 140 to 230 MPa. Al6060 is corrosion resistant and benefits from good weldability plus good formability. This aluminium alloy is using in architectural sections, truck and trailer flooring and furniture [78].

2.9 Interlayers in bimetallic joints

Differences in the properties between two surfaces of the solid metal and overcast alloy may prohibit the bonding of dissimilar materials. In some bonding processes it is possible to make bond only by surface preparation, while using an interlayer is a usual method to overcome bonding difficulties. An interlayer is a layer between two surfaces to help them make a better bond [68, 71]. An ideal interlayer should have the following properties:

- A thermal expansion coefficient between the solid substrate and the cast metal.
- Wetting easily by the cast metal.
- Not decreasing the qualities of the final product of the process after alloying.
- The melting temperature of the interlayer should be lower than melting temperature of the casting metal to be able to fully/semi melt by casting metal.

Difference between the CTEs of two sides of a bond is an important factor for those bonds that their production process includes changing in temperature or their working temperature varies in a wide range. So, considering CETs of different materials is important. For example, the CTE of aluminium-tin bearing alloy at 25 °C (23 µm/ (m·K)) is two times of steel (12 µm/ (m·K)), so after casting Al-Sn around steel, a big gap forms between two sides. Moreover, an interlayer can play an important role to decrease that deteriorate effect; to reach this goal, the CTE of interlayer should be between the CTE of two sides of bond [80]. The linear CTE of aluminium and steel are

demonstrated in Table 2-2. Zinc as a most common interlayer for aluminium alloys/steel joints is widely used in different bonding processes such as resistance welding [81] and laser beam brazing [82]. In addition to zinc, gallium [83] and nickel interlayers (coatings) [84] are also utilised in different joining processes, which are discussed below:

Researchers have used zinc interlayer to bond steel and aluminium by different methods such as Laser Beam Welding (LBW) and Tungsten Inert Gas (TIG) [77, 78, 79]. The zinc coating can successfully inhibit the vulnerable surface of steel from oxidation and the low melting temperature (420 °C) of zinc and high solubility of zinc in aluminium in elevated temperatures can also prevent it from aggregating around the interface [87]. So, the zinc coat dissolves in aluminium and acts as a scarifiable layer in temperatures higher than 600 ºC. These are seemingly crucial properties to make zinc well suited as an interlayer in the aluminium overcasting process. However, few studies have been reported so far on microstructure and properties of bimetallic joints formed by overcasting of molten Al over Zn coated steel [87]. Figure 2-6 shows a Al-Zn binary equilibrium phase diagram.

A study by Eustathopoulos et al. [88] showed that the formation of a continuous layer in the joint caused by interfacial reaction, leading to the formation of intermetallic compounds [88].

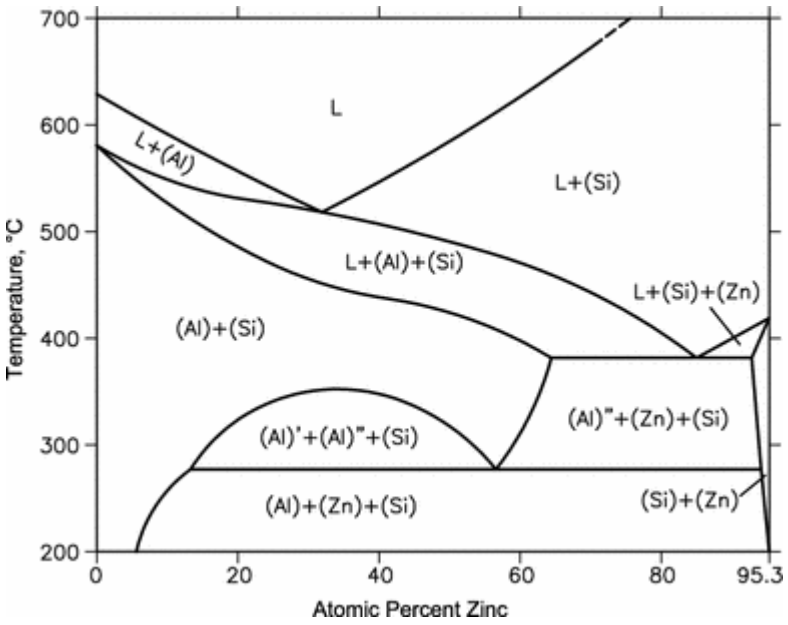

Figure 2-6- Al-Zn phase diagram [89].

Gallium forms a eutectic liquid phase with aluminium at 29 ºC and has a high solubility in aluminium [90]. Al alloys containing Ga are brittle, due to the rapid penetration by Ga in the Al grain boundaries. It can also disrupt the oxide layer on the aluminium surface [83]. Shirzadi et al. has developed a method in which a minimal quantity of gallium, about 1 mg/cm^2, was gently applied to the surfaces without disrupting the oxide layer to braze two surfaces of aluminium [83]. The assembly was then immediately and rapidly heated to around 500 ºC to allow the gallium to diffuse and homogenise into the aluminium after penetrating and disrupting the oxide. The heating process lasts no longer than 1 or 2 minutes. During bonding, the sample was subjected to a level of pressure close to the yield strength of the aluminium at the bonding temperature (10MPa). This produced a strong joint in which the bond position was hardly visible by optical microscope. Microstructure of the brazed joint demonstrated in Figure 2-7 [83]. The line of the joint is hardly visible in the micrograph. Such an application of gallium could inspire its use in other bonding processes such as compound casting.

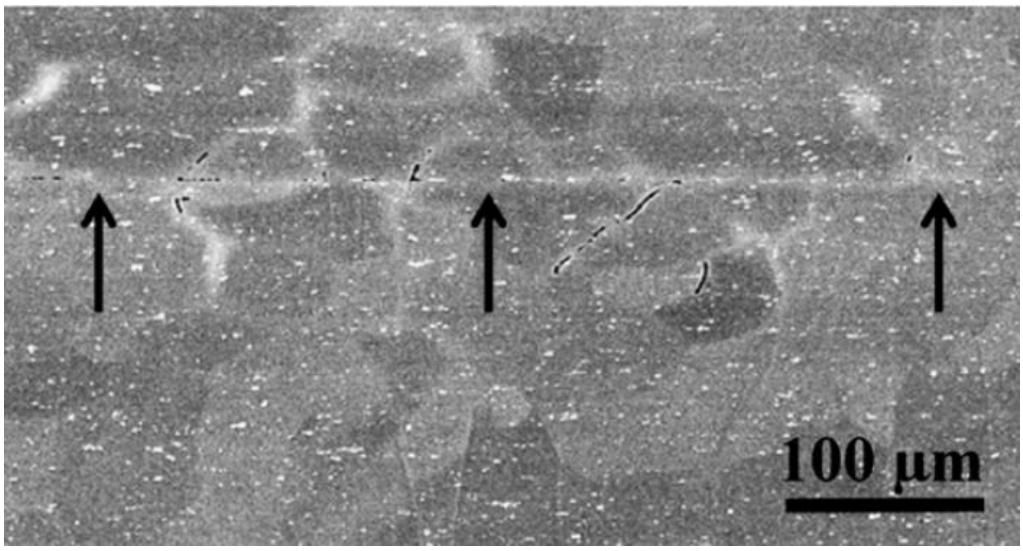

Figure 2-7- SEM micrograph of a brazed joint. The black arrows show the position of the brazed line. White particles demonstrate Al_3Fe [83].

Nickel coating on steel used by Han to modify the intermetallic phases that form between liquid aluminium and solid steel [91]. Han noticed that using Nickel coated steel increased the strength and ductility of the bimetallic joint [91]. Also, Nickel coat

bonds well to aluminium oxide and can improve weldability. Nickel coating on natural aluminium oxide reduced surface strain [92].

2.10 Kinetics of formation of an interlayer

The formation of an intermetallic layer in the bimetallic joint resulted from the interaction of liquid Al and solid steel; This can be considered as diffusion-controlled reaction because the movement of iron atoms across the solid and liquid is much higher than diffusion of iron atoms throughout intermetallic interfacial layer [93].

In formation of an interaction layer, the flux is proportional to the chemical potential gradient when the diffusion is rate (dx/dt) limiting where x is thickness and t is time. Since the chemical potentials on both sides of the interaction layer are assumed fixed, k is considered independent of thickness. However, the gradients of the elements are proportional to the thickness of interaction layer. As the diffusion constant is independent of thickness of interaction layer, the density, composition or topology of the interaction layer is assumed inert and rigid. So the parabolic regime, dx/dt is k_P/x, and x^2 is proportional to t [85, 86]. Therefore, the parabolic equation for oxide layer inspires the implication of parabolic law for the formation of intermetallic interlayers in Al/Fe bimetallic joints. The consistency of the experimental thickness measurements with Equation (2-1) for solid Fe/liquid aluminium reactions has been reported in previous studies [87, 88, 89].

$$x^2 = kt \qquad \text{Equation (2-1)}$$

In Equation (2-1), x is thickness of intermetallic layer, t is the time of diffusion, and k rate constant, which can be related to temperature using Arrhenius equation (2-2):

$$k = k_0 \exp\left(-\frac{Q}{RT}\right) \qquad \text{Equation (2-2)}$$

In equation (2-2), Q activation energy in kJ mol^{-1}, K_0 temperature-independent pre-exponential (m^2/s) and T temperature in Kelvin, R is gas constant. Therefore, the formation of intermetallic interlayers in Al/Fe bimetallic joints can be described by parabolic law.

2.11 Imperfections in bimetallic joints

Imperfections and failure are key factors in bonding materials, however only few relevant reports found imperfections and failure of bimetallic joints in overcasting process. So, imperfections in similar processes of metal matrix composites and fibre reinforced metal matrix composites studied to have a better understanding of imperfections and failure mechanisms of overcasting process. Specifically, the thermal cycle of components in metal matrix composites and overcast parts are very similar and comparable. Also, as in overcasting process, one side of the bond is in solid state while the other side of the bond in the beginning is in liquid state and solidifies gradually, the most similar process is in solidification of metal matrix composites, so imperfections of metal matrix composites studied.

In casting of metal matrix composite from liquid temperature, considerable thermal stresses could develop in the steel substrate that is used for reinforcement. These stresses arise from different thermal expansion characteristics of the matrix and reinforcement materials. In particular, residual stresses develop in ceramic-metal composites because the thermal expansion coefficient of the ceramic phase is lower than that of the matrix metal; as a result; the ceramic phase is subjected to large compressive thermal stresses during cooling. The larger the mismatch in the coefficient of thermal expansion (CTE) between the fibre and the matrix, and the greater the magnitude of difference in temperature, the larger is the magnitude of residual stress that develops in the composite [75].

An important property that depends upon the thermal stresses generated during composite fabrication, secondary processing and subsequent service is related to composite's resistance to thermal fatigue. Thermal cycling impairs the strength and ductility of composites reinforced with continuous fibres, whiskers and particles. In general, the thermal fatigue resistance depends upon the amplitude of the temperature cycle, its frequency, and the CTEs of the reinforcement and matrix materials. The strength degradation of thermal cycled composites is usually attributed to the mismatch of thermal expansion coefficient as well as formation of brittle reaction products in the interface. Thermal cycling reduces the strength of cast aluminium-matrix composites as the number of cycles and the temperature amplitude are increased. Generally, interfacial debonding is the primary mode of failure. The use of

stress absorbing compliant layers with coefficient of thermal expansion (CTE) values intermediate between the reinforcement and the matrix materials has been proposed to reduce the incidence of interfacial debonding and failure during thermal cycling [75]. Figure 2-8 shows the fracture surface of a bond of aluminium to steel. The figure demonstrates the fracture propagated through the $Al_{7.4}Fe_2Si$ phase. The bond failed in $Al_{7.4}Fe_2Si$ phase that has a cleavage plane [98].

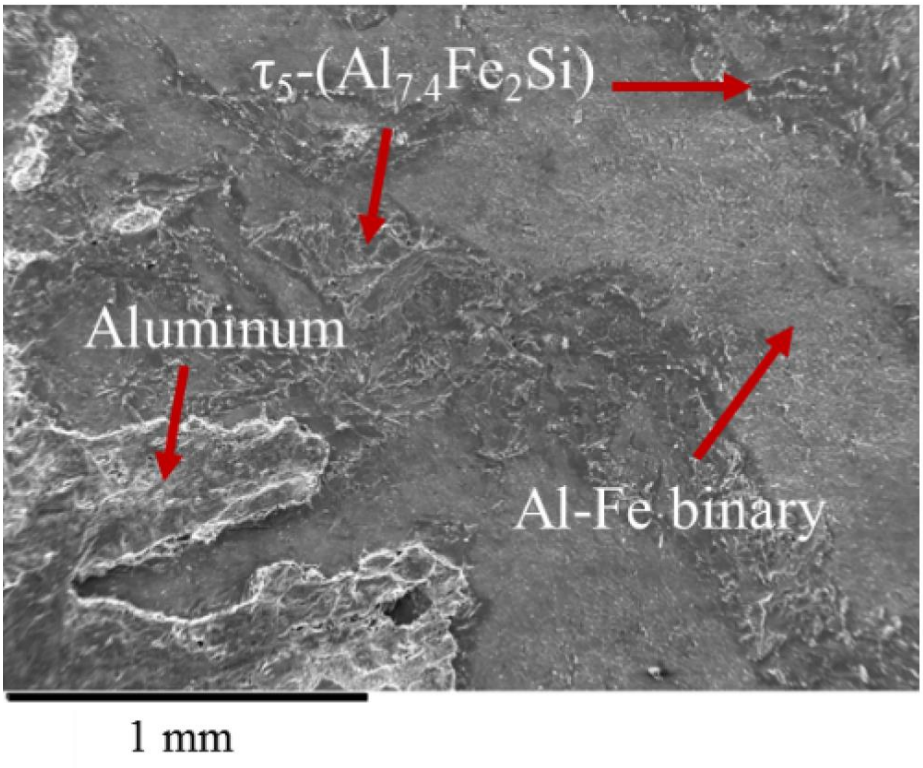

Figure 2-8- Fracture surface of steel/aluminium bond [98].

Chapter 3 Experimental methods

This chapter gives a detailed description of materials, processes and characterisation used in this piece of work. They include overcasting of pure aluminium and its alloys around solid steel substrate. Then followed by a range of microstructural and mechanical characterisation methods such as OM, SEM, EDX, TEM, XRD and tensile test.

3.1 Mater*ials*

The overcast alloys were prepared in the laboratory from commercially pure aluminium, 99.9 wt. % pure Tin and Al-50Si master alloy. Composition, supplier and purity of the materials used in the preparation of aluminium and its alloys are listed in Table 3-1. Composition of the commercially pure aluminium measured by inductively coupled plasma atomic emission spectroscopy, this alloy used to make the overcasting alloys. Composition of aluminium alloys after casting also are reported.

Table 3-1- Compositions of the raw materials used in this study (wt.%)

	Supplier	Purity	Al	Sn	Cu	Zn	Bi	Fe	Ni	Sb	As	Cd	Mg	Si	Mn	Pb	Ti	Cr
Aluminium	Coleshill Aluminium Ltd,	99.2%	Rem	0.03	0.03	0.07	-	0.40	0.03	-	-	-	0.03	0.30	0.03	0.03	-	-
Al-50Si	Norton Aluminium Ltd	99.6%	Rem	0.01	0.08	0.02	-	0.32	0.01	-	-	-	0.28	51.0	0.02	0.02	0.09	0.03
Sn	William Rowland Limited	99.9%	-	Rem	<0.01	0.02	0.015	<0.01	0.01	0.015	0.013	0.006	-	-	-	-	-	-

All the alloys melted in clay graphite crucibles at 750 ºC by using electrical resistance furnaces. The melts were stirring before casting to ensure chemical homogeneity of the chemical composition. To make sand moulds, dried sand mixed with sodium silicate, moulded in designed dimensions and dried at room temperature for one week. Figure 3-1 shows the sand mould used in this experiment.

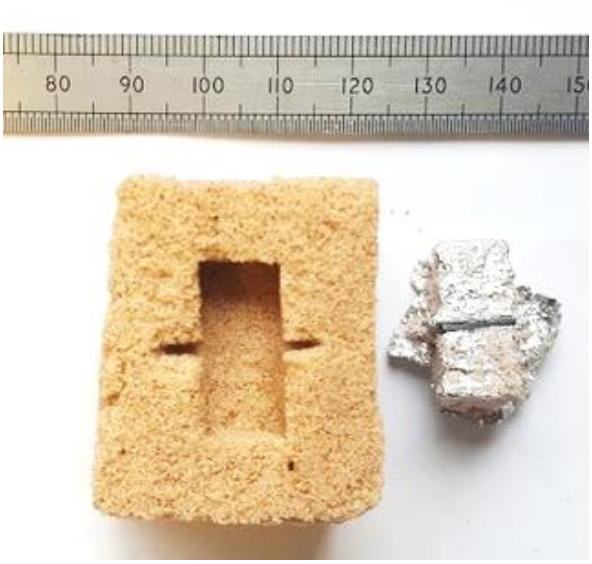

Figure 3-1- Sand mould and the aluminium-zinc coated steel overcast. Sand moulds with similar dimensions were used for all of the experiments.

To check the composition of the aluminium alloy, compositions of the castings analysed using Worldwide Analytical Systems, AG, Foundry Master, Optical Emission Spectroscope (OES) after making the alloy. Dependent to the requirements of the experiments, the quantity of the melt was varied from 1 kg to 4 kg.

Table 3-2 shows the composition of the steels of the uncoated steel, zinc coated and nickel coated steel used in the experiments. All of the steel plates were cut from a big sheet of steel. Size of the zinc coated and uncoated steels used in the overcasting process was 0.44×10×10 mm^3 while the thickness of the zinc coat was 12 µm. Moreover, 1.2×10×10 mm^3 nickel coated steel was used with thickness of 7 µm nickel coat and supplied by Tata Steel. The company data sheet confirms that the nickel plated steel was diffusion annealed and cold rolled after nickel plating.

Nickel-zinc coated steel by 1.2×10×10 mm^3 size and 80 µm nickel-zinc coats were used in this experiment.

Table 3-2-The nominal chemical composition of different alloys (wt. %)

Element	Al	Fe	Si	C	Cu	Mn	P	Sn
Al-1Si	Rem	0.103	1.3	-	0.011	0.006	0.005	0.000
Al-7Si	Rem	0.122	7.23	-	0.004	0.005	0.002	0.000
A-12.2Si	Rem	0.224	12.4	-	0.013	0.022	0.003	0.000
Al-20Sn-7Si	Rem	0.161	7.44	-	0.031	0.032	0.002	20.312
Al 6060	Rem	0.222	0.451	-	0.051	0.054	0.002	0.292
Uncoated steel	0.038	Rem	0.05	0.072	0.01	0.26	0.01	-
steel of the zinc coated steel	0.038	Rem	0.05	0.072	0.01	0.26	0.01	-
steel of the nickel coated steel	0	Rem	0.01	0.048	0.01	0.26	0.009	-
steel of the nickel-zinc coated steel	0	Rem	0.01	0.048	0.01	0.26	0.009	-

3.2 Overcasting process

The sand mould made out of a mix of dried sand and sodium silicate and dried in atmosphere for at least one week before of the overcasting tried. Figure 3-2 shows the dimensions of the sand mould and the cast part. The moulds were preheated at 250 ºC inside furnace for at least one hour before casting in order to eliminate the moisture in the mould. Then the mould cooled to room temperature and the steel substrate was inserted inside the mould. The steel substrates were at room temperature when fixed in the moulds.

Melt prepared in a large graphite crucible and stirred manually to maintain homogeneity. The melt temperature measured to make sure of the designed temperature ±1 ºc. Then melt was poured into the mould and cooled down to room temperature or held in the time and temperature that was designed in advance.

The casting process performed at room temperature. Then the moulds moved to furnace based on the design of experiment. Holding time demonstrates the time from when the mould moved into the furnace to the time when mould moved out of furnace.

Table 3-3 shows the variables used in the experiments. These variables used to make samples with different processing conditions. In most of the cases, for each processing condition in least 4 samples made to ensure the repeatability of the results.

A steel mould with similar design of the sand mould but different dimensions used. The overall size of 30×20×90 mm^3 and a cavity size of 10×10×40 mm^3 used for casting in steel mould.

YCT model YC-727UD thermometer and K type thermocouple used to measure temperature with an accuracy of ±0.01 ºC.

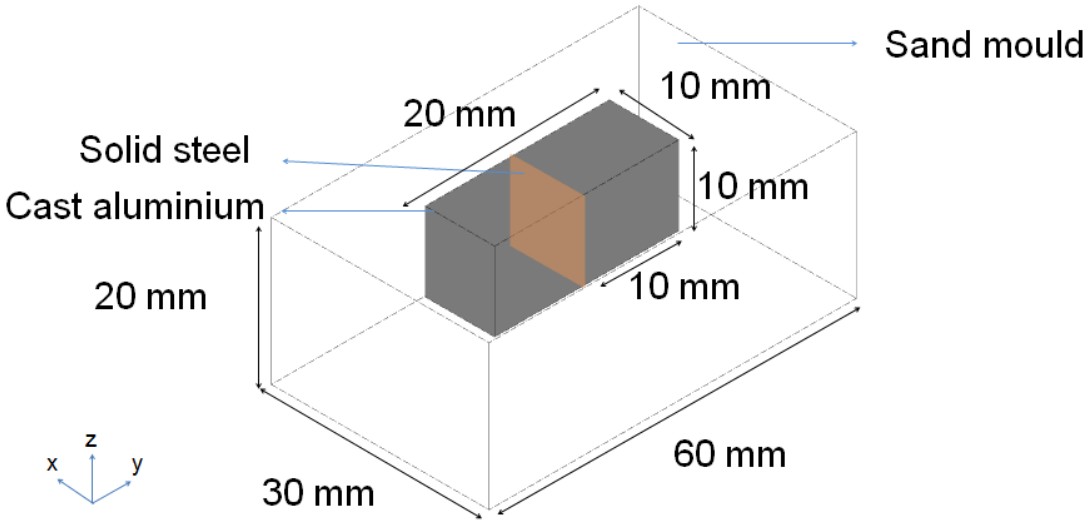

Figure 3-2- Schematic illustration of the sand mould and the cast.

Table 3-3- Variables of the materials processing conditions

Overcasting temperature, ºc	Type of substrate	Overcast Al composition	Melt Holding time/ minutes
750	Uncoated steel Gallium/zinc coated steel Zinc coated steel Nickel coated steel Nickel/zinc coated steel	Aluminium Al1Si Al7Si Al12.2Si Al20Sn Al20Sn7Si Al6061	0 1 5 10 30

3.2.1 Chemical composition of the cast

To verify the composition of the cast is near the designed chemical composition, the chemical composition of all of the alloys was checked by using “Worldwide Analysis System (WAS) AG, Foundry master”. Samples were polished with 120 grit SiC paper to produce flat surfaces for analysis. The machine was calibrated with standard piece of CITZAF correction package prior to analysis. On every single sample at least 5 tests were performed and an average result was recorded as the final composition.

3.3 Materials characterisation

3.3.1 Sample preparation for metallography

Avoid separation of steel and overcast aluminium during sectioning of the bimetallic specimens, the cast part was mounted in Bekelite prior to metallography. X-y plane of as cast part was mounted to keep consistency at all samples. Then the mounted samples were grounded by using abrasive SiC papers with the grits of 120, 800, 1200, 2400 and 4000. The samples did not etch. To make sure there is no artificact on the

surface of every sample, they cleaned in water in ultrasonic vibrator for 10 minutes after cleaning by washing liquid and water.

3.3.2 Optical microscopy

The microstructures were observed by using a Zeiss Optical Microscope equipped with a computer and a digital camera, AxioCam ICc3. “Axioshop 2 MAT0” software was used to acquire images from the camera and perform image analysis. The quality of the microscopic images was sufficient to measure the topographic parameters such as crack.

3.3.3 Electron microscopy

Scanning Electron Microscopy (SEM) was used with a field emission gun Zeiss Supra 35 machine, equipped with an Energy Dispersive X-ray spectroscopy (EDX) Octane Super SDD EDX and back-scattered electron detection (BSE) facility. The machine operated in an accelerating voltage between 5 to 20 kV. Secondary and back-scatter electron imaging modes used to analyse the as-solidified microstructures. Carbon tape was used to connect the mounted samples to the SEM specimen holder. Figure 3-3 illustrates a schematic of the principle of SEM.

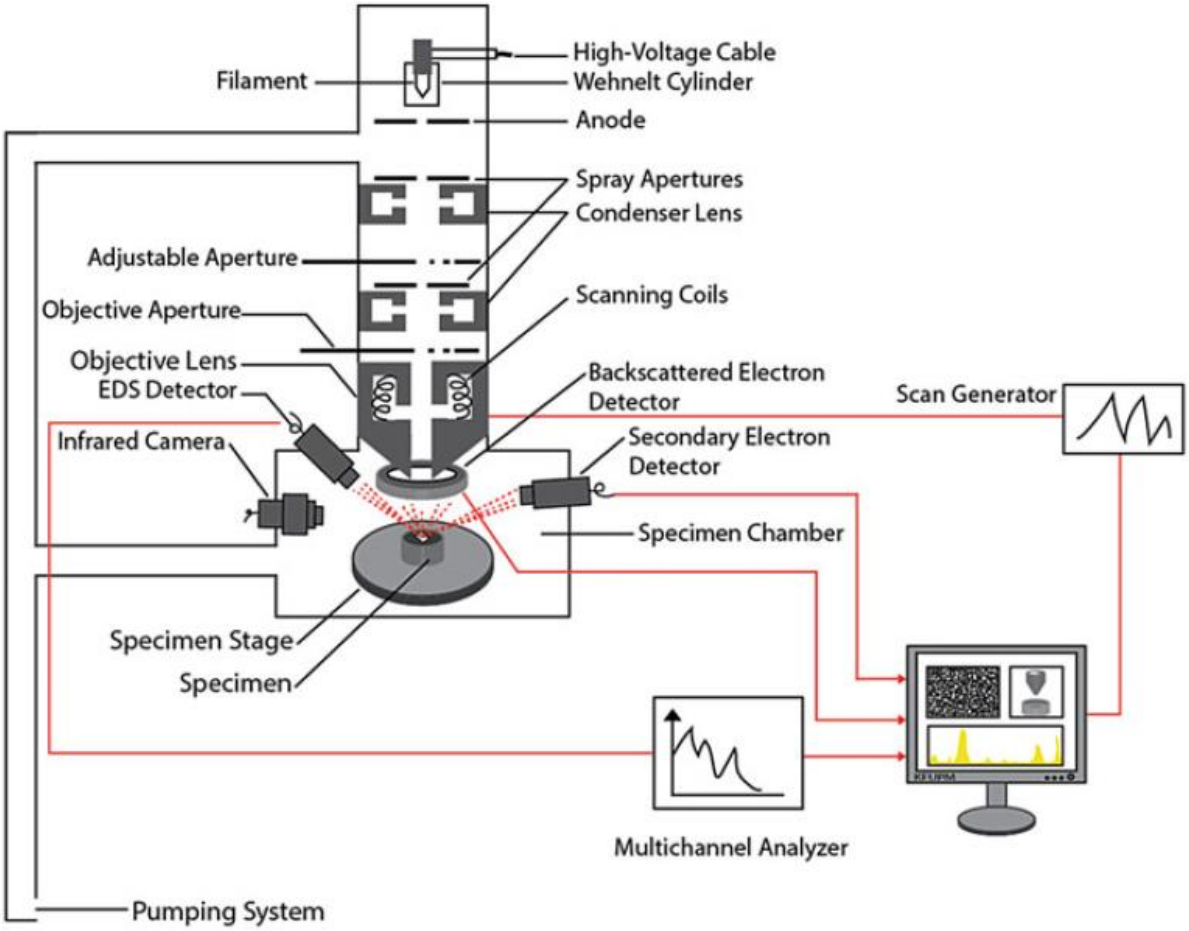

Figure 3-3- Schematic of the principles of scanning electron microscope [99]

3.3.4 Sample pre preparation

FIB (Focused Ion Beam) used to cut out the TEM specimens from the regions of interest of the bi-metal overcast samples. A Carl Zeiss Crossbeam 340 DualBeam FIB/SEM was set in SEM mode with 5kV used Ion beam operation to cut the trench 30kV at 3nA and then 30kV, 1.5nA, 30kV pA, 30kV, 300pA. Samples were then lifted out and attached to a TEM grid. Both of the TEM samples of about 20×8×0.1 μm^3 were then thinned using 30kV 100pA and 50pA. Then cleaned using 5kV 20pA. Such a TEM specimen preparation ensures to keep the brittle intermetallic phases present in the aluminium/steel interface intact. Figure 3-4 shows the microstructure and the schematic of the samples prepared by FIB to characterise using TEM. Figure 3-4 illustrates the TEM sample preparation by using FIB.

The prepared samples used for both optical Microscopy and SEM characterisation.

3.3.5 TEM

The TEM operated at 200kV to identify the intermetallic phases formed in the bond, Jeol 2100 F analytical TEM (Transmission Electron Microscopy) equipped with EDAX EDXS in dark field mode was used. TEM analysis used to understand the change in the selected area of the intermetallic compounds formed. The crystallographic features of the intermetallic phases were investigated to understand the mechanism of formation of the phases between solid steel and liquid aluminium during overcasting process.

Micrograph of the interaction layer of pure aluminium and zinc coated steel that held at 750 ºC for 0 minutes is demonstrated at Figure 3-4 (a). Figure 3-4 (b) demonstrates the schematic of the microstructure and the position of 2 samples extracted from the cast part. The average thickness of the interaction layer formed between aluminium and steel is about 80 micron and too big to characterise in TEM at once. Therefore, the TEM sample was focused in the regions of steel/IMC and aluminium/IMC. Figure 3-4 (c) shows the sample ready to be extracted from the border of steel and intermetallic compound layer and Figure 3-4 (d) shows the sample ready to extract from the border between aluminium and intermetallic layer.

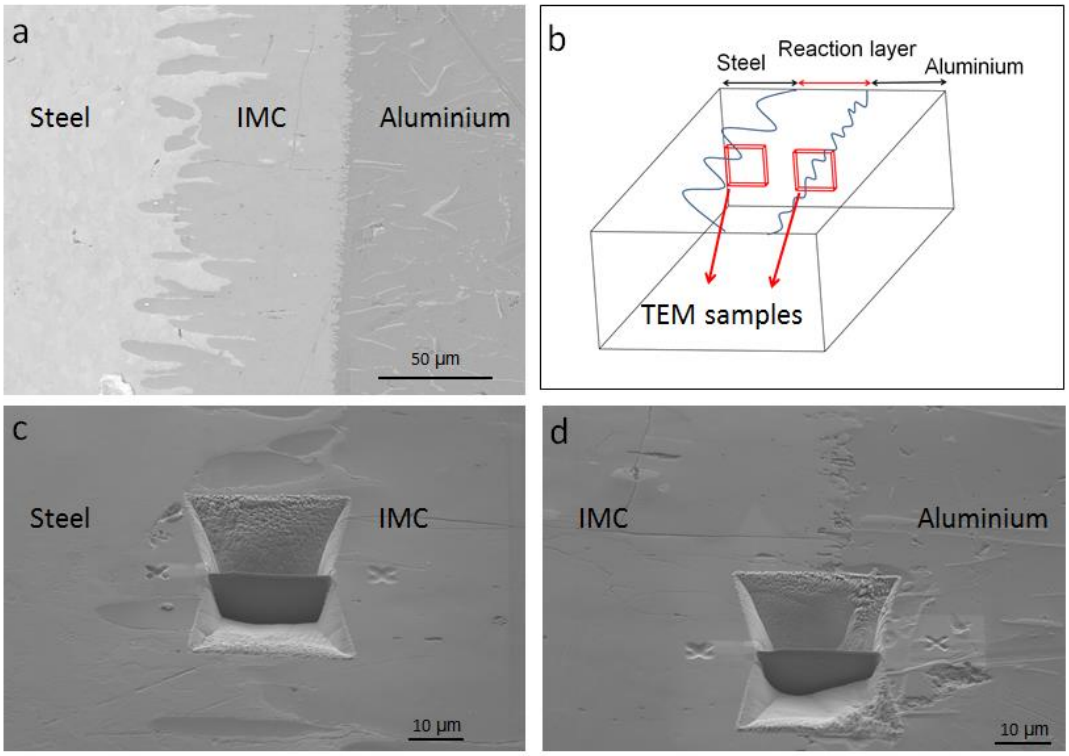

Figure 3-4 – Illustration of the TEM sample preparation using Focused Ion Beam (FIB) (a) SEM Micrograph of as-cast microstructure of interface between pure aluminium and zinc coated steel. After overcasting, the sample held at 750 ºc for 10 minutes. (b) Schematic of TEM sample preparation using a FIB (c) TEM lamellae of the region between IMC and steel, prepared for puck-up and final thinning (d) TEM lamellae of the region between IMC and aluminium, prepared for puck-up and final thinning.

3.3.6 XRD

Different phases identification were performed by using X-ray diffractometry (XRD) Bruker D8 Advanced X-ray diffractometer with Cu-Kα sourced that the energy is 8.04 keV, which corresponds to an x-ray wavelength of 1.5406 Å. The wave was filtered through nickel absorber at a voltage of 40 kV, a current of 40 mA. The following parameters were used to perform the characterisation: 2Θ range from 10-100º, step size: 0.009172 º, step time: 61.59998s. By compare of the extracted peaks from the spectra to the standard pdf files by using Crystallographica Search-Match V2,1,1,0 software, different phases characterised.

3.3.7 Tensile test

To measure the bond strength of the bimetals, they were cast into blocks of a certain size. Figure 3-5 shows the dimensions and the schematic of a sample while the red arrows demonstrate the direction of forces to determine bond strength. The bond strength of at least 3 bimetallic overcast samples were measured on every processing condition of the as cast samples without cutting them. The load-displacement curves were determined using a Universal Materials testing machine (Instron® 5569) operated at a cross head speed 3.4 mm/min. The Instron® 5569 machine was connected to a computer for automation and calculation of the average value of maximum load to break bimetallic bond was determined from 3 to 5 tensile tests.

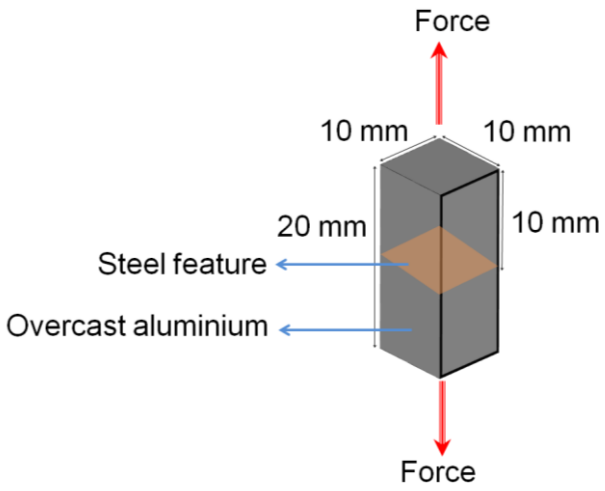

Figure 3-5- Schematic of the tensile test samples.

It should be noticed that for the samples that fall part apart after overcasting, the bond strength was reported zero.

Chapter 4 Effects of coating on overcasting pure aluminium on steel

4.1 Introduction

There are different parameters that control the bonding of dissimilar joint of aluminium around steel. An important factor is surface condition of the solid steel or the coating of the steel. The current research performed a comprehensive study of the effects of interaction between liquid aluminium and steel in different surface conditions, uncoated, zinc coated, nickel coated and zinc/nickel coated. This chapter presents results and discussion on the effect of substrate, surface condition and holding time of melt prior to solidification of overcasting pure aluminium over mild steel substrate with and without coating to understand the evolution of microstructure on the interface of aluminium and steel of bimetallic joint.

It is critical to choose appropriate and suitable materials process parameters in overcasting to make sound dissimilar joint of aluminium/steel. It is also critical to investigate the effects of different materials and process parameters on formation of intermetallic compound on the joint interface. The interface reaction behaviour in different coatings will be compared and discussed; also, the effects of holding time on formation of intermetallic compound in the joint will be studied.

The experiments presented in this chapter show the microstructure of the reaction layer formed between aluminium and steels with different surface modifications. It is studying how surface conditions govern the reaction between liquid aluminium and solid steel. Interaction couples in different surface conditions studied: interaction between liquid aluminium and the coating conditions of gallium-zinc coated steel uncoated steel, zinc coated steel, nickel coated steel and zinc-nickel coated steel. Moreover, the kinetics of the formation of interaction layer between aluminium and steel in the aforesaid surface conditions were studied. To study the kinetics, the overcast samples were held at 750 ºC in furnace for 0, 1, 5 and 10 minutes. The objective of this chapter is to understand the fundamental aspect and kinetics of interaction between liquid aluminium and solid steel in different surface conditions.

Pieces of uncoated steel, zinc coated steel and nickel coated steel with equal sizes that described earlier in chapter 3 were used in overcasting processes.

4.2 Aluminium /uncoated steel

Four samples of Al/uncoated steel were made by similar process and materials: one sample was cooled down in atmosphere and at room temperature right after overcasting, the second held in furnace at 750 ºC for 1 minute, the third held in furnace at 750 ºC for 5 minutes and the fourth held in furnace at 750 ºC for 10 minutes.

Figure 4-1 shows the microstructure of the cross section of the joint between uncoated steel and pure aluminium after holding for 10 minutes at 750 ºC. Formation of the interaction layer in uncoated steel with aluminium is not uniform; similar results were found by Rezaei et al. that noticed that the interaction between aluminium and uncoated steel is not uniform [100].

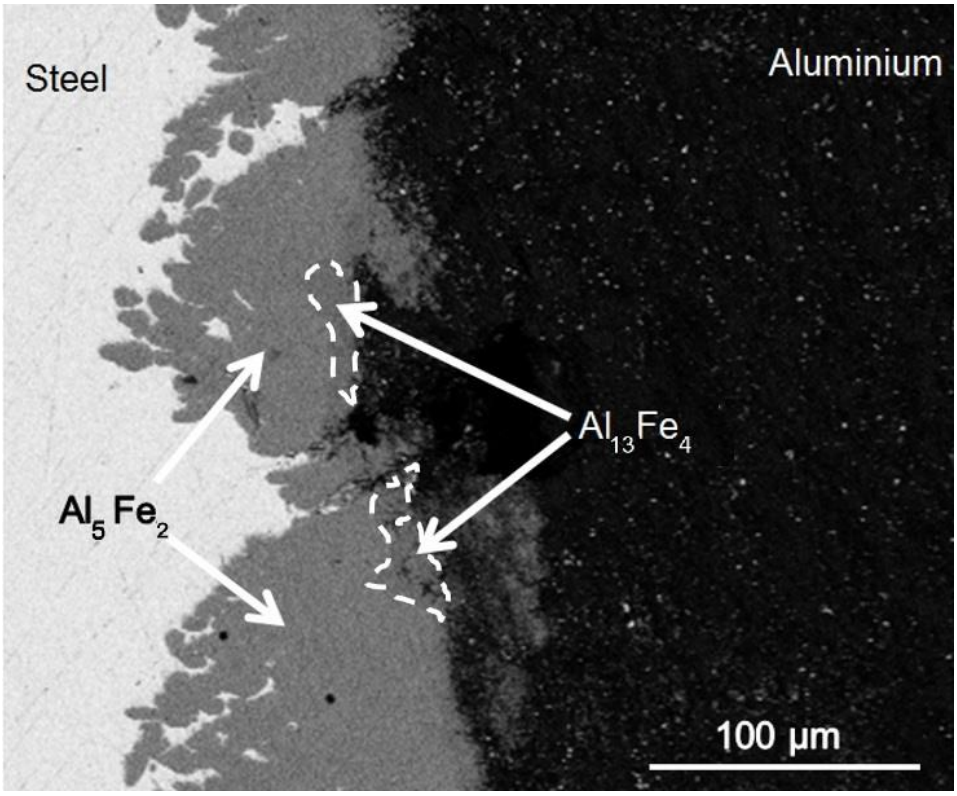

Figure 4-1- SEM microstructure of the interaction between uncoated steel and overcast pure aluminium after holding at 750 ºC for 10 minutes.

Aluminium and steel reacted in specific points of the joint and then the reaction region grows alongside the bond towards the steel. Most of the reaction layer is Al_5Fe_2 with a finger like morphology while a narrower layer of $Al_{13}Fe_4$ formed between Al_5Fe_2 and

aluminium. Moreover, a thin layer of $Al_{13}Fe_4$ intermetallic phase formed between aluminium and the Al_5Fe_2 intermetallic phase. Al_5Fe_2 intermetallic phase build the largest fraction of the interaction layers that form in the interdiffusion between aluminium and steel and following parabolic growth law.

Before overcasting, surface of the mild steel was polished and every oxide or dirt was removed, however vulnerable surface of uncoated steel was oxidised before being touched by liquid aluminium in 750 ºC. That layer of oxide could prevent the steel to be touched by liquid aluminium uniformly alongside the bond and the steel did not interacted with aluminium after overcasting. After one minute of keeping at 750 ºC, interaction between aluminium and steel initiates in random areas where there is a lack of oxide layer on steel and liquid aluminium touches solid steel and intermetallic forms. The intermetallic had been growing by time at high temperature of 750 ºC until IMCs touch each other alongside of the interaction layer however still oxide layers may stop the IMCs to touch each other after growth. Figure 4-2 (a) shows the interaction layer between aluminium and uncoated steel after holding at 750 ºC for 10 minutes. The steel is lighter and aluminium is darker while the grey layers of IMCs formed in between. Figure 4-2(b) demonstrates high magnification of the white dashed rectangular at figure (a). The figure focused on the bond between two particles of IMC. EDS map of 3 different elements of iron, aluminium and oxygen are shown in the figure. The lighter area in Figure 4-2(b) is IMC and the darker area is iron oxide. The iron oxide separates two pieces of IMC from each other.

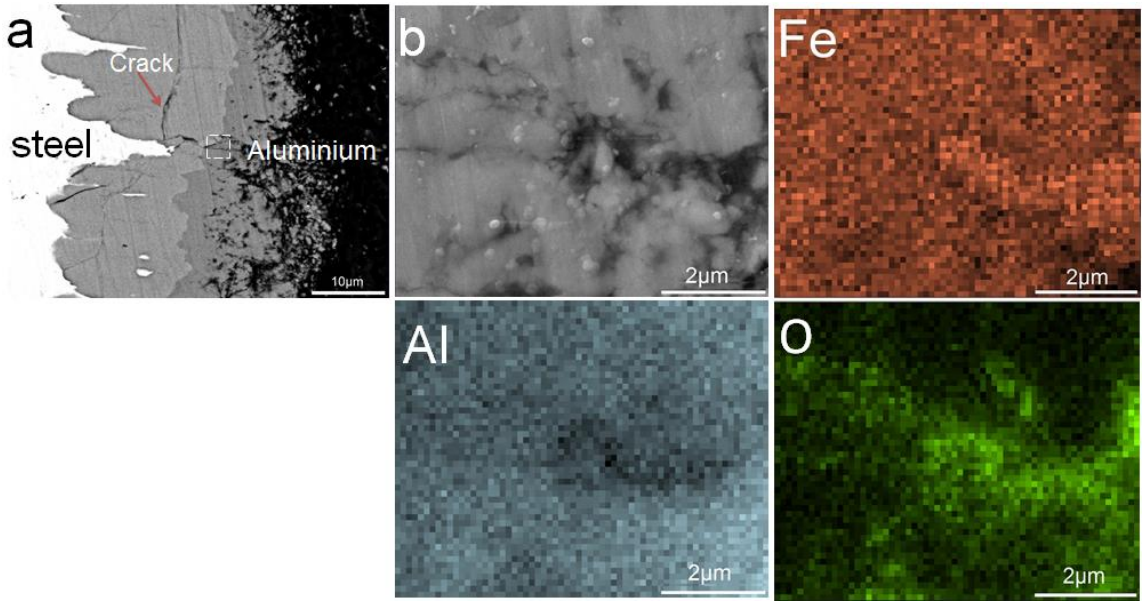

Figure 4-2- (a) Microstructure of the interaction layer between uncoated steel and pure aluminium after holding at 750 ºC for 10 minutes. (b) Higher magnification of the white rectangular of figure a. EDX map analysis of oxygen, aluminium and iron of figure b.

4.3 Aluminium / Zinc coated steel

Figure 4-3a shows the micrograph of the cross section of the zinc coated steel. The zinc coat distributed uniformly and the thickness of the zinc coat is 12±1 µm. Figure 4-3b and c show the EDX map of the microstructure of the cross section, (b) demonstrates iron and (c) demonstrates zinc of the surface.

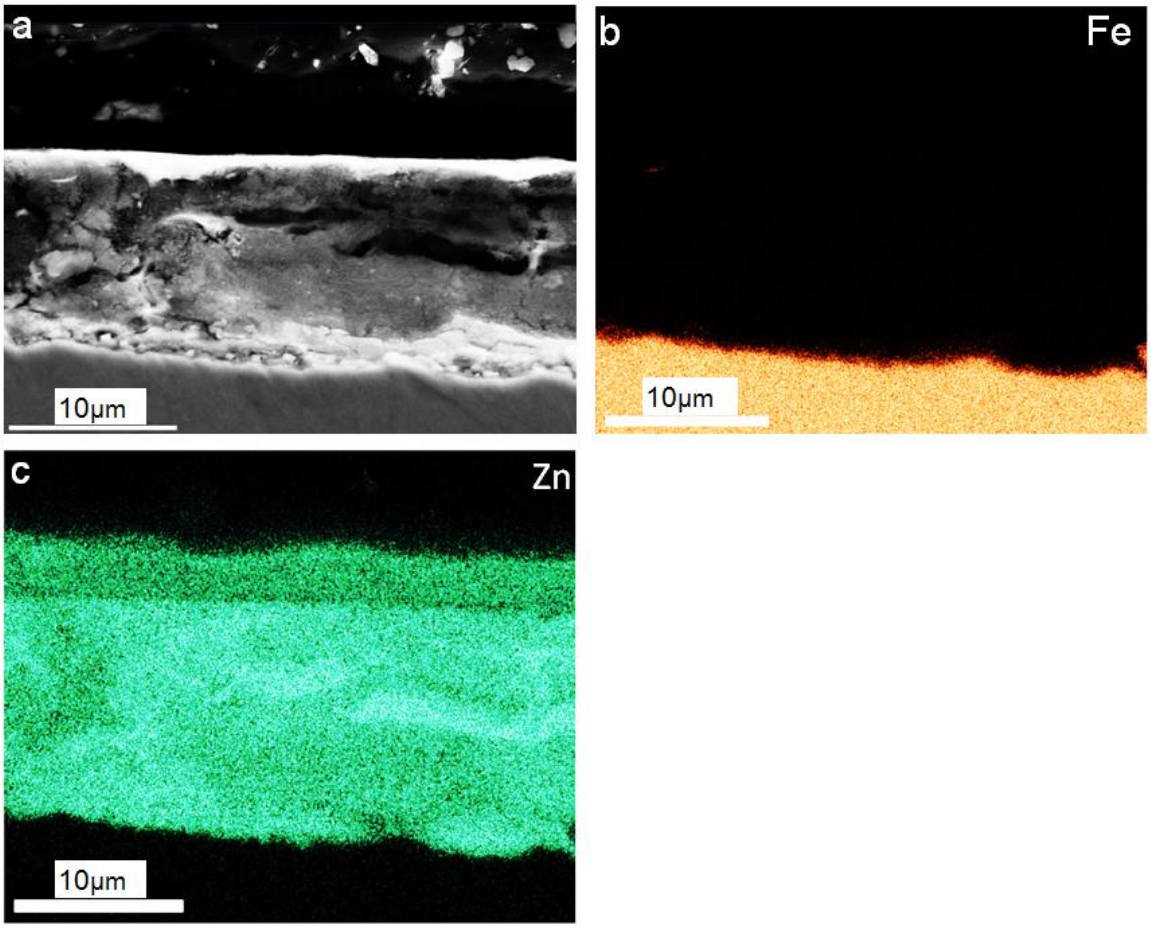

Figure 4-3- (a) SEM micrograph of the cross section of the surface of a zinc coated steel. The zinc coat is uniform with a thickness of 11-12 micrometre on top of steel (b) the iron at the micrograph (c) the zinc of the micrograph.

To study and compare the cooling rate of the steel mould and sand mould, the cooling rate was measured. Figure 4-4 shows the cooling curve of the sand mould in blue line and the steel mould in red line. As soon as overcasting was initiated, the temperature reached 750 ºC and then gradually dropped by an average rate of 0.63 K/s (750/ 500 ºC) in the sand mould. However, the steel mould, after casting at 750 ºC dropped by an average rate of 5 K/s (750/500 ºC).

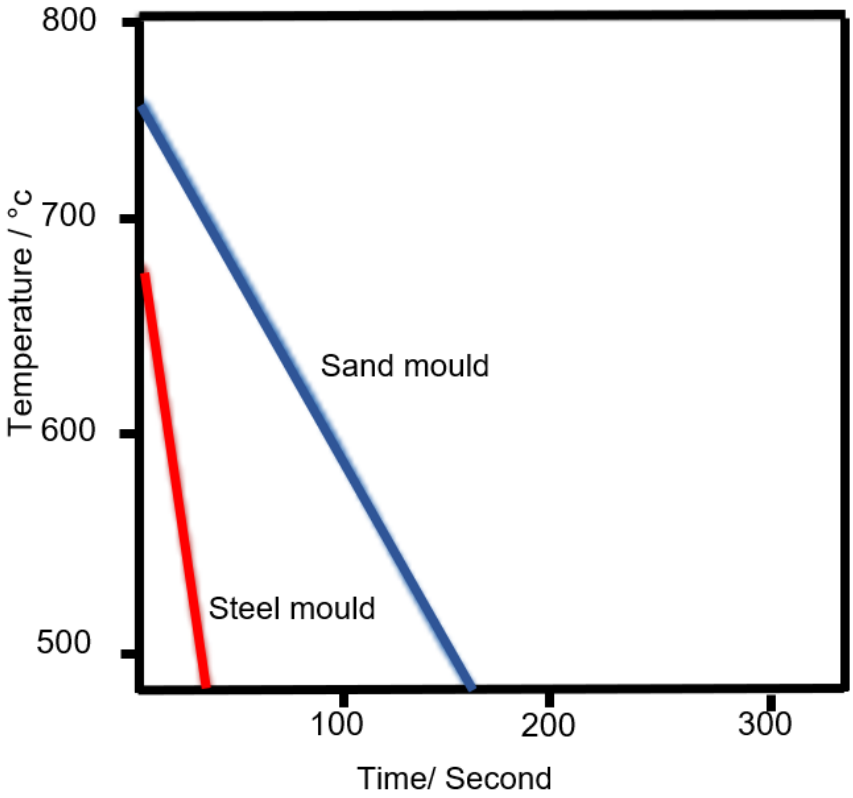

Figure 4-4-Results of the thermal measurement of the overcast aluminium around zinc coated steel from 750 ºC in room atmosphere. The red line demonstrates the cooling curve of the aluminium cast in steel mould and the blue line demonstrates the aluminium cast in sand mould.

4.3.1 Microstructure and morphology

Figure 4-5 a and b demonstrate the interaction between liquid aluminium and zinc coated steel. Figure 4-5 a shows the microstructure of the cross section of interaction between liquid aluminium and zinc coated steel and cooling down at high rate of 5 K/s (750/500 ºC) in steel mould. The correspondent EDX line scan shows 10% zinc at 2 µm on the interaction layer. Figure 4-3 shows the primary thickness of the zinc coat was about 12 µm, so it is possible to conclude that most of the zinc coat dissolved in the liquid aluminium and 2 µm thick zinc by 10% dilution remained on the surface at high rate of cooling rate of 5 K/s (750/500 ºC). It is also noticeable at Figure 4-5a that no interaction detected between aluminium and steel; no intermetallic compound is visible in the micrograph nor stable proportion of Al/Fe at the EDX line scan is visible.

However, despite no interaction at the high speed cooling rate of 5 K/s (750/500 ºC) in steel mould, the interaction between aluminium and steel at low speed cooling rate

of 0.63 K/s (750/500 ºC) in sand mould formed intermetallic compound layer. Figure 4-5 b shows the finger like feature of the interaction between aluminium and steel. The reaction layer is continuous however the thickness varies alongside the interface. This phenomenon demonstrates the fact that the rate of dissolution of the zinc coat was higher than the rate of formation of intermetallic layer. It should be considered that Figure 4-5a and b are in different magnifications.

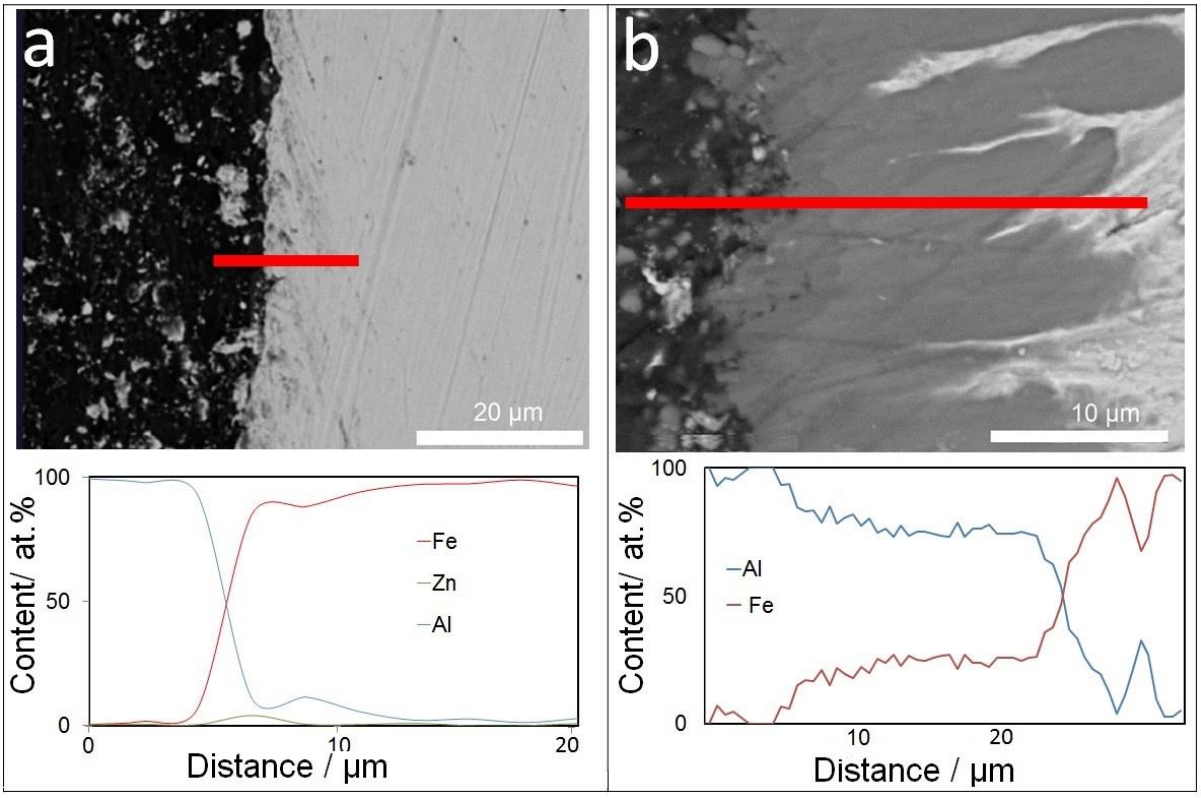

Figure 4-5- SEM micrograph of the interaction between zinc coated steel and overcast aluminium and the corresponding EDX line scan of the red line (a) steel mould (b) sand mould. Both of the samples cooled in room atmosphere after casting at 750 ºC.

4.3.2 Intermetallic layer

Figure 4-6 shows the SEM micrograph of the cross section of interaction between overcast aluminium on top of zinc coated steel after holding in furnace in 750 ºC for 10 minutes. This is the typical interface morphology of dissimilar overcast of liquid aluminium of annealing and is similar to the finding of other researchers [101]. Finger like feature IMC growth from aluminium towards steel while the maximum thickness of the IMC was measured 150 µm. The graphs in Figure 4-6 show EDX line scan of the

corresponding red lines. The line scan shows the finger like feature is Al_5Fe_2 intermetallic compound. Figure 4-6b shows a higher magnification of the yellow rectangular of Figure 4-6a that is darker grey. The EDX line scan shows the darker area is $Al_{13}Fe_4$ and was formed between Al_5Fe_2 and aluminium. The $Al_{13}Fe_4$ interface with Al_5Fe_2 is flatter than the interface with aluminium. In overcasting process, a finger like feature layer of intermetallic compound develops and identified as Al_5Fe_2. The interface of the intermetallic layer and steel is flatter than the interface of the intermetallic layer and aluminium. Also, the growth of the intermetallic layer into the steel has a preferred orientation that results formation of a non-uniform, finger-like feature interface between the intermetallic phase and the steel substrate.

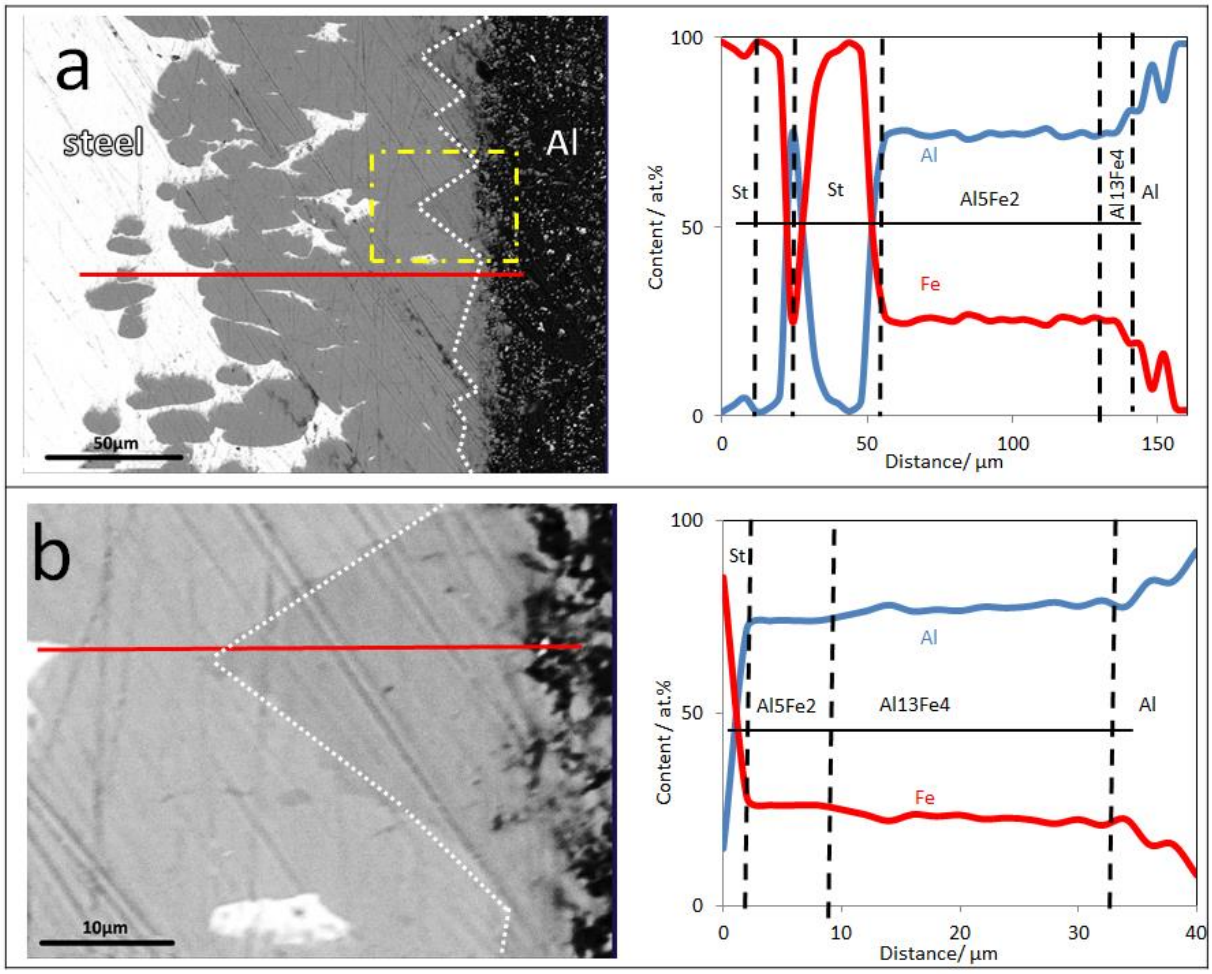

Figure 4-6- (a) SEM micrograph of cross-section of overcast aluminium around Zn coated steel substrate and (b) region near the aluminium side outlined by yellow rectangle taken in higher magnification, together with composition profile across the distance shown as red line.

4.3.3 Formation and growth of the intermetallic compound layer

Zinc coat is usually applied on surface of steel to provide corrosion protection. However, the strong effect of the zinc coat on reaction between aluminium and steel and build-up of reaction layer on the joint is considerable for researchers, so they asked for a deeper study on the kinetics of the role of zinc on reaction of aluminium and steel [95]. For example, Springer [95] assumed the zinc coat on the steel has no effect on the results of the experiment because of the small quantities of the zinc coat in comparison with the high amount of aluminium. However, the current research shows different effects imposed by different coatings while the volume of every coat was small in comparison with the volume of liquid aluminium.

Figure 4-5b and Figure 4-6 show a continuous intermetallic compound layer alongside the joint of overcast aluminium on top of zinc coated steel in different holding times. The microstructure development of the intermetallic layer in each bond observed by SEM and the phase composition was identified by EDX line scan.

The zinc coated steel was in room temperature when the liquid aluminium cast at 750 ºC touched the surface of the zinc coat. Figure 2.6 shows the eutectic temperature of the zinc-aluminium phase diagram at 382 ºC, 95% zinc and 5% aluminium. So, interaction of only 5 wt.% of the liquid aluminium and the solid zinc can form eutectic of aluminium-zinc. As the volume of zinc is less than the volume of the liquid aluminium, the zinc coat was dissolved in the liquid aluminium. However, the cooling rate of 5 K/s (750/500 ºC) was fast enough to keep 5% of the zinc on the surface of the steel while the major parts of the zinc coat was dissolved in the aluminium. Figure 4-5a shows the microstructure of the zinc coated steel in touch with aluminium that cooled fast.

At cooling rate of 0.63 K/s (750/500 ºC) when the liquid aluminium touches the zinc coat, the zinc coat dissolved in the liquid aluminium and Al_5Fe_2 intermetallic phase forms.

As the activation energy of $Al_{13}Fe_4$ is higher than Al_5Fe_2, formation and growth of $Al_{13}Fe_4$ intermetallic phase is more difficult than Al_5Fe_2 at about 700 ºC [68]. So, a higher input energy is required for forming and growth of the $Al_{13}Fe_4$ intermetallic phase.

In all of the studies of the literature reviewed, including solid state and liquid state processes, the Al_5Fe_2 phase was always the major part of the intermetallic layer.

Aluminium-Iron phase diagram shows different intermetallic in the system, however, only two phases of Al_5Fe_2 and $Al_{13}Fe_4$ were formed in the overcasting process. The Al-Fe phase diagram, Figure 2.4 demonstrates AlFe, $AlFe_3$, $AlFe_2$, $Al_{13}Fe_4$ and Al_5Fe_2, however in the current experiment just Al_5Fe_2 and $Al_{13}Fe_4$ phases formed out of 5 phases. Despite the fact that all of those phases are stable at room temperature, just 2 out of 5 phases formed in the current experiment. Windmann defined specific conditions for formation of AlFe and Al_2Fe; high temperature of minimum 920 ºC, long annealing (in this case holding time) and the consumption of aluminium substrate is needed to form AlFe and Al_2Fe. Windmann [102] used a thin coat of aluminium on top of steel, after interaction of all the aluminium coat in high temperatures, the Fe riched phases formed [102]. However, in the current experiment overcasting is happening at 750 ºC and steel is always in touch with aluminium. Therefore, only Al_5Fe_2 and $Al_{13}Fe_4$ intermetallic phases form at the bond. Moreover, Naoi noticed that interdiffusion coefficient of FeAl, $FeAl_2$ and $FeAl_3$, should be more than two orders of magnitude smaller than at T= 550-640 ºC [68].

4.3.4 Development of the grain structure of the intermetallic compound layer

Morphology of the grains of the intermetallic layer changed by change in holding time. Change of the thickness of the interaction layer is different for Al_5Fe_2 and $Al_{13}Fe_4$ intermetallic phases. Figure 4-7 demonstrates change of the thickness of the different intermetallics of the interaction layer by holding time. The minimum and maximum thickness of every layer shown by error bars to demonstrate the scatter of data.

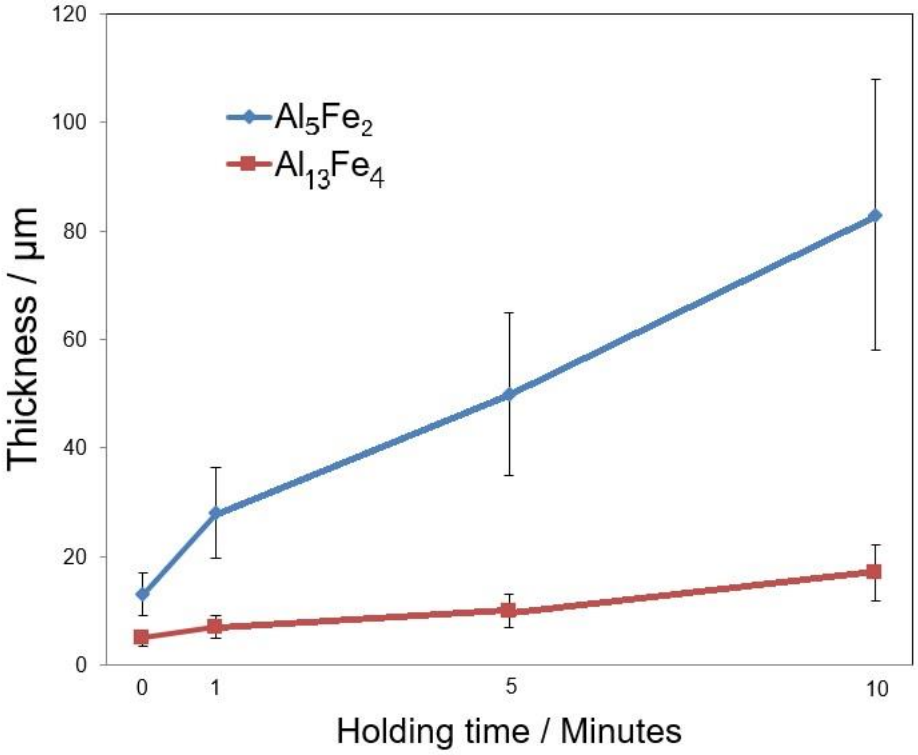

Figure 4-7- Average thickness of the intermetallic compound layer in the joint interface for both of the intermetallic phases of Al_5Fe_2 and $Al_{13}Fe_4$ when pure aluminium is overcast on top of zinc coated steel.

Figure 4-8 shows the layer thickness plotted as a function of square root of time after reaction at 750 ºC for steel with different surface conditions. The minimum and maximum thickness of every layer shown by error bars to demonstrate the scatter of data. Figure 4-8 shows that the growth of the reaction layer follows parabolic law in samples with different surface conditions. **d** is thickness of the interaction layer; **k** is surface dependent rate constant and suggests that formation of reaction layer is controlled by diffusion of aluminium and the element at the surface of the solid steel and **t** is time by second. All the surface conditions interacted with aluminium at the first instance however nickel coated steel was the only sample didn't interact with aluminium at the first second and the intermetallic compound was detected when nickel coated steel and aluminium have been in touch at 750 ºC for minimum 60 seconds. To compare the rate of formation of intermetallic compound in different surface conditions, the slop of every line is calculated. Zinc coated steel has the highest slope of 2.4 $\mu m/s^{-1/2}$ then correspondingly nickel-zinc coated steel by 2.15

μm/s$^{-1/2}$, nickel coated steel by 1.6 μm/s$^{-1/2}$ and uncoated steel by 0.97 μm/s$^{-1/2}$ have the highest to lowest rate of interaction with aluminium.

$$d = k\sqrt{t} \quad \text{Equation (4-1)}$$

$$k_{Zn} > k_{NiZn} > k_{Ni} > k_{Un}$$

Other researchers demonstrated that interaction of liquid aluminium and solid steel follows parabolic law [87, 7]. However, the current research approves that parabolic law is not the only factor that is controlling formation of interaction layer.

The best method to show a parabolic growth is to plot IMC thickness as a function of square root of time to measure the respective rate constant, Figure 4-8 demonstrated IMC thickness as a function of square root of time. The first IMC of nickel coated steel is forming after a period of time holding at 750 ºC while zinc coated steel has the highest rate of interaction with aluminium.

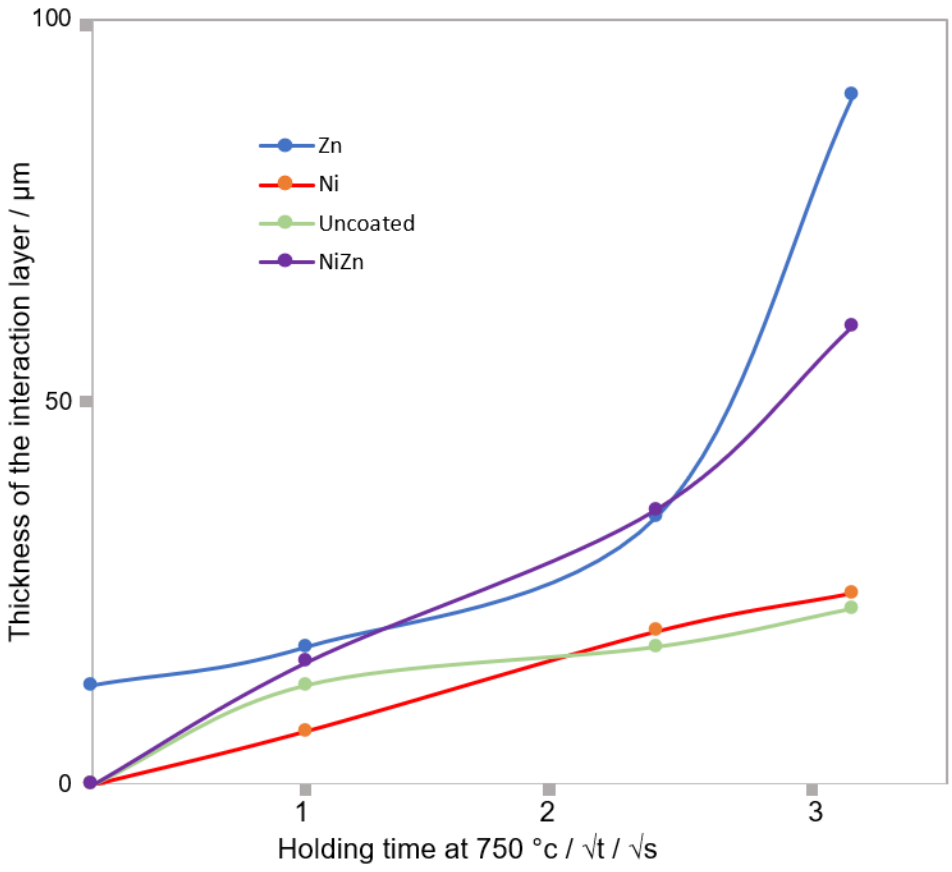

Figure 4-8- Average thickness of the interaction layer in the joint interface for different surface conditions in different periods of time. The graph demonstrates thickness of the IMC for zinc, nickel, nickel-zinc coated and uncoated steel which had been in touch with pure aluminium at 750 ºC in different square roots of holding time.

4.3.5 TEM investigation of the interaction layer

The object of using TEM to study the joint is to provide a detailed investigation of complex reaction layers of interaction between solid steel and liquid aluminium. Also, TEM has investigated the relationship between the orientation of the formed intermetallic layer and the substrates of steel and aluminium in order to understand the mechanism of growth of the intermetallic phases into the steel and aluminium substrates.

Takata et al. [103] used TEM and EBSD (electron backscatter diffraction) to study the dislocation density and density of high/low angle grain boundaries and concluded preferential diffusion can be because of the anisotropic volume change during the phase transformation of α-iron and Al_5Fe_2 intermetallic phase.

In order to study the microstructure, a zinc coated steel that pure aluminium was overcast on and held at 750 ºC for 10 minutes was examined. The micrograph of the sample and the lamellas extracted with FIB to use in TEM is shown in Figure 4-9 and Figure 4-10.

The steel/IMC border shows the steel region next to the intermetallic. Steel region doesn't show any incoherent intermetallic in the low magnification however the intermetallic region has varying coherent in high magnifications.

Cheng et al. reported $FeAl_2$ in the same area that was characterised by using EBSD. Cheng et al. noticed that $FeAl_2$ only formed between Fe_2Al_5 and steel and gradually replaced the top peak of the original finger-like steel substrate[104].

The microstructure of the intermetallic region shows a lamella-like contrast. This contrast is observed through random magnifications. The diffraction pattern recorded from this region maybe indexed as Al_6Fe_2, as described by Burkhardt et al. [73]. The microstructure observed is similar to that reported by Rong et al. [105] and the crystal structure is the same but with a composition of Al_5Fe_2.

The high-resolution micrograph shows significant number of localised defects along with the lower magnification images. It is likely that the presence of defects in the microstructure gave rise to reflections that are forbidden in a perfect crystal. Hence [001] reflection is observed in the diffraction pattern.

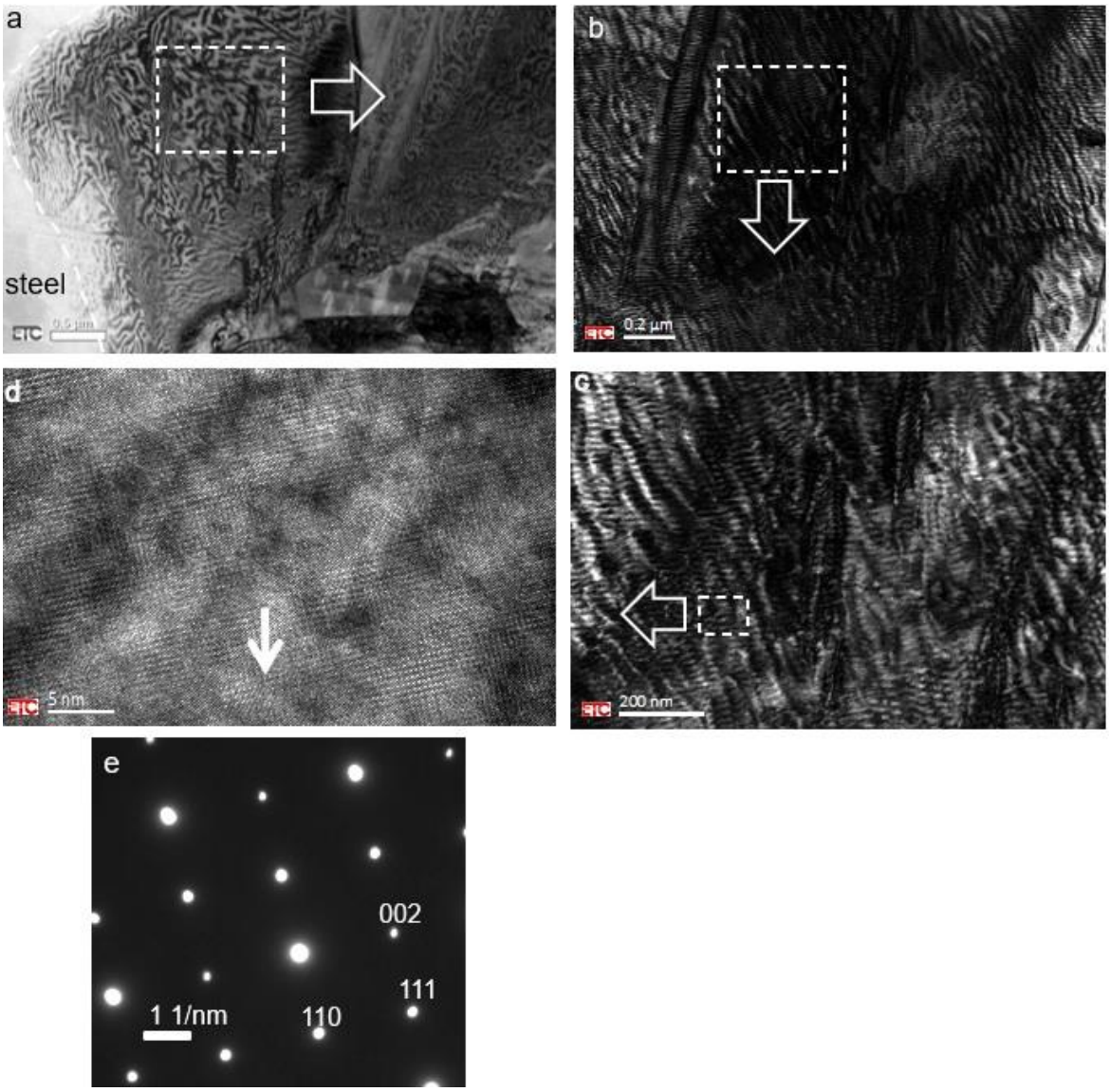

Figure 4-9- TEM microstructure of the bond between steel and intermetallic compound layer. Figures a, b, c and d show a higher magnification of white dashed rectangle of their former micrograph. (e) Corresponding electron diffraction pattern of c maybe indexed as Al_6Fe_2.

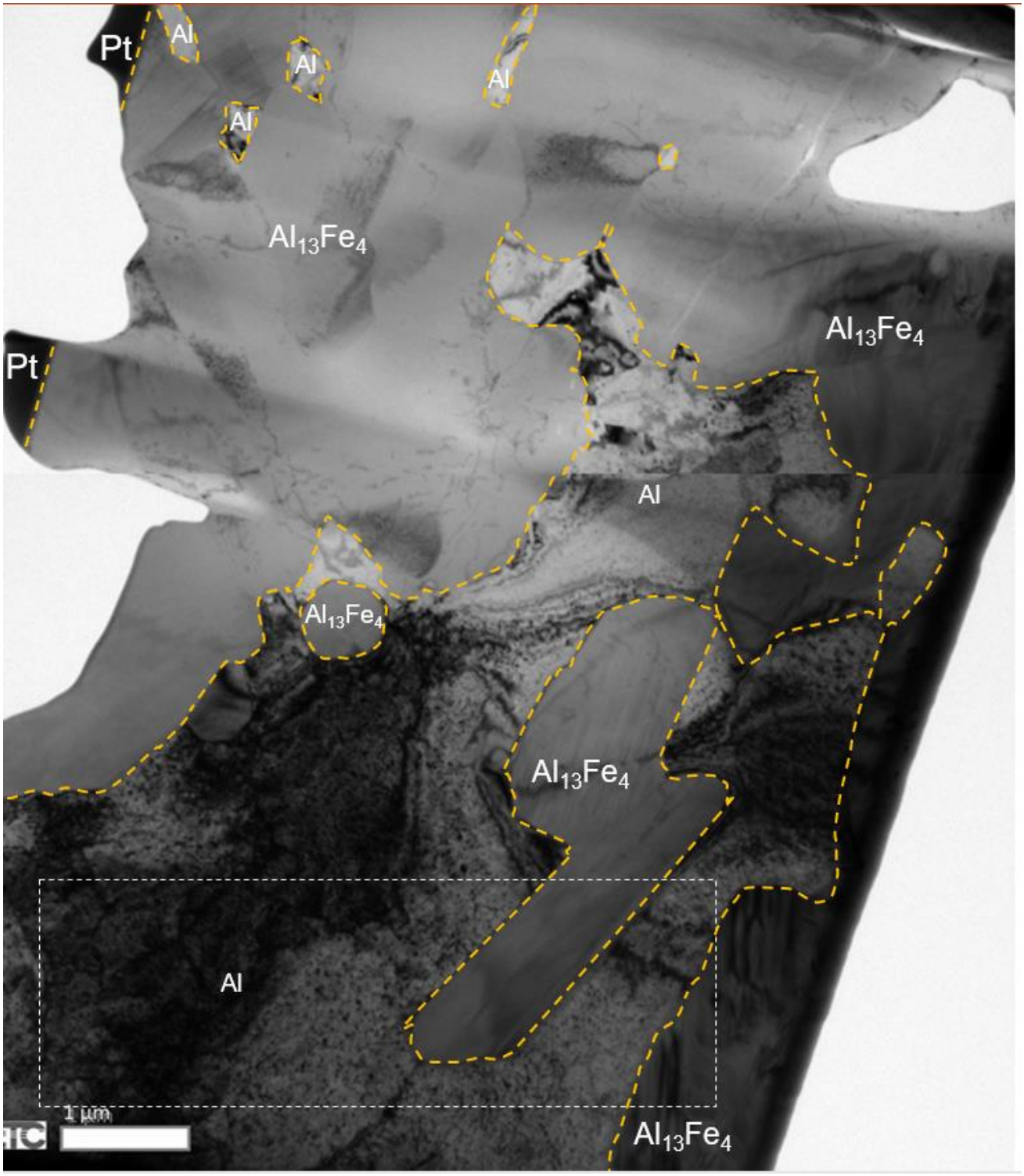

Figure 4-10 - TEM micrograph of the reaction layer between intermetallic compound layer and aluminium.

Figure 4-11 shows the TEM microstructure of the white dashed rectangle of Figure 4-10. The aluminium/IMC area shows long particles of IMC growth in the liquid aluminium. There seems to be some amount of coherency as observed by interface that are straight. Aluminium matrix seems to contain some contrast which is not visible

in the diffraction pattern and likely be due to defect structure or smaller gap zone. The diffraction pattern from the IMC was recorded in 3 different orientations [100], [110] and [101]. There is combination illustrates that the IMC are indeed $Al_{13}Fe_4$ phase. The microstructure as well as the diffraction patterns show the presence of nano scaled twins. The forbidden reflection observed in the diffraction pattern are due to the presence of twin, which has been reported in the literature [106].

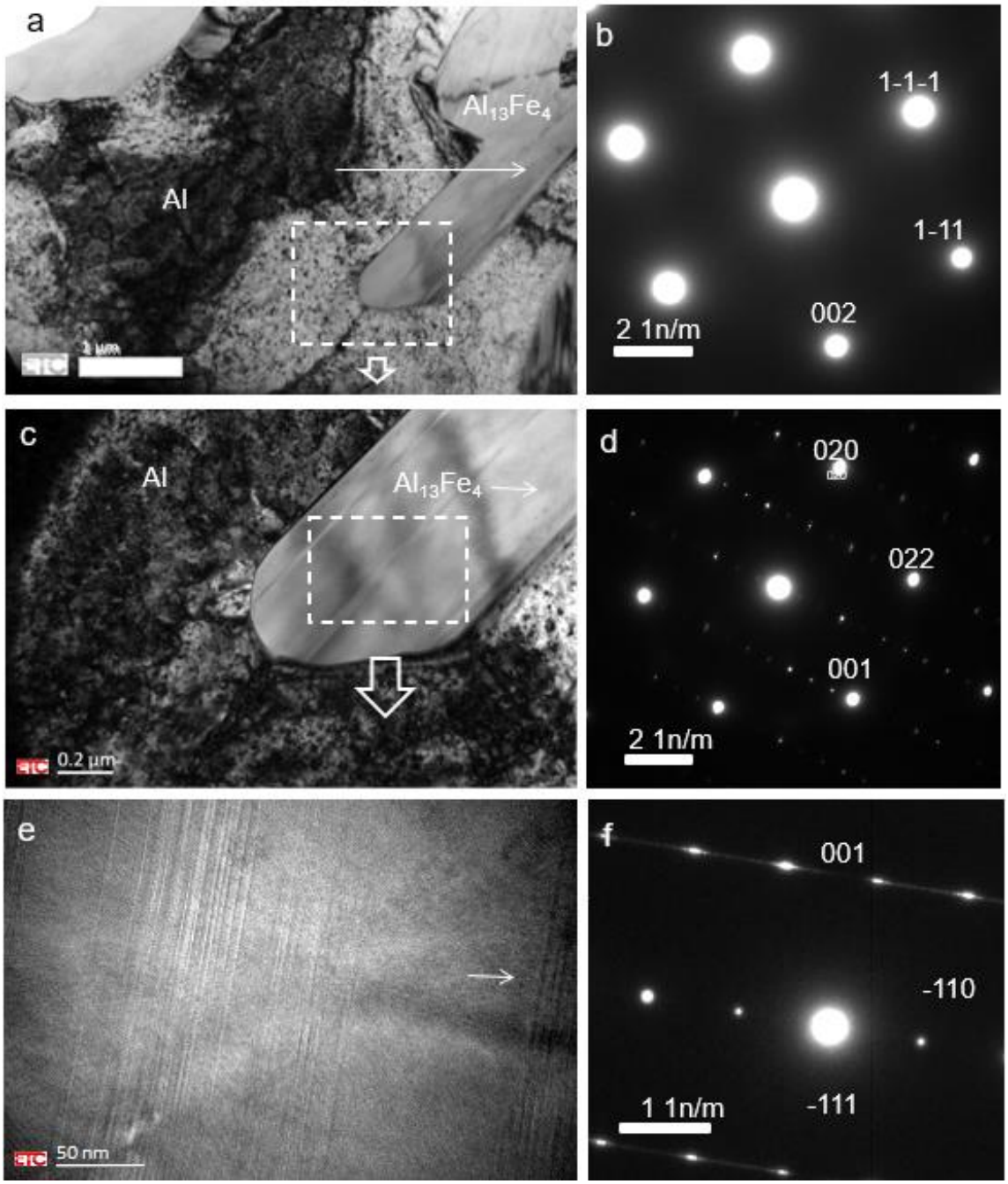

Figure 4-11- TEM microstructure of the white dashed rectangle of Figure 4-10. (b, d & e) show higher magnifications of each other correspondingly, (c) diffraction pattern of aluminium, produced from the aluminium part of figure a. (f) diffraction pattern of figure d demonstrates $Al_{13}Fe_4$.

4.3.6 Surface of the fracture

Figure 4-12 (a) shows the cross section of the surface between uncoated steel and overcast aluminium. No interaction detected on the surface while a lack of connection between two surfaces demonstrates a longitudinal crack all along the surface. Figure 4-12 (b) shows the cross section of the surface between overcast pure aluminium and zinc coated steel after holding in 750 °c for 10 minutes. Cracks initiated in the interaction layer and propagated alongside the bond. Figure 1-1

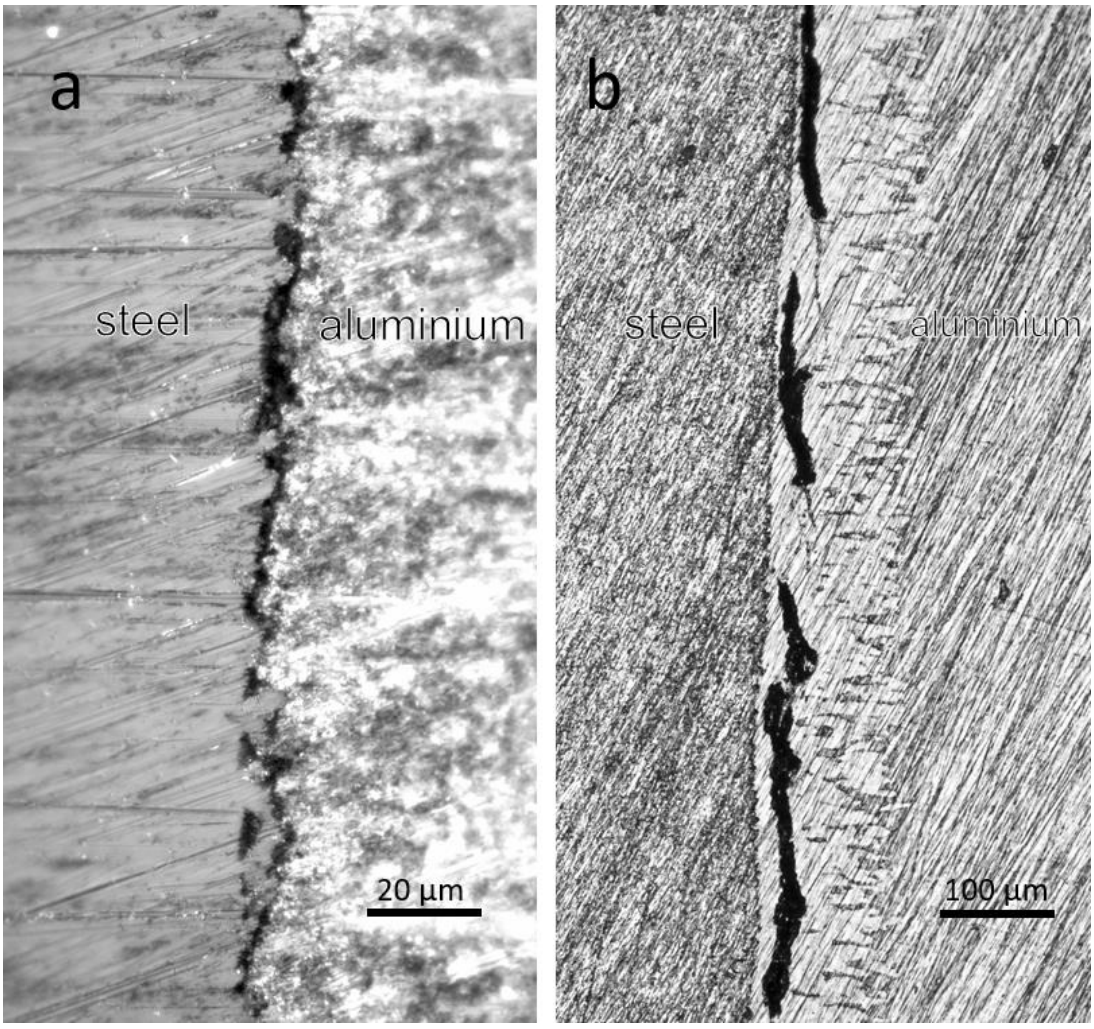

Figure 4-12- Cross section of the overcast surface of (a) aluminium/uncoated steel, (b) aluminium/zinc coated steel that held in 750 °c for 10 minutes.

The fracture surfaces and EDX map analysis of the tensile test sample of the zinc coated steel remained in pure aluminium at 750 ºC for 10 minutes for both of the steel and aluminium sides of the fracture surface is demonstrated in Figure 4-13 and Figure 4-14 correspondingly. The flat fracture surfaces demonstrate existence of a certain cleavage plane that facilitates the failure in a specific phase.

The tests revealed that overall composition of the fracture surfaces for both sides is Al 79%, Fe 20%, Si 1% at%, suggests fracture of the tensile test propagated in the $Al_{13}Fe_4$ phase. The impurity of silicon inside the aluminium measured 0.03 wt% and the impurity of silicon in the steel measured 0.05 wt% however 1 at% silicon in the fracture surface shows propagation of the crack in a high concentrated area. Also, no aluminium was found on the surface of the steel side of the fracture surface while the entire surface covered by $Al_{13}Fe_4$ intermetallic phase. This finding demonstrates that the bonding of aluminium to $Al_{13}Fe_4$ intermetallic compound has been the weakest bond.

Surprisingly, both of the EDX composition analysis and topography of the fracture surfaces of aluminium and steel sides were matched. However Springer [95] and Albridght [107] reported non-fully matched fracture surfaces. Springer reported that tensile strength of the pure aluminium and steel is mainly governed by the formation of Kirkendal porosities.

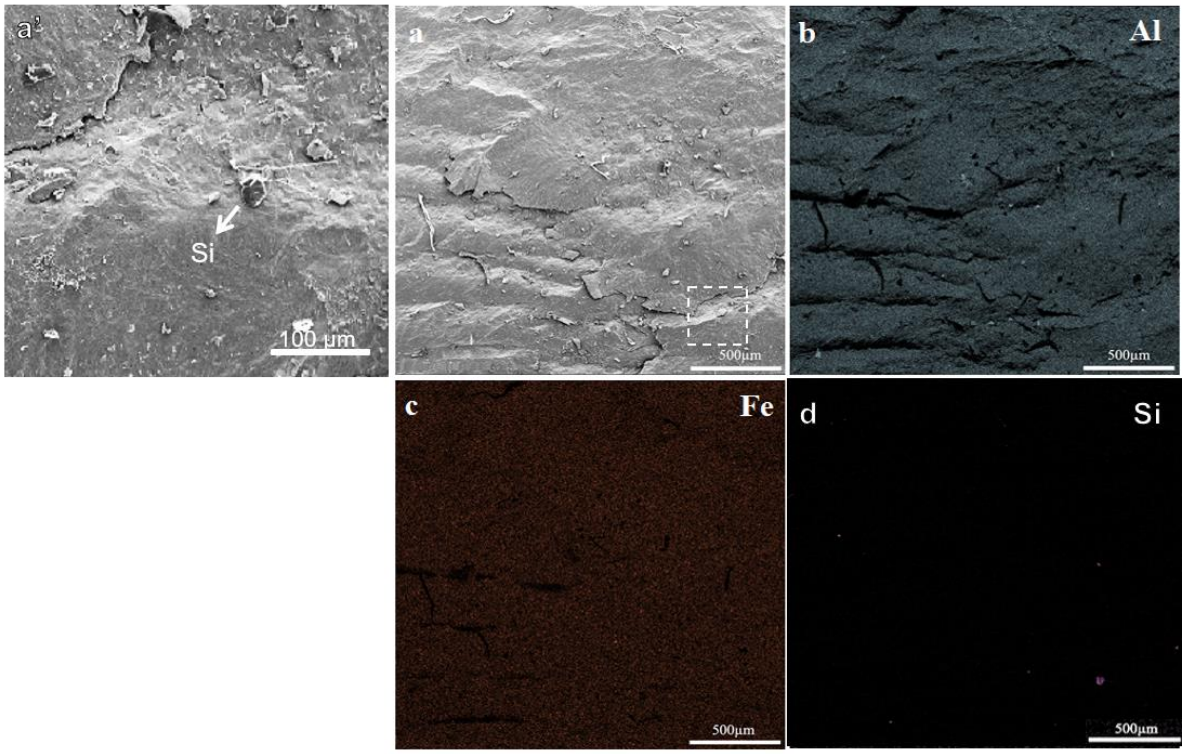

Figure 4-13 – (a)-The steel side of the SEM graph of the fracture surface of the zinc coated steel that was held at pure aluminium for 10 minutes at 750 ºC (a') higher magnification of the dashed rectangular of image a (b) Aluminium (c) Iron (d) Silicon. Overall composition measured Al 79%, Fe 20%, Si 1% at%.

Study of the aluminium side of the fracture surface reveals the aluminium in the back of $Al_{13}Fe_4$ phase of the surface. A lighter aluminium rich section is visible in Figure 4-14 (a') and EDX map of aluminium.

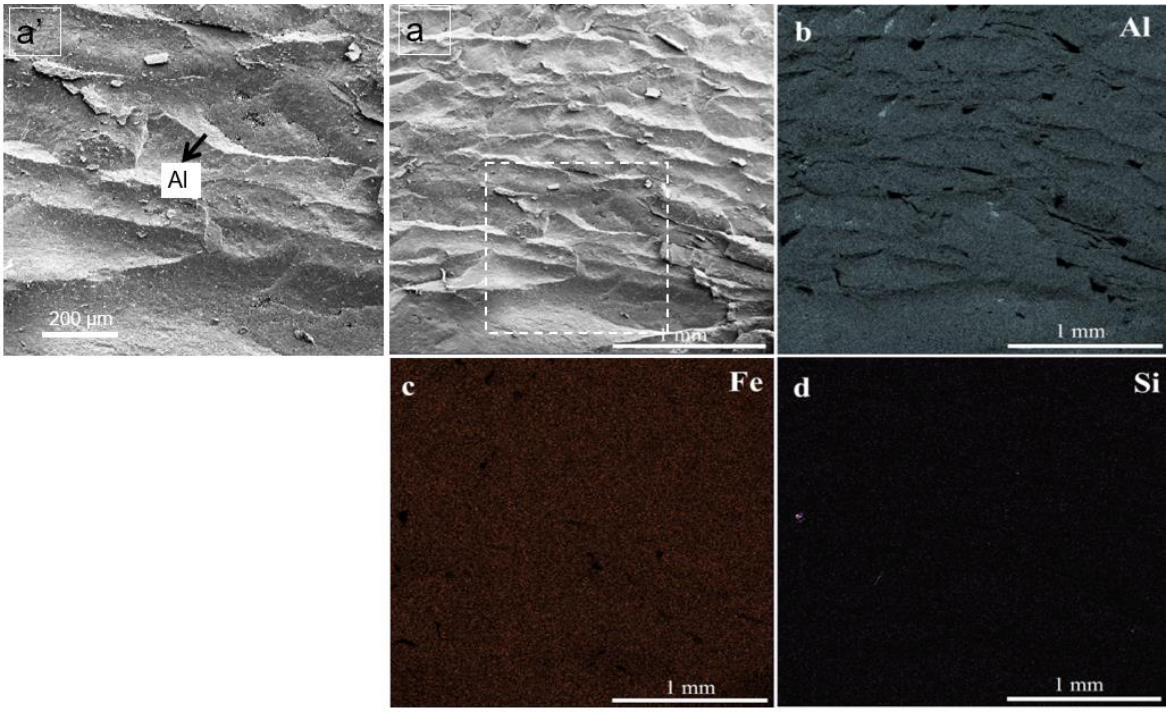

Figure 4-14-(a) The aluminium side of the SEM graph of the fracture surface of the sample that held for 10 minutes in 750 ºC (a') higher magnification of the dashed rectangular in figure a (b) EDX map of Aluminium (c) EDX map of Iron (d) EDX map of Silicon. Overall composition measured Al 79%, Fe 20%, Si 1% at%.

4.4 Pure aluminium / Gallium-zinc coated steel

Gallium used in a technique of aluminium soldering, called Galliuminium [108], also Shirzadi developed a flux free brazing method to bond aluminium alloys by implementation of a minimal thickness of liquid gallium [83]. Moreover, Shirzadi developed a method for diffusion bonding of aluminium to steel and other metallic alloys with stable surface oxide films. In this method the surface of the bond is polluted by gallium [109]. Considering application of gallium in bonding aluminium to aluminium or steel demonstrates possible application of gallium in bonding aluminium to steel in overcasting process.

To examine the effects of gallium on bond between aluminium and steel, zinc coated steel of 10×10×0.44 mm^3 that was polluted to gallium was used to bond to aluminium. The steel was washed by water and then cleaned by ultrasonic bath of ethanol and then dried out by drier. In order to pollute the surface of steel to gallium, a warmed (about 40 ºC) soft cloth containing pure gallium was smeared to the surface of the zinc

coated steel. The polluted zinc steel was fixed in sand mould and the pure aluminium of 750 ºC was cast over the gallium polluted zinc coated steel in atmosphere while the steel was at room temperature.

The microstructure of the samples were studied after mounting and polishing. The microstructure was similar to the typical aluminium overcast zinc coated steel with no significant change. More detail of the microstructure and mechanical properties of gallium-zinc coated steel that shared with zinc coated steel demonstrated in section 4.

4.5 Aluminium / Nickel coated steel

4.5.1 Nickel coated steel

Figure 4-15 shows the micrograph of the cross section of the nickel coated steel. The EDX map demonstrates the iron of the substrate and the nickel of the coat. The nickel coat uniformly distributed on the surface of the steel and the thickness of the nickel coat was measured about 3 µm. The EDX line scan shows gradual reduction of nickel from 90 at. % on surface of steel to 20 at. % in the depth of 8 µm of the steel. This gradual change of the composition can be resulted from the diffusion annealing in the production process of the nickel coated steel. The steel fixed in sand mould and pure aluminium of 750 ºC was cast over the nickel coated steel in atmosphere while the steel has been at room temperature.

Five samples were made by similar process and materials and different holding times. Development of the intermetallic compound layer of the nickel coated steel as a function of holding time was studied by scanning electron microscope and EDX.

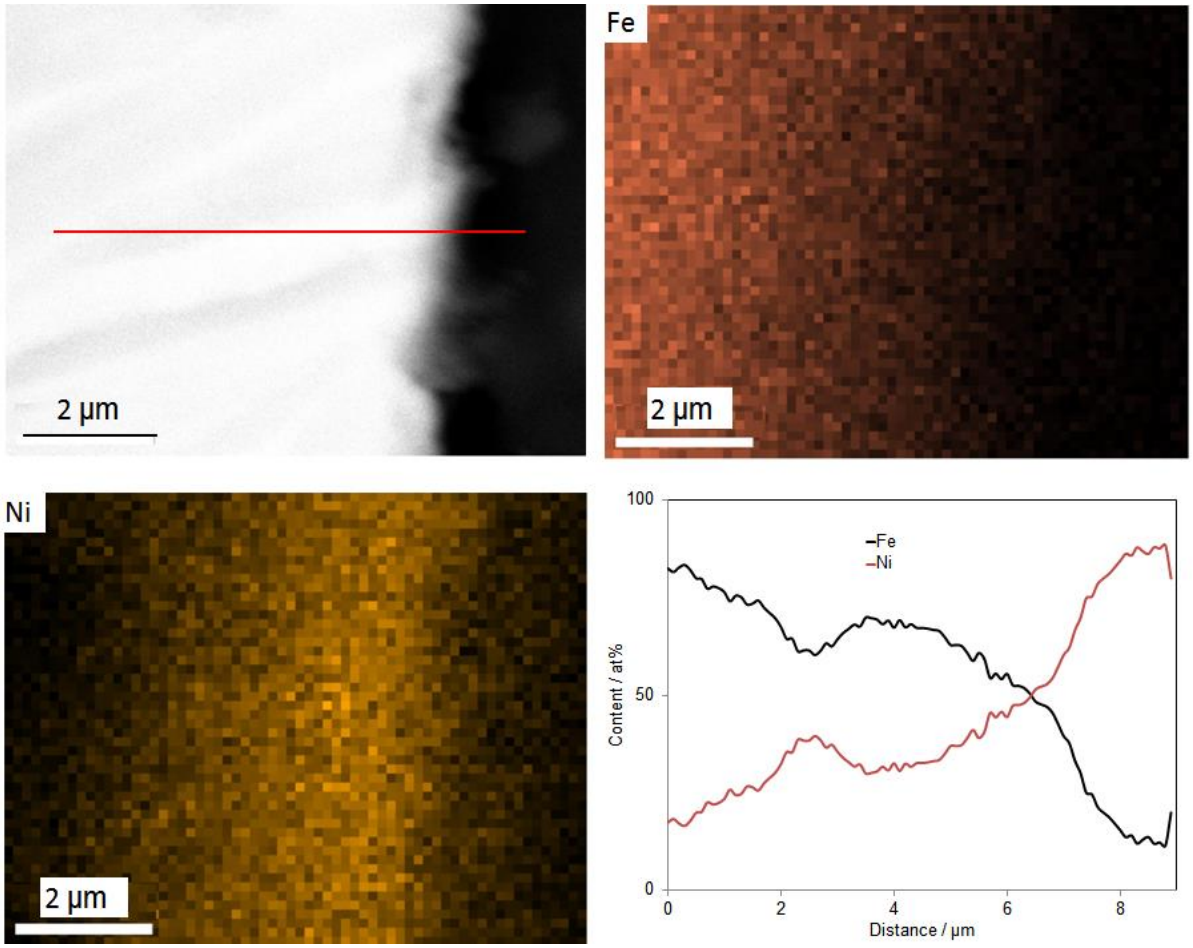

Figure 4-15- Micrograph and SEM map of the nickel coated steel.

Figure 4-16 shows the SEM microstructure of interaction layer of nickel coated steel and overcast aluminium held at 750 ºC for 1 minute. Non-uniform IMC was formed alongside the interface while some areas remained intact.

4.5.2 Holding in 750 °c for 1 minute

Holding overcast aluminium/nickel coated steel at 750 ºC for 1 minute had two main effects. Firstly, islands of intermetallic compound were formed at the joint that is presented at Figure 4-16. Secondly, the nickel coat was dissolved in the liquid aluminium and the dilution of nickel dropped in the surface of the joint. The EDX characterisation on the interaction zone shows less than 20% of nickel on the bond that is presented at Figure 4-18. This is a unique character of nickel coated steel that after one minute of holding at 750 ºC, still there is a 20% diluted nickel coat on the

surface of the interaction layer. Most of the formed intermetallic is Al_5Fe_2 while a small section of $Al_{13}Fe_4$ formed.

The nickel coat was survived on the steel coat in temperature of 750 ºC in touch with liquid aluminium for one minute and gradually dissolved in the liquid aluminium. At same time, the intermetallic islands start to initiate.

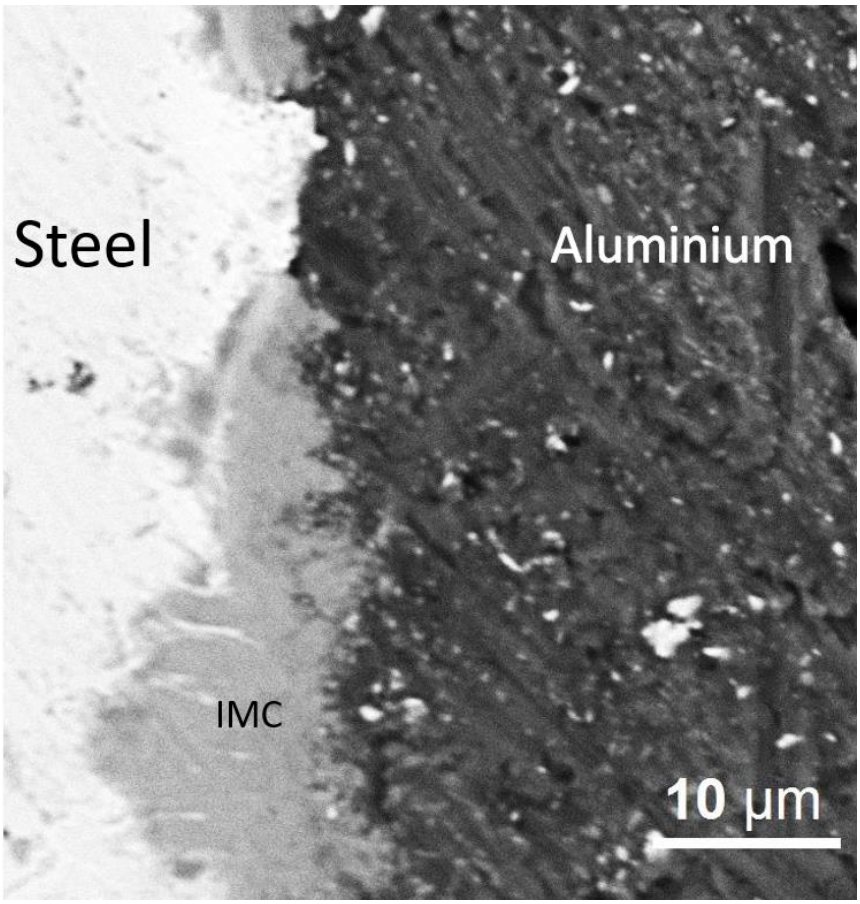

Figure 4-16- SEM microstructure of overcast pure aluminium on top of nickel coated steel after holding at 750 ºC for 1 minutes. Intermetallic compound formed on the interface however the IMC didn't cover all of the bond between the nickel coated steel and the overcast aluminium.

Microstructure of overcast aluminium on top of nickel coated steel that cooled to room temperature after overcasting shown at Figure 4-17a. Also Figure 4-17b to f demonstrate EDX map of cumulative and different elements. Figure 4-17 b and c show the aluminium solidified on the surface of the steel with no penetration. Figure 4-17 d demonstrates silicon that despite presence of less than 1 wt% in the liquid was one of the first elements solidified at the surface of the nickel coated steel. Figure 4-17e

shows the iron of the microstructure. There are some parts of iron visible in the nickel dominated are and aluminium side however no IMC formed. So even if iron diffused to the aluminium, no IMC formed. Figure 4-17f shows the nickel of the interface. Similar to Figure 4-15, the nickel coat is intact. So, it can be concluded that no interaction between nickel coated steel and liquid aluminium formed.

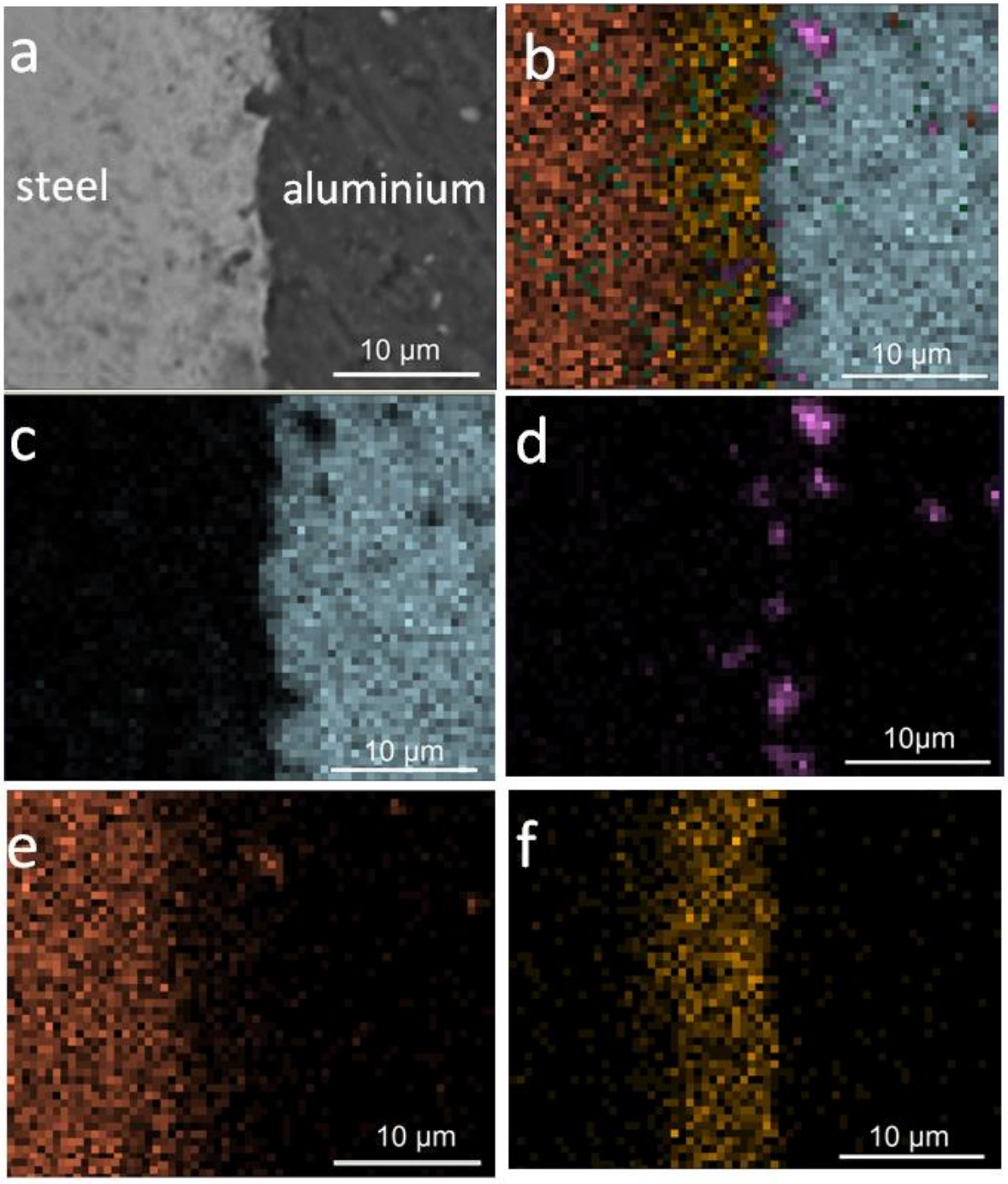

Figure 4-17- (a) SEM Microstructure of the interaction layer, overcast pure aluminium over nickel coated steel, cooled at room atmosphere (b) cumulative EDX map of the corresponding micrograph (c) aluminium EDX map (d) silicone EDX map (e) iron EDX map (f) nickel EDX map.

4.5.3 Holding in 750 °c for 10 and 30 minutes

Figure 4-18 shows the microstructures of the cross sections of the nickel coated steel and overcast aluminium after holding for 1 minute, 10 minutes and 60 minutes at 750 ºC. The morphologies of the intermetallic layer after 1 minute and 10 minutes are different with the morphology of the zinc coated steel that will discuss later at this chapter. Figure 4-18d shows the microstructure of the cross section of the pure aluminium overcast on top nickel coated steel after holding at 750 ºC for 60 minutes. Despite the microstructures of the samples held for 1 and 10 minutes, microstructure of the sample that held for 10 minutes at 750 ºC has slim and longer morphology of the morphology of intermetallic layer. This is similar to the microstructure of the zinc coated sample that will show later in this chapter.

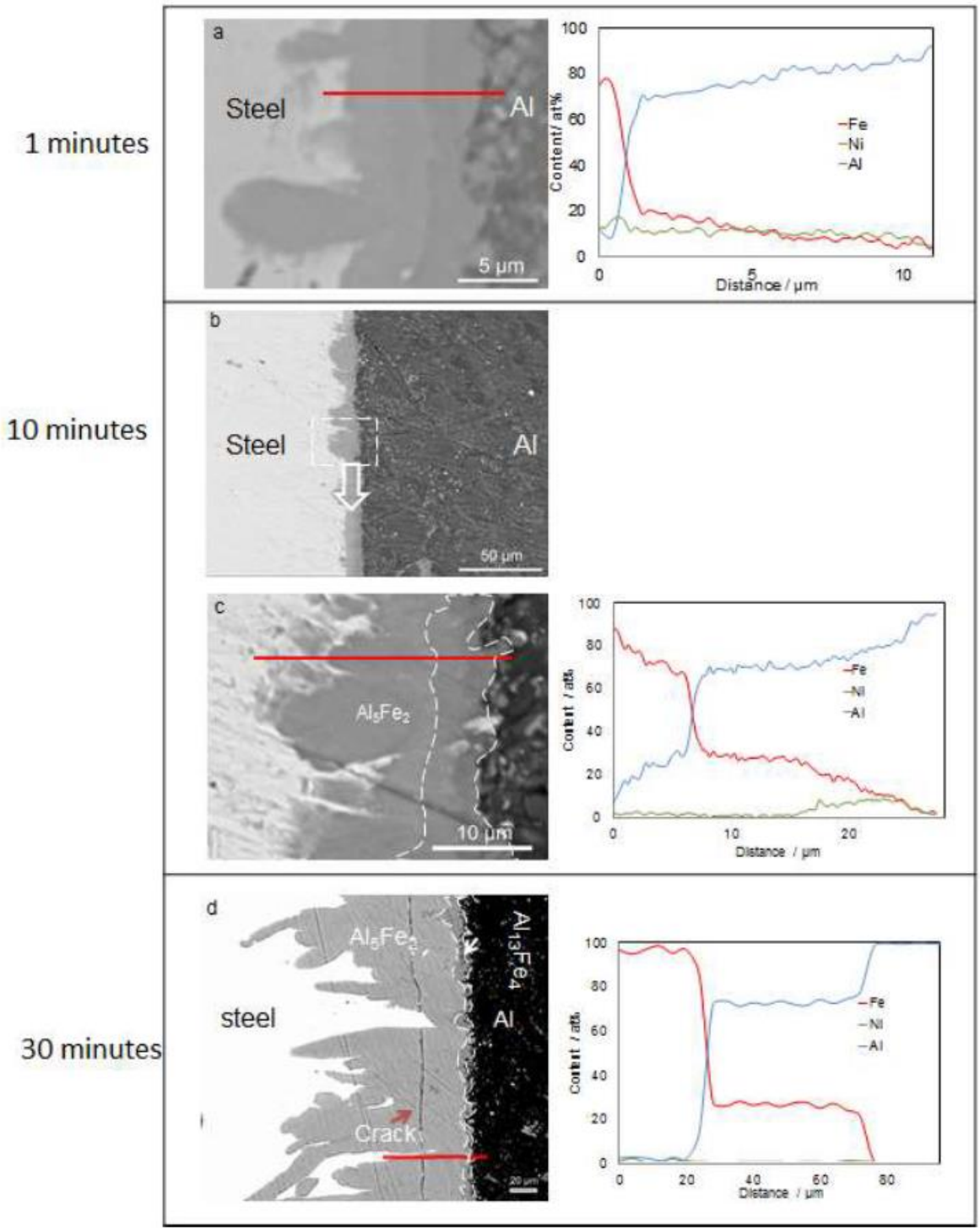

Figure 4-18- SEM micrograph o of overcast pure aluminium on top of nickel coated steel (a) held at 750 ºC for 1 minute and the EDX line scan of the corresponding red line (b) held at 750 ºC for 10 minutes (c) high magnification of rectangular of image b and EDX line scan of the corresponding red line (d) SEM micrograph of overcast pure aluminium on top of nickel coated steel that held at 750 ºC for 30 minutes and EDX line scan of the corresponding red line. Longitudinal crack formed at the sample after 30 minutes of holding.

Microstructure of the nickel coated steel in high magnifications that was in touch with liquid aluminium at 750 ºC for 1 minute and the corresponding EDX map analysis of the micrograph presented at Figure 4-19. The samples cleaned at ultrasonic vibrator for 10 minutes before any characterisation, so there is no artificial dirt at the surface of the samples. Figure 4-19 shows steel in left and aluminium on right side of the micrograph. Also, there are some particles of aluminium/iron phases in different sizes in aluminium. The iron/aluminium phases were visible on the aluminium side of uncoated steel. However, in nickel coated steel, the aluminium/iron intermetallic phases are visible in aluminium while the nickel coat is still on top of steel. On the surface of steel, a mix of nickel and iron characterised while aluminium diffused to some extend to the surface of steel.

The most prominent feature of Figure 4-19 is that after 1 minute of holding in 750 ºC, iron characterised in aluminium while the nickel coat is still between aluminium and steel and did not dissolved in aluminium. There are two possible scenarios for the presence of steel in aluminium despite presence of nickel between aluminium and steel. First scenario is that characterised iron could diffuse in aluminium from an area that entire of nickel dissolved in aluminium. It means the iron visible in this EDX map came from a section that entire of the nickel coat removed. So, after removing entire of the nickel coat, iron could diffuse to the liquid aluminium and aluminium/iron intermetallics formed. The second scenario is the possibility of diffusion of iron/nickel of the steel surface into the aluminium. Figure 4-15 shows the EDX land scan of the nickel coat and demonstrates presence of 90 at% nickel on the surface of the steel while the amount of nickel is reducing to 50 at% at 2 micron and reaches to 10 at% at 8 micron far from the surface. Figure 4-15 proves there have been always some amounts of iron on the surface of steel, so it could diffuse to the liquid aluminium. Considering the fact that diffusion of nickel to aluminium needs higher temperature and time, iron may diffuse into aluminium and interacted with aluminium to form iron/aluminium IMC while nickel did not diffused at a same rate.

Moreover comparison of Figure 4-15 and Figure 4-18c shows that in the interaction layer of nickel coated steel/pure aluminium, maximum 90 at.% of nickel reduced to 10 at.% and maximum 70 at.% of iron reduced to 30 at.% after holding the joint at 750 ºC for 10 minutes, instead aluminium diffused to the interaction layer.

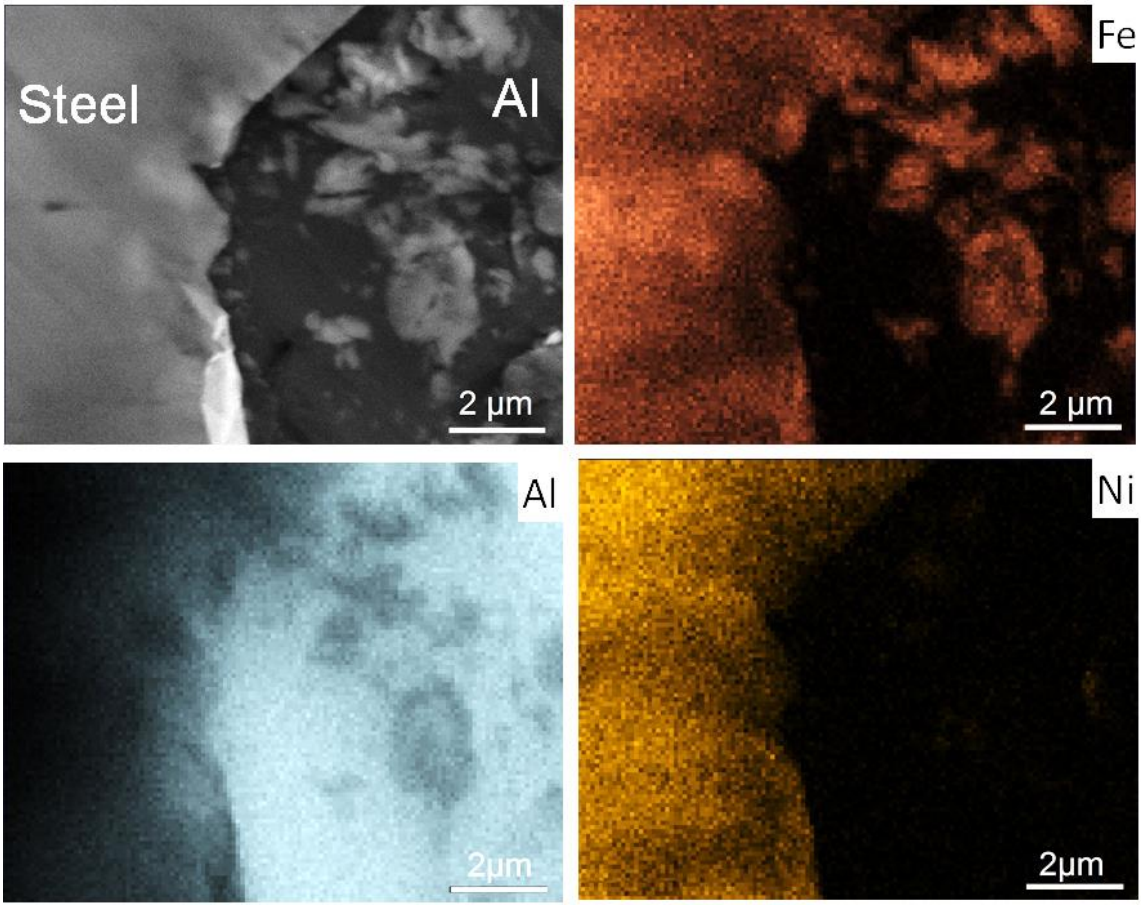

Figure 4-19- Microstructure of the joint between aluminium and nickel coated steel after holding at 750 °c for 1 minute. EDX map scan of iron, aluminium and nickel.

The fracture surface of pure aluminium/nickel coated steel joining that held at 750 °C for 10 minutes characterised by using XRD. Analysis of two sides of the fracture shows presence of Al_5Fe_2 and $Al_{13}Fe_4$ IMCs on the surfaces. Figure 4-20 shows the XRD spectra of the fracture surfaces.

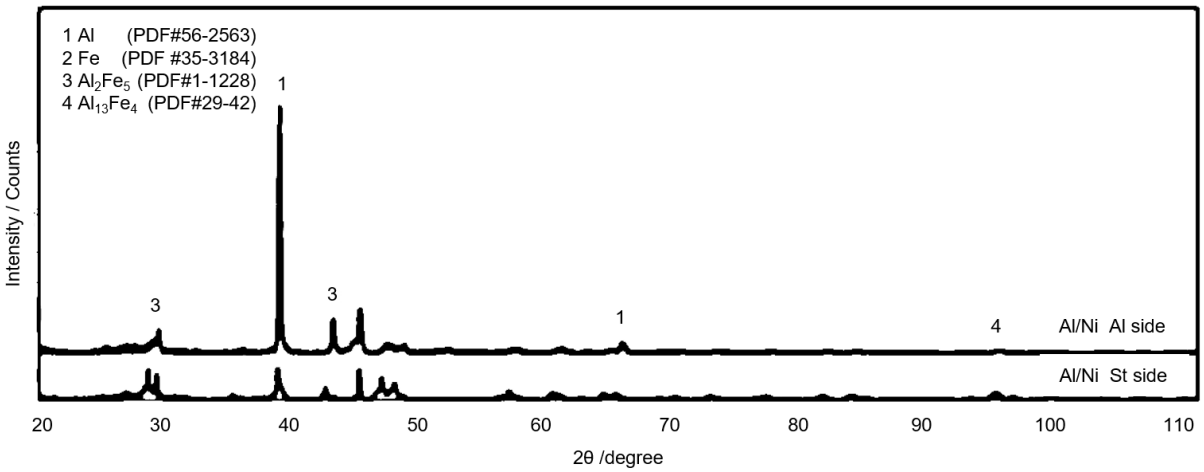

Figure 4-20 - XRD spectra of fracture surface of the joints after tensile test. Two sides of aluminium side and steel side of fracture surface. Pure aluminium/nickel coated steel bimetallic joint that held at 750 °C for 10 minutes.

4.6 Pure aluminium / NiZn coated steel

High speed of formation of intermetallic layer in the joint of zinc coated steel and aluminium is leading to a low strength bond. However, low speed of formation of intermetallic layer of nickel coated steel and aluminium in the beginning is leading to formation of no bond and then formation of intermetallic layer in a very low speed. So, a coat made of mix of zinc and nickel was used to control the speed of formation of the intermetallic layer in the joint.

Nickel-zinc coated steel of 10×10×1.2 mm^3 cut from a sheet of steel. Figure 4-21 presents the cross section of the surface of nickel-zinc coated steel and the corresponding EDX map. The yellow demonstrates nickel, the green demonstrates zinc and they both show the thickness of the coat is about 2-3 µm.

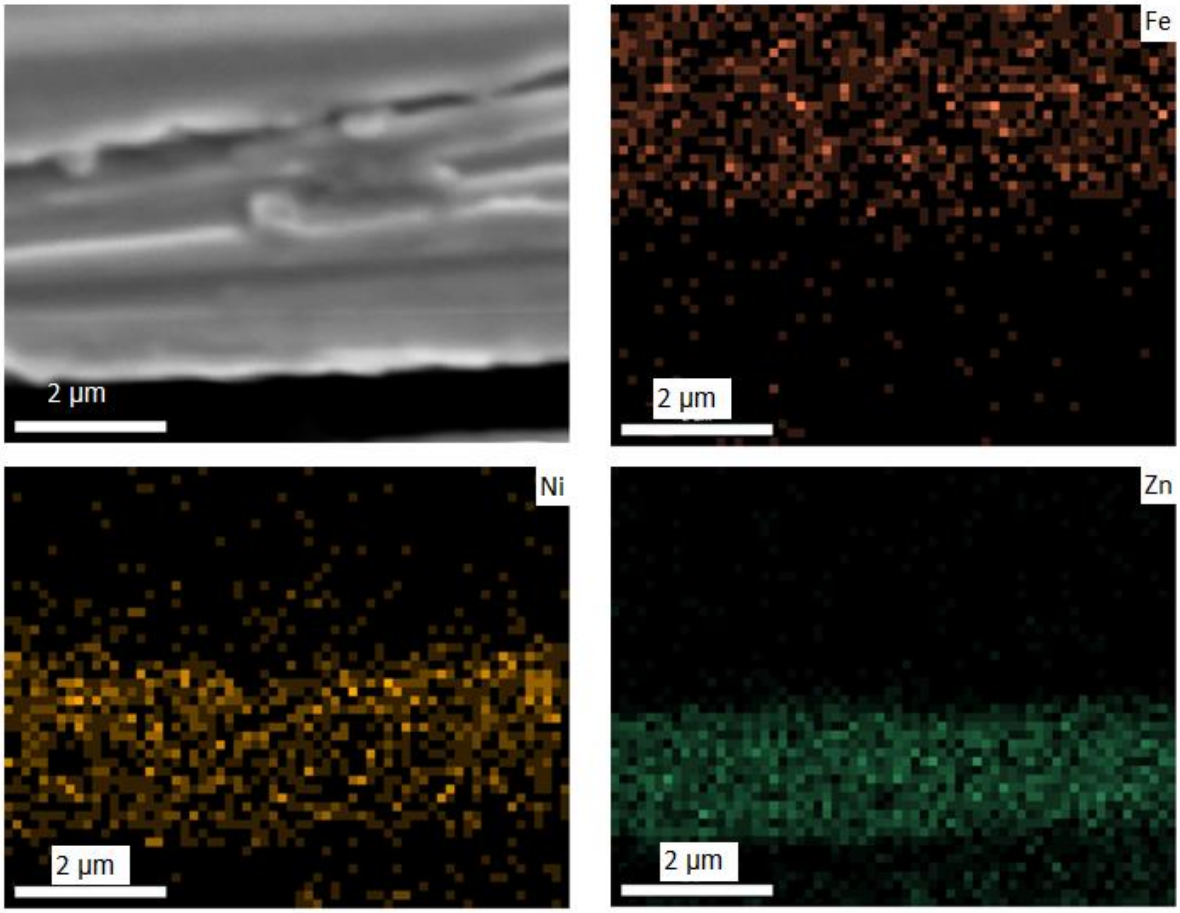

Figure 4-21-Microstructure and EDX map of the nickel-zinc coat of the steel. EDX analysis shows 25wt% nickel vs 75 wt. % zinc at the coat.

The steel was washed by water and then cleaned by ultrasonic bath of ethanol and then dried out by drier. The nickel zinc coated steel fixed at sand mould and the pure aluminium of 750 ºC cast over the uncoated steel in atmosphere while the steel was at room temperature. Four samples made by similar process and materials: one sample cooled down in atmosphere and at room temperature right after overcasting, the second held in furnace at 750 ºC for 1 minute, the third held in furnace at 750 ºC for 5 minutes and the fourth held in furnace at 750 ºC for 10 minutes. The samples mounted, polished and characterised after cooling down at room atmosphere.

4.7 Imperfections

4.7.1 Cracks

Two types of crack detected on the bond. The first type of crack formed between the $Al_{13}Fe_4$ intermetallic phase and aluminium that is shown in Figure 4-22. Kajihara described the reason of formation of this crack by faster diffusion rate of aluminium into iron rather than the slow diffusion of iron atoms into aluminium [110]. Kajihara used diffusion bonding while both of the aluminium and steel have been at a same temperature (550-640 ºC). However, in overcasting, aluminium was at 750 ºC and steel was at room temperature. Finally, diffusion of aluminium in iron is even higher and it is expected to detect a bigger crack at the area.

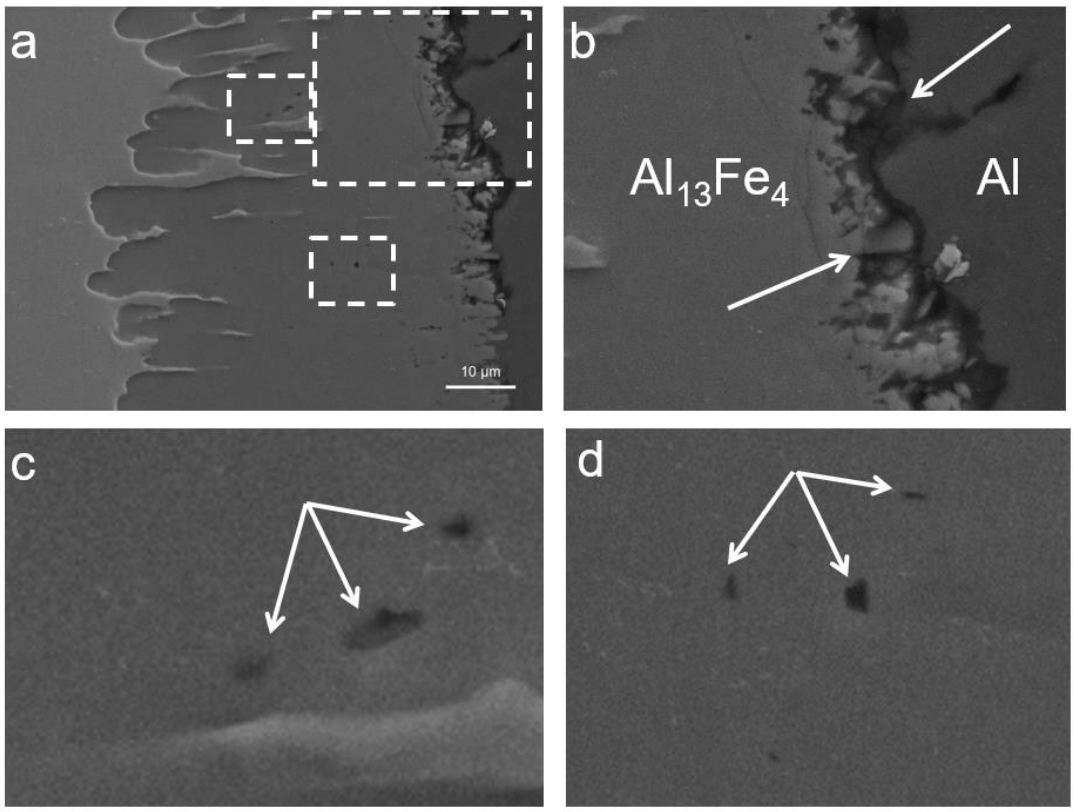

Figure 4-22-(a) SEM micrograph of the bond between zinc coated steel and aluminium that was held at 750 ºC for 1 minute. (b) High magnification of the big white rectangular. Arrows show the crack formed between $Al_{13}Fe_4$ intermetallic phase and aluminium. (c) and (d) high magnification of the smaller white dashed rectangles in a. White arrows show pores formed by Kirkendal effect.

The second type is longitudinal cracks detected alongside the bond at Al_5Fe_2 intermetallic phase and caused by the mismatch of thermal expansion coefficients of aluminium, steel, $Al_{13}Fe_4$ and Al_5Fe_2. The second type is shown in Figure 4-18. Table 4-1 indicates the thermal expansion coefficients of different phases. The parabolic growth of the intermetallic layer of the samples that cracks detected at Al_5Fe_2 were similar to the parabolic growth of the intermetallic layer of the samples without crack. So, it is possible to conclude that the cracks were produced during cooling process and there was no crack during formation of the intermetallic layer and finally the cracks had no effect on the growth of the intermetallic layer. Figure 4-18 shows a crack at Al_5Fe_2 intermetallic phase. These cracks were formed despite from the type of the coating however the chance of crack increases by increasing the thickness of the interaction layer. Longitudinal crack is visible at Figure 4-18 d for interaction of pure aluminium and nickel coated steel after holding at 750 ºC for 30 minutes. No longitudinal crack is visible at the interactions with less holding time. A longitudinal crack on aluminium/uncoated steel interaction layer shown at Figure 4-2a. Surface conditions had no visible effect on formation of longitudinal cracks.

Table 4-1- Thermal expansion coefficient of different phases [111, 112].

Phase	Thermal expansion coefficient/ $10^{-6}\,K^{-1}$
Aluminium	23.5
Iron	12.2
$Al_{13}Fe_4$	19.7
Al_5Fe_2	18.9

4.7.2 Kirkendal effect

Porosities in reaction layers and border of interfaces can be formed by Kirkendal effect [113]. Kirkendal effect can form small pores and develop them when the mutual diffusion rate of two components in a diffusion couple are very different with each other. By Kirkendal effect some pores form by interdiffusion on the side of the couple with higher diffusion rates. Such pores occur on the side of the element with faster diffusion rates and vacancies move to the opposite direction of the dominant diffusion flux. The pores detected at Al_5Fe_2 intermetallic phase. The pores formed by Kirkendal

effect are shown by white arrows at Figure 4-23c and d and Figure 4-23b at aluminium / zinc coated steel held at 750 ºC for 10 and 30 minutes. Pores formed by Kirkendal effect formed in thicker interaction layer despite the type of the coating.

4.8 Kinetics of interaction

The kinetics of reaction zone growth for every coating described earlier. In addition to the kinetics of formation of the IMC layer at the bond, there is another kinetic of separation of the IMC pieces, those separate from the steel plate and move towards the liquid aluminium. The IMC pieces distributed at aluminium after 10 and 30 minutes holding at 750 ºC are visible in Figure 4-23 (a) and (b) respectively.

Separation of the IMC pieces from the steel plate leaded to decreasing of the overall size of the steel plate. Thickness of the steel plate in Figure 4-23 b excluding the IMC between aluminium and steel is maximum 300 µm while the primary thickness was 440 µm. This phenomenon demonstrates some parts of the steel plate are separated from the main part and some parts of the steel plate were moved towards the liquid aluminium. The EDX line scan of Figure 4-23 d demonstrates presence of 20% (at%) iron and 80% (at%) aluminium suggests $Al_{13}Fe_4$.

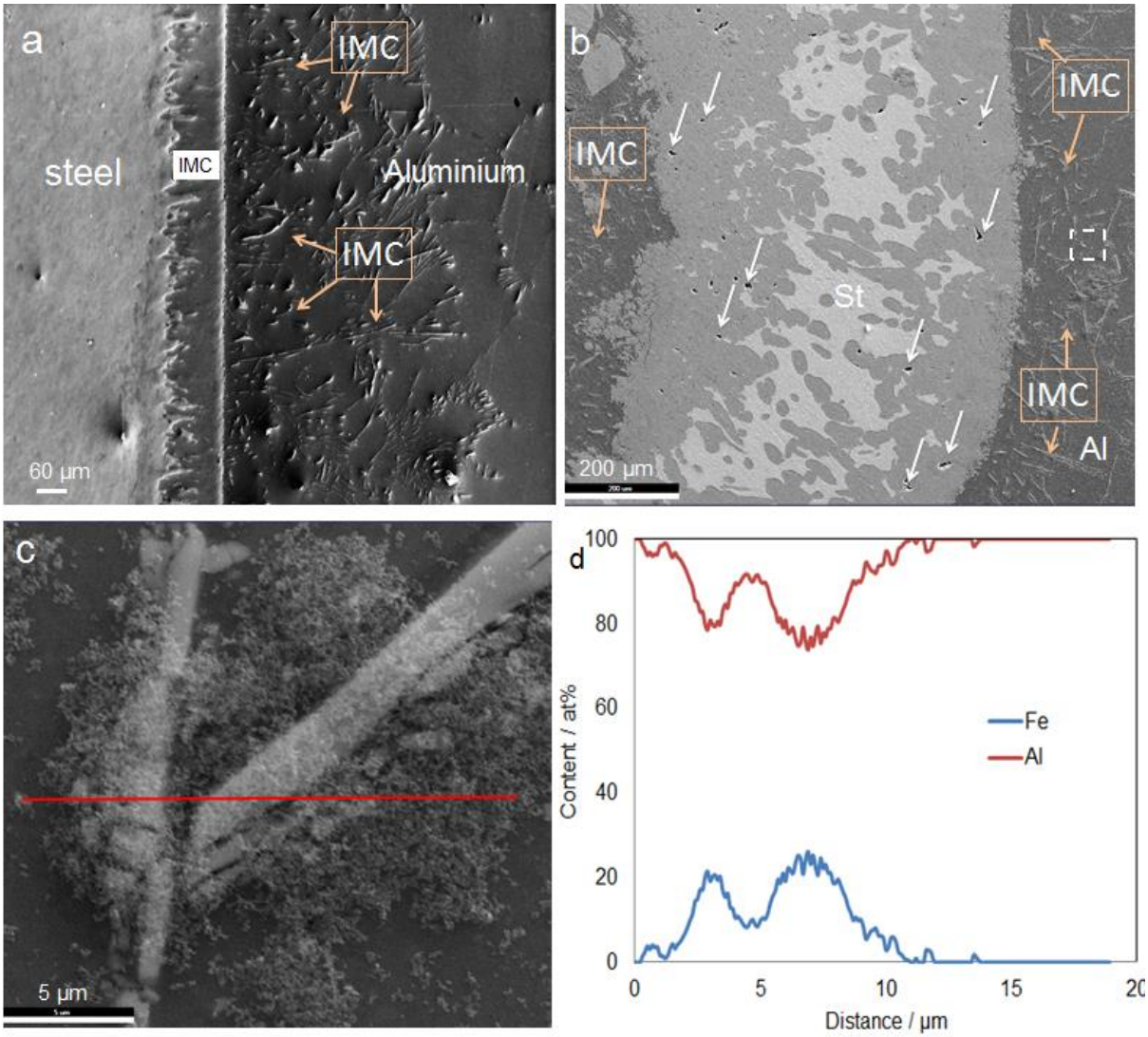

Figure 4-23- (a) SEM microstructure of pure aluminium overcast on top of the zinc coated steel and held at 750 ºC for 10 minutes. IMC pieces separated from the main steel are visible in the aluminium (b) SEM microstructure of pure aluminium overcast on top of the zinc coated steel and help at 750 ºC for 30 minutes. IMC pieces separated from the main steel are visible in the aluminium. Pores formed by Kirkendal effect shown by white arrows. (c) SEM microstructure of the dashed rectangle at b (d) EDX line scan analysis of the red line at c.

4.9 Bond strength

Tensile test performed in order to compare the bond strength in different surface conditions. To find the best geometry and design of sample, to compare the bond strengths, many size and geometries have examined and tested. The sketch and sizes of the tensile test sample and direction of tensile test demonstrated at chapter 3. Each fixed process condition tested at least 3 times and the bond strength demonstrated at

Figure 4-25 shows the average of the measurements. It worth to mention that the big error bars of the bond strength graph demonstrate the unsteady nature of the bond strength in bonding aluminium to steel by using overcasting process. After performance of tensile test, all of the samples visually tested and it revealed that all of the samples have broken in the interaction layer. This shows the weakest part of the bond has been the interaction layer. The measured bond strengths are very lower than both of the steel and aluminium. Tensile strength of pure aluminium is about 85 MPa and the tensile strength of mild steel about 400 MPa [116, 117]. Typical Load/Displacement graph of tensile test of a sample of nickel-zinc coated steel that held at 750 ºC for 1 minute presented at Figure 4-24.

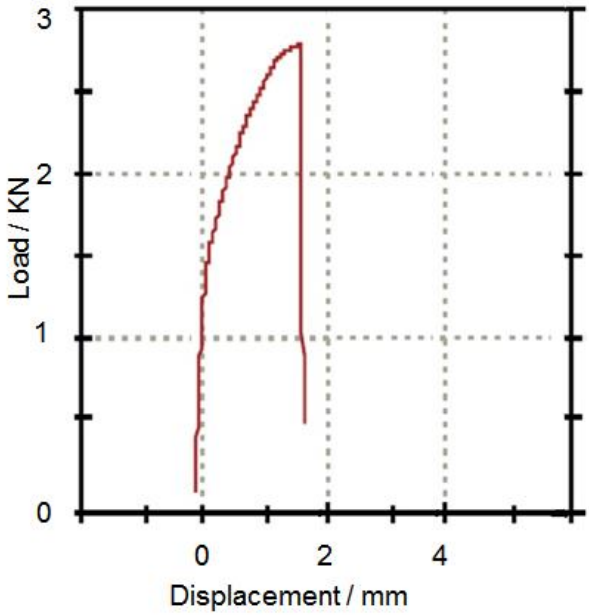

Figure 4-24- Load/Displacement graph of tensile test of the Ni-Zn coated steel held at pure aluminium at 750 ºC for 1 minute.

Yilmaz et al. bonded aluminium to steel by using friction welding process. Yilmaz et al. noticed maximum bond strength under optimised conditions when the size of interlayer is optimum. Yilmaz et al. found 2 µm is the optimum thickness of the interaction layer that can lead to the maximum bond strength of 63 MPa [116].

Uncoated steel has made no bond with pure aluminium after overcasting at 750 ºC. Even after holding at 750 ºC for 1 minute. In some samples that held for 1 minute at

750 ºC, a bond formed however they have been very fragile to measure by the tensile test machine and they were breaking before measurement of the bond strength. Actually, an oxide layer was formed on the surface of the mild steel and the oxide layer was stopping the aluminium to touch the surface of steel, diffuse and make a bond. The uncoated samples that held for 5 and 10 minutes at 750 ºC were diffusing into the surface of steel in some minor areas and were making bond, so the average bond strength measured less than 10 MPa.

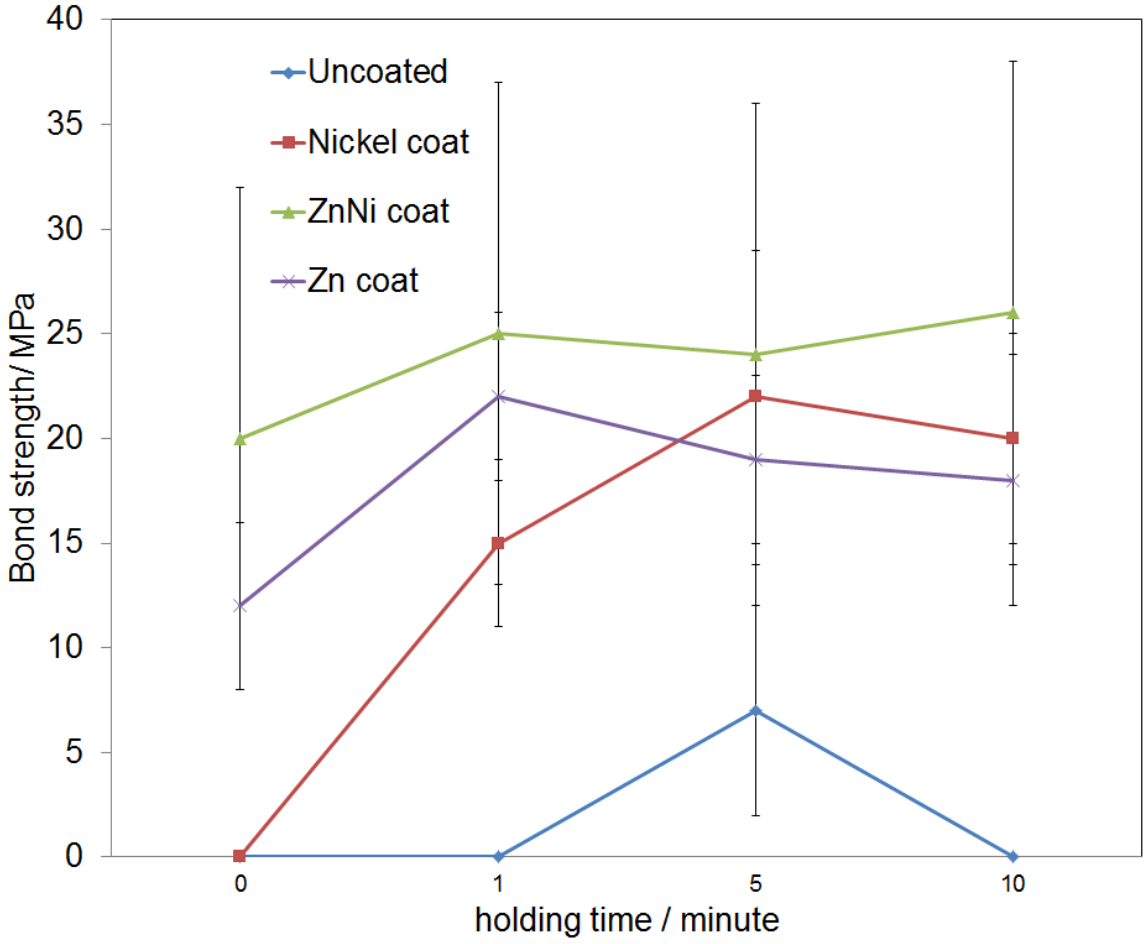

Figure 4-25- Average of bond strength of pure aluminium overcast around steel by different surface conditions of uncoated, nickel, zinc-nickel and zinc for different holding times.

Average bond strength of aluminium/nickel coated steel was measured zero while it was 15 MPa in the samples held for 1 minute at 750 ºC. Nickel coat on top of steel was not affected just after overcast of pure aluminium on top of the nickel coated steel, so no bond formed between aluminium and the nickel coated steel. When the nickel coated steel was in touch to aluminium, the nickel started to dissolve in aluminium

however the steel substrate did not touch the liquid aluminium, so there was no interaction between steel and aluminium. When the nickel coated steel remained in touch with liquid aluminium for 1 minute, more than 80% of the primary nickel coat dissolved in aluminium and aluminium interacts with the steel in substrate and a bond formed. The microstructure of the formed intermetallic layer and the remained of the nickel coat can be seen at Figure 4-18. Following the interaction of the steel and aluminium and formation of the IMC, average bond strength of 15 MPa was achieved. The formed IMCs was covered some parts of the bond and not the entire surface. Holding the sample at 750 ºC for 5 minutes helped the IMC to expand to the entire surface between aluminium and steel. The holding time helped the nickel coated steel held for 5 minutes at 750 ºC to achieve to the maximum strength of 22 MP. Holding the bond at 750 ºC for 10 minutes increased the IMC thickness to 30 µm and dropped the bond strength to 20 MPa.

Zinc coated steel has been wet by liquid aluminium and 18 µm IMC has formed after overcasting. Holding at 750 ºC for 1 minute increased the thickness of the interaction layer to 33 µm and the bond strength to 22 MPa. Keeping in high temperature for 5 and 10 minutes increased the thickness of IMC while the bond strength dropped.

Zinc/nickel coated steel wet by aluminium and a 15 µm thick IMC was formed that leaded to 20 MPa bond strength between aluminium and steel. While keeping at 750 ºC for 1, 5 and 10 minutes increased the IMC thickness from 30 µm to 75 µm, the average bond strength remained approximately fixed around 24 ±1 MPa.

Chapter 5 Effects of alloying elements on overcasting of different aluminium alloys on steel

5.1 Introduction

The objective of this chapter is to study the overcasting process of different aluminium alloys on coated steel substrates in order to understand the effects of alloy chemistry on the development of the interaction layer and imperfection at the aluminium/steel joint interface and the bond strength of the bimetallic couple. Two kinds of coated steel substrates are chosen for this study. They are zinc coated and nickel coated steel substrates similar to that used in the overcasting of commercially pure aluminium as reported in Chapter 4. The aluminium alloys include binary Al-Si alloys (eg. Al-1 wt.%Si, Al-7 wt.%Si and Al-12.2 wt.%Si) and two commercially available alloys of Al-20 wt.%Sn-7 wt.%Si and Al6060. The chemical composition of Al6060 presented at chapter 3.

5.2 Effect of silicon content on overcasting of Al-Si alloy on Ni coated steel

To study the effects of silicon content on the interphase interaction of aluminium and galvanized steel, aluminium alloy was melt with different percentages of silicon (Al-1Si, Al-7Si and Al-12.2Si) was overcast over zinc coated and nickel coated steels and held at 750 ºC for 0, 1, 5, and 10 minutes.

Figure 5-1(a-c) show SEM micrographs and composition profiles of cross sections of nickel coated steel overcast with binary Al-Si alloys with Si content ranging from 1 to12.2wt% were prepared from holding the melt at 750°C for 10 minutes around the steel substrate prior to solidification.

For Al-1wt%Si /nickel coated steel sample, an interaction (IMC) layer of 25 μm was found between steel and aluminium alloy, as shown in Figure 5-1. The interface between interaction layer and aluminium alloy was found to be rather flat with maximum perturbation of 5μm. However, the thickness of the interaction layer appeared to be 21 μm with a maximum perturbation of 7 μm.

The composition profile across the interaction layer revealed, there were Al_5Fe_2 phase near the steel substrate and Al_8Fe_2Si phase near the aluminium alloy.

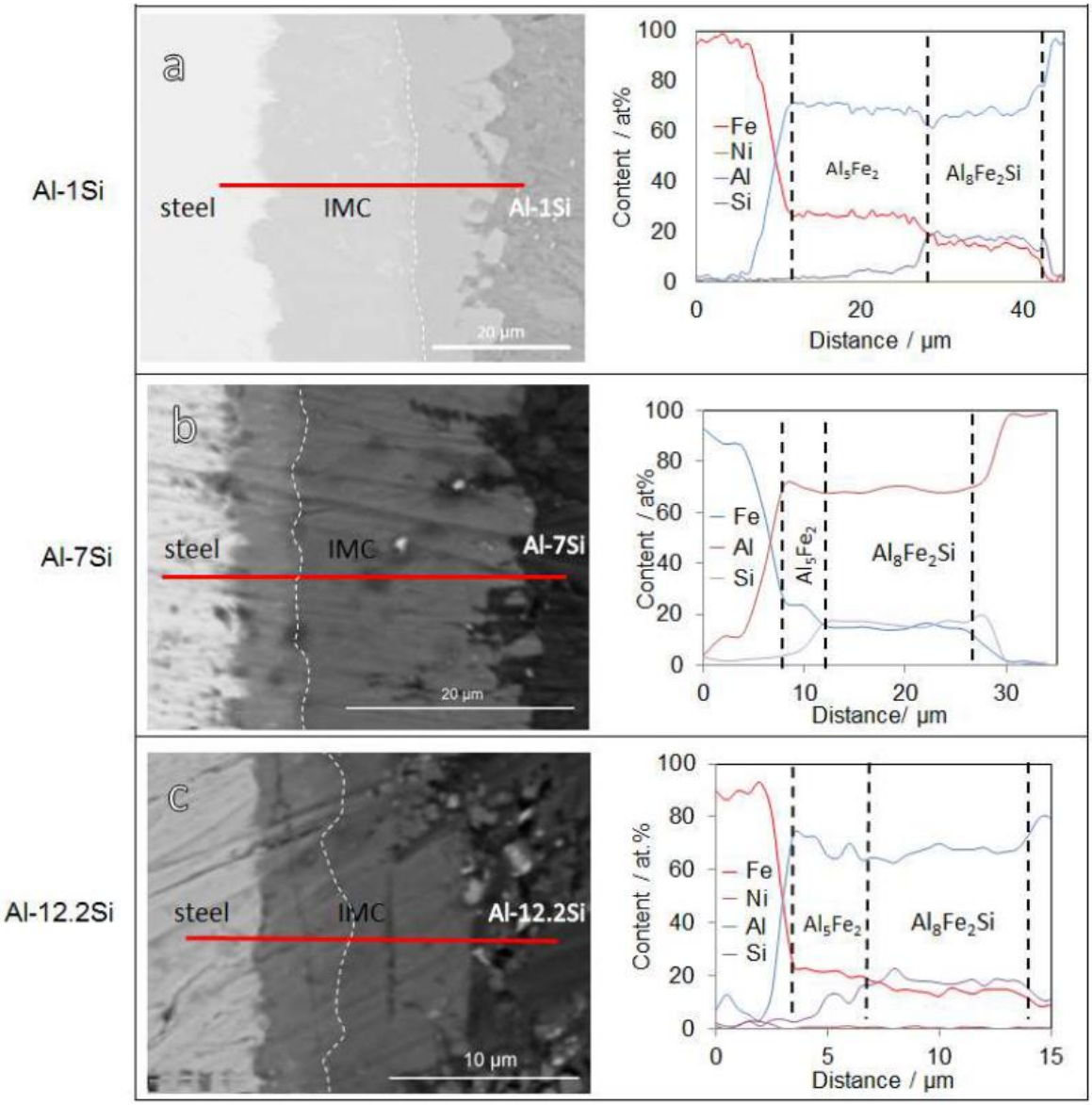

Figure 5-1- Micrographs of the interaction layer between nickel coated steel and different aluminium alloys: (b) Al-1Si, (c) Al-7Si, (d) Al-12.2Si (wt.%).

Figure 5-1 demonstrates the cross-section micrographs of the interaction layers of nickel coated steel and aluminium alloys after holding for 10 minutes. While, the interaction layer of pure aluminium and nickel coated steel is shown in Figure 5-1 (a), the micrographs of Al-1Si, Al-7Si, Al-12.2Si alloys/steel interaction layers are

presented in Figure 5-1 (b-d), respectively. It is worth to mention that due to finger-like feature shape of pure aluminium/steel joints, which discussed earlier at chapter 4, only a small portion of the interaction layer is shown in Figure 5-1 (a). The surface of the aluminium/IMC joints was approximately flat with perturbations of maximum 5 µm in all alloys. However, the surface of the IMC/steel joints were not similar in all alloys and the maximum perturbation was changed in maximum of 140 µm for pure aluminium to maximum 4 µm for Al-Si alloys. In all of the interaction layers, two distinctive layers of IMC can be observed, in which, the layer next to the aluminium alloy was darker than the IMC layer next to the steel.

In order to study the chemical composition changes across the IMC layers, EDX line scan analysis were performed on the interaction layer of all samples. The results are demonstrated in the right column of Figure 5-1. It can be seen in all samples that after holding the joint at 750 ºC for 10 minutes, very low amount of nickel (maximum 3 at.%) was detected in the interaction layer of steel/pure aluminium and steel/Al-7Si joints. As it was discussed earlier at chapter 4, the $Al_{13}Fe_4$ and Al_5Fe_2 intermetallic phases form in the interaction layer of steel/pure aluminium. This is in agreement with EDX line scan results of Figure 5-1 (a). Moreover, EDX line scans of the steel/Al-1Si, steel/Al-7Si and steel/Al-12.2Si joints, complemented with XRD analysis results, imply the formation of Al_5Fe_2 and Al_8Fe_2Si intermetallic phases next to the steel and aluminium alloys, respectively. Results of XRD analysis are presented and discussed later in section 5.3.

EDX line scan performed in all of the interaction layers of Figure 5-1 demonstrated at right side of every micrograph. After holding the joint at 750 ºC for 10 minutes, very low amount of nickel was detected in the interaction layer. Maximum 3 at.% of nickel was detected at the interaction layers of steel/pure aluminium and steel/Al-7Si joints. The detected nickel was near the steel side of the interaction layer in both of the cases.

EDX line scan of the interaction layer of the steel/pure aluminium shows formation of $Al_{13}Fe_4$ and Al_5Fe_2 intermetallic phases on the bond. That is discussed earlier in chapter 4. EDX line scans of the steel/Al-1Si, steel/Al-7Si and steel/Al-12.2Si show formation of Al_8Fe_2Si next to the aluminium alloy and formation of Al_5Fe_2 intermetallic phase next to the steel side of the interaction layer. Results of XRD analysis confirm

formation of the mentioned intermetallic phases and will be presented later in this chapter.

The XRD analysis shows presence of Al_5Fe_2, $Al_{13}Fe_4$ and Si in the fracture surfaces of the joints of Al-1Si, Al-7Si and Al-12.2Si. As all of the fractures were happened in the intermetallic layers of the bonds, IMCs were detected on the surfaces of samples with different processing conditions. The characterised phases of XRD are in line with the phases that characterised SEM and EDX analysis. Moreover, the Al_8Fe_2Si IMC that detected on the interaction layer and fracture surface, was reported before [90] and the micrograph of the fracture surface is presented at Figure 2-8.

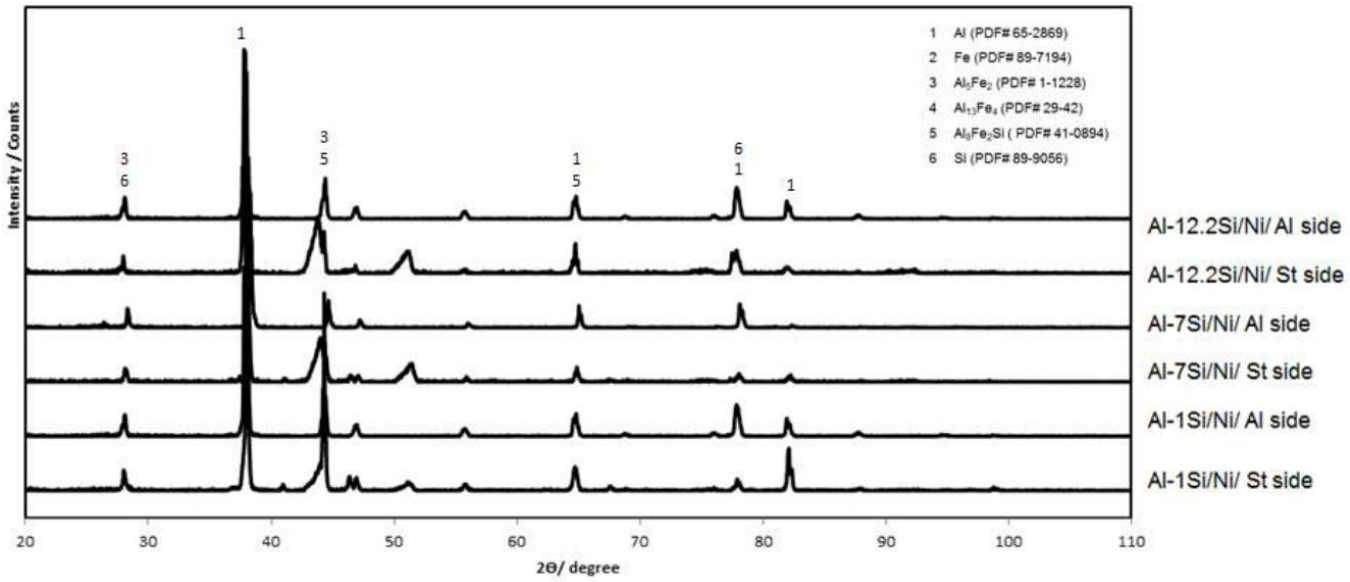

Figure 5-2- XRD spectra of fracture surface of the joints after tensile test. Two sides of every fracture surface characterised. One side is from the steel side of the fracture surface and the other side from the aluminium of the fracture surface.

Table 5-1 shows a plot of thickness of interaction (IMC) layer that was formed after overcasting of Al-Si alloy on Ni coated steel by holding the melt at 750°C for 10mins, as a function of Si content. The thicknesses of Al_5Fe_2 and Al_8SiFe layers clearly decreased with increasing Si content. However, the decrease in thickness of Al_5Fe_2 layer is more significant compared to that of Al_8Si_2Fe layer. The reduction in the thicknesses of intermetallic compound layers can be attributed to the lowering of atomic diffusion and reaction kinetics as a result of silicon addition in the melt. The

role of silicon on the kinetic of reaction between the aluminium alloy melt and the solid steel will be discussed later in chapter 6.

Table 5-1- Thickness of the Al_5Fe_2 and Al_8Si_2Fe intermetallic layers change in different alloy compositions. The interaction of nickel coated steel and different aluminium alloys that were held at 750 ºC for 10 minutes.

	Al_5Fe_2 / µm	Al_8Si_2Fe / µm
Al-1Si	19	13
Al-7Si	10	7
Al-12.2Si	9	7

5.3 Effects of steel substrate coating on the development of interaction layer during the overcasting

Figure 5-3(a-d) show SEM micrographs of cross sections of overcast Al-7wt%Si on steel substrates coated with either nickel or zinc layers after holding the melt at 750 °C for 0 and 10mins.

In 0min holding time, the zinc coated steel produced an uneven interaction (IMC) layer that is shown in Figure 5-3a. However, in 0min holding time, the nickel coated steel produ (Figure 5-3b) as compared to that found in zinc coated steel.

As the melt holding time increased to 10mins, the overall thickness of the interaction layer between the steel and the aluminium alloy increased in both coated steel substrate as shown in Figure 5-3(c-d). The interface between steel and interaction layer appeared to be flat for both coated steel substrates. However, the interface between the interaction layer and the aluminium alloy appeared rough for both coated steel substrates.

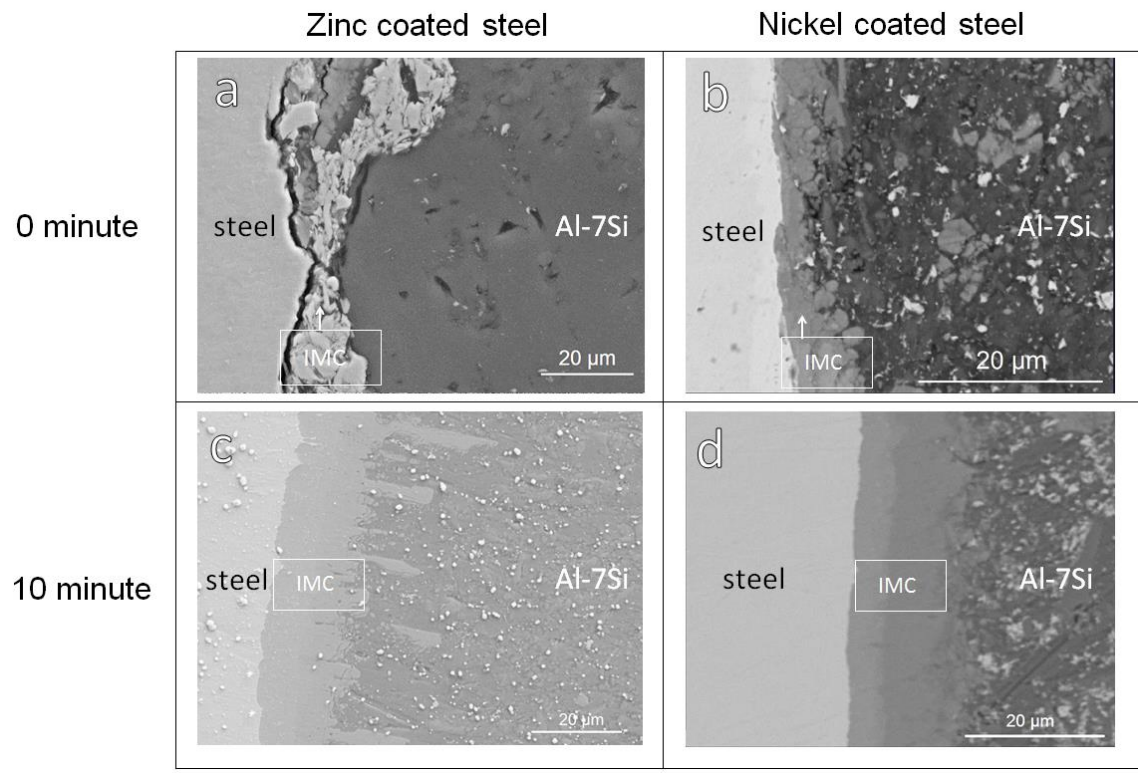

Figure 5-3- SEM micrographs of cross sections of overcast Al-7wt%Si onto various coated steel prepared by holding the melt at 750°C for various holding time: (a) zinc coated steel with 0 min holding time; (b) nickel steel with 0min holding time; (c) zinc coated steel with 10min holding time and (d) nickel coated steel with 10min holding time.

Table 5-2 give a list of measured thickness of the interaction layer and bond strength of overcast samples prepared using various alloy composition, coating of steel substrate and holding time. In a given alloy composition and coating of steel substrate, the thickness of interaction layers increased with increasing holding time Al-1Si composition had the highest rate of increasing in thickness of interaction layer of both zinc coated and nickel coated surface conditions. Al-7Si and Al-12.2Si alloys had approximately same increasing rate with nickel coated steel. Thickness of interaction layer of Al-1Si, Al-7Si and Al-12.2Si increased approximately in a similar low rate in compare with the thickness of interaction layer of same alloys with nickel coated steel.

Table 5-2- average thickness and bond strength of the interaction layer in different processing conditions

No.	Holding time/ minute	Alloy composition	Steel coating	Thickness of the interaction layer	Bond strength average /MPa
1	0	Al-1Si	Zn	10	0
2	1	Al-1Si	Zn	14	0
3	5	Al-1Si	Zn	19	6
4	10	Al-1Si	Zn	20	6.25
5	0	Al-1Si	Ni	0	16
6	1	Al-1Si	Ni	5	17
7	5	Al-1Si	Ni	15	13
8	10	Al-1Si	Ni	27	14
9	0	Al-7Si	Zn	20	0
10	1	Al-7Si	Zn	23	0
11	5	Al-7Si	Zn	25	8
12	10	Al-7Si	Zn	26	0
13	0	Al-7Si	Ni	0	0
14	1	Al-7Si	Ni	3	12
15	5	Al-7Si	Ni	10	20
16	10	Al-7Si	Ni	17	31
17	0	Al-12.2Si	Zn	18	0
18	1	Al-12.2Si	Zn	19	4.5
19	5	Al-12.2Si	Zn	20	4.5
20	10	Al-12.2Si	Zn	25	0
21	0	Al-12.2Si	Ni	0	0
22	1	Al-12.2Si	Ni	5	29
23	5	Al-12.2Si	Ni	10	15.9
24	10	Al-12.2Si	Ni	17	7.6

To identify the responsible phases for failure, the fractured surfaces of steel/aluminium alloys joints after bond strength test, were analysed using XRD. Figure 5-2 shows the XRD patterns of fractured surfaces of overcast Al-1wt%Si, Al-7wt%Si and Al-12.2wt%Si onto nickel coated steel samples. Whereas, aluminium and Al_5Fe_2 peaks are detected in all of the samples, $Al_{13}Fe_4$ peaks are detected only in both sides of surfaces of pure aluminium/nickel coated steel joint. Moreover, in all of the fracture surfaces of Al-Si alloys, Al, Al_5Fe_2, Al_8Fe_2Si and Si were detected. The phases detected at XRD are in line with the phases that EDX analysis suggested earlier at this chapter and chapter 4.

5.4 Overcasting of Al-20Sn-7Si alloy onto steel

Al-20wt%Sn-7wt%Si is a commercially available alloy that is normally used in bearing components. Figure 5-4 shows as cast microstructure of Al-20wt%Sn-7wt%Si, together with X-Ray maps of aluminium, silicon and tin elements. The microstructure

consisted of cellular α-Al matrix (dark) with Si (grey) and Sn (white) phases on the cell boundaries.

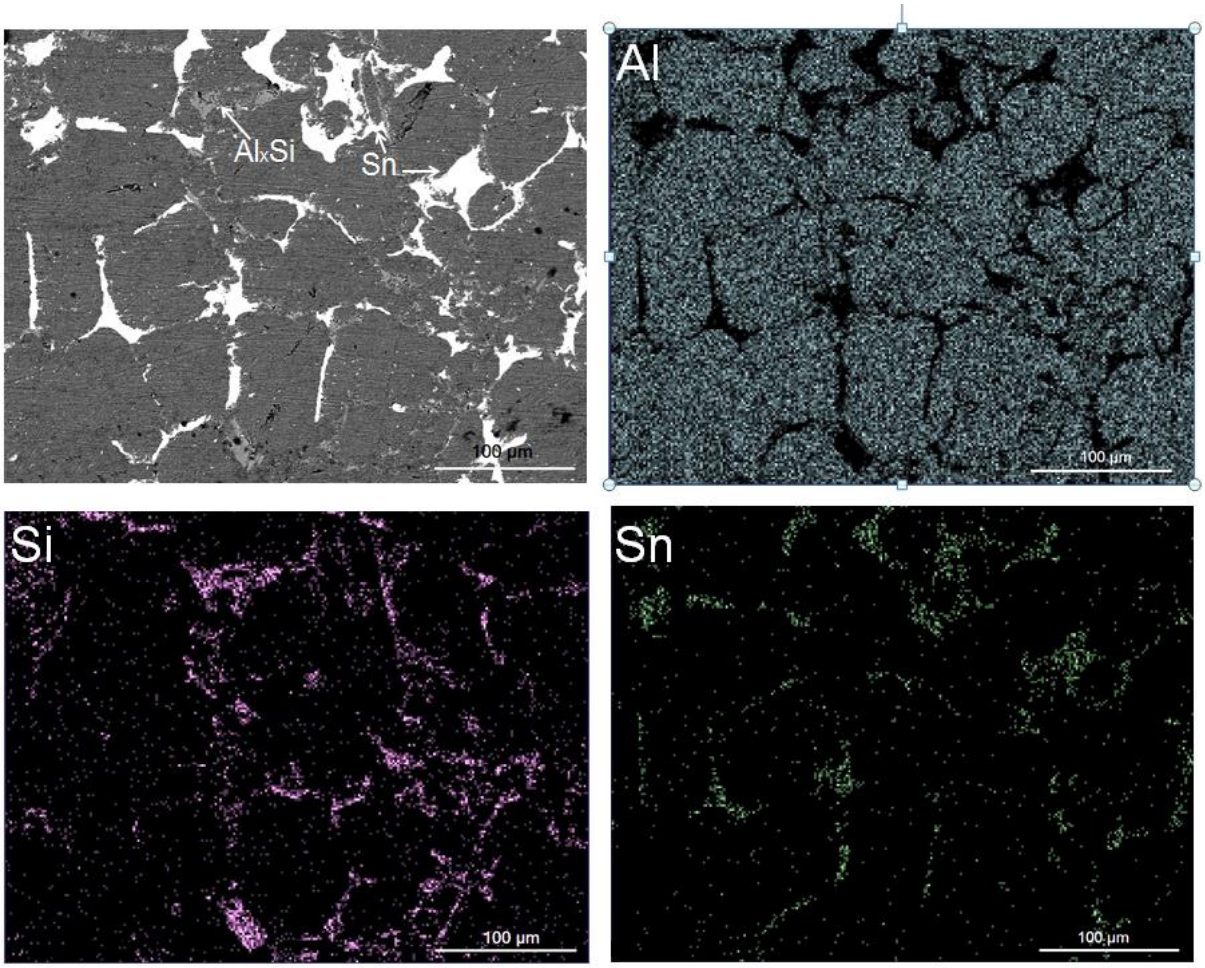

Figure 5-4- SEM micrograph of as cast Al-20wt%Sn-7wt%Si alloy. X-Ray Map using Al, Si and Sn elements to illustrate chemical distribution within the microstructure.

Figure 5-5(a) shows SEM micrograph of cross section of overcast Al-20wt%Sn-7wt%Si onto nickel coated steel prepared after holding the melt at 750 ºC for 1 minute The Al-20wt%Sn-7wt%%Si melt interacted with the nickel coated steel to form an interaction layer. Figure 5-5 (b) shows a region in Figure 5-5 (a) marked by white dashed rectangle in high magnification. It revealed finger-like features of intermetallic compound (IMC) developed from the interface towards the steel.

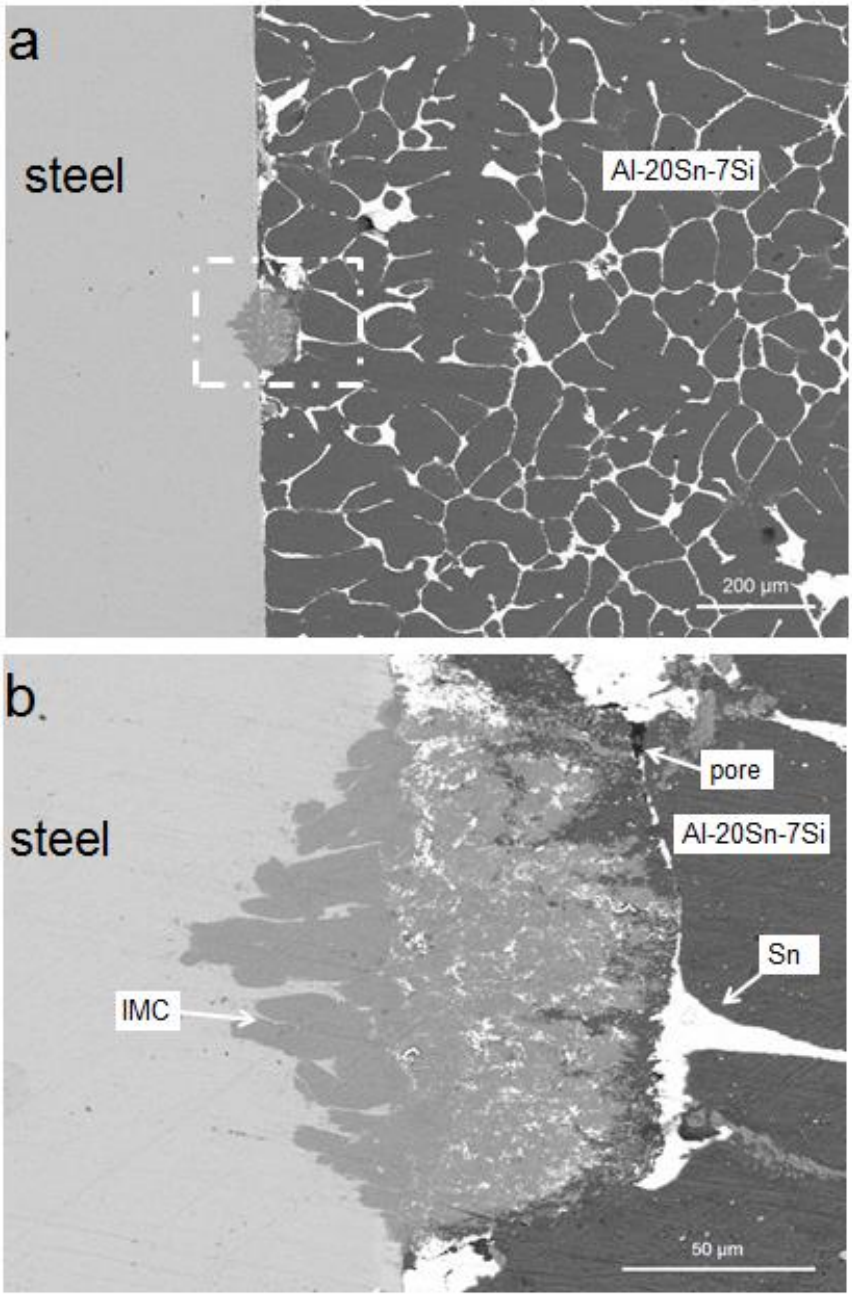

Figure 5-5- (a) SEM micrograph of the cross section of overcast Al-20Sn-7Si onto nickel coated steel prepared by holding the melt at 750 ºC for 1 minute. (b) High magnification of the white dashed rectangle at figure a.

Figure 5-6 shows a typical microstructure of cross-section of overcast Al-20wt%Sn-7wt%Si onto nickel coated steel prepared by holding the melt for 10 minutes: SEM micrographs taken in low magnification (a) and high magnification (b) from region highlighted by white box in (a) and composition profile across the interaction layer (c). It can be seen that an approximately uniform interaction layer of overall thickness 9±2

μm was formed alongside the border between steel and the alloy as shown in Figure 5-6(a). The interaction layer highlighted by the square white box in Figure 5-6(a) was examined in higher magnification, the interaction layer comprised of a light region with thickness of 2 μm next to steel and a dark region of thickness of 7±2 μm next to the aluminium alloy side, as shown in Figure 5-6(b).The light interaction layer has a composition corresponded to Al_5Fe_2 and the dark interaction layer has a composition corresponded to Al_8Fe_2Si, as shown in Figure 5-6(c) .

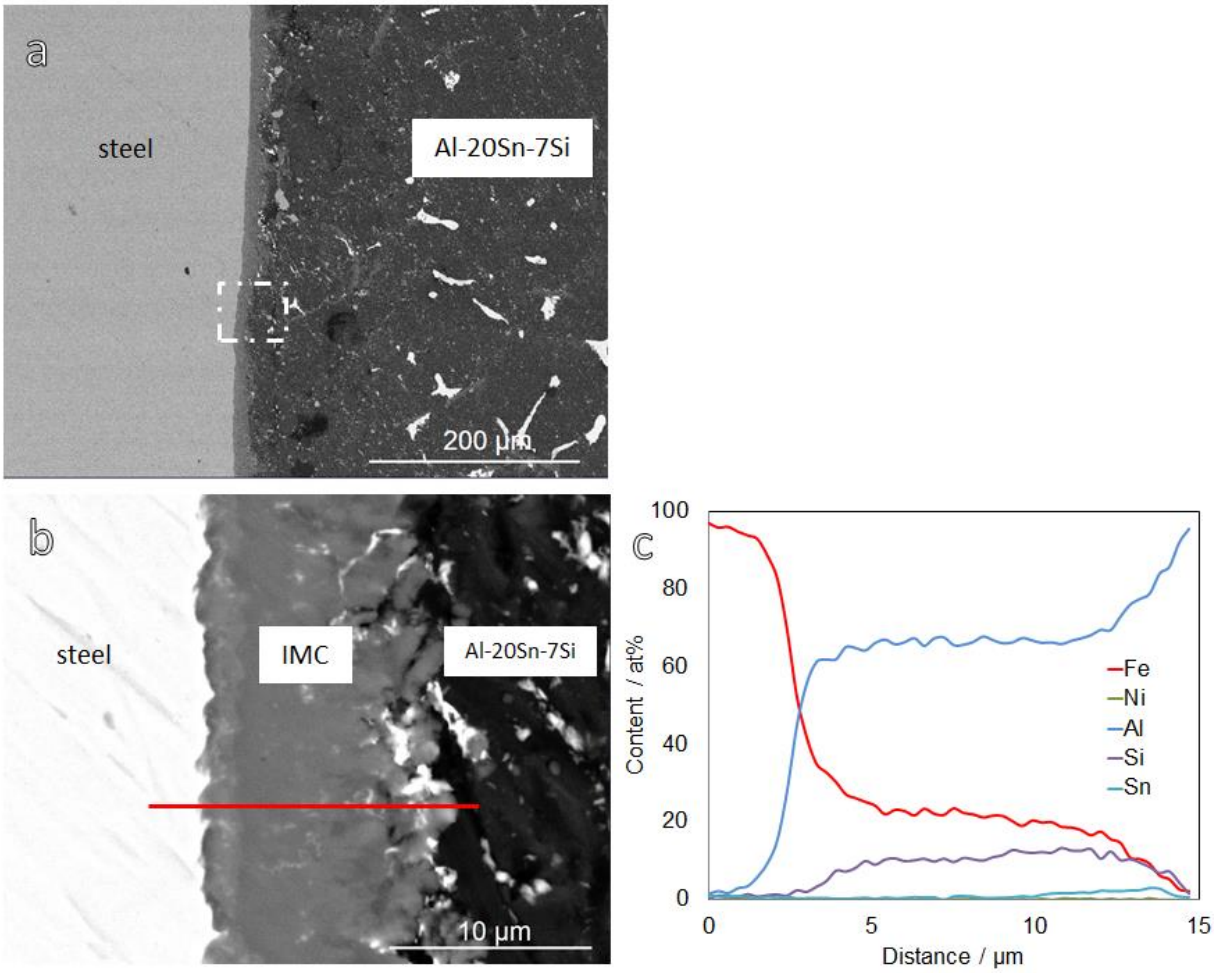

Figure 5-6- SEM micrograph of the cross section of overcast Al-20Sn-7Si onto nickel coated steel prepared by holding the melt at 750 ºC for 10 minute. (b) High magnification of the white dashed rectangle at figure a. (c) EDX line scan of the red line at (a).

Based on the EDX line and map scan results showed in Figure 5-5 and Figure 5-6, complemented with microstructural results it can be concluded that during overcasting of Al-20Sn-7Si, Sn segregates to the interface of IMC and aluminium alloys. Formation

of Sn particles in the interaction layer was decreases the bond strength of Al-20Sn-7Si/steel joints drastically. Figure 5-7 shows thickness of the interaction layer in overcast Al-20Sn-7Si on nickel coated steel and zinc coated steel prepared by holding the melt at 750 ºC for various time.

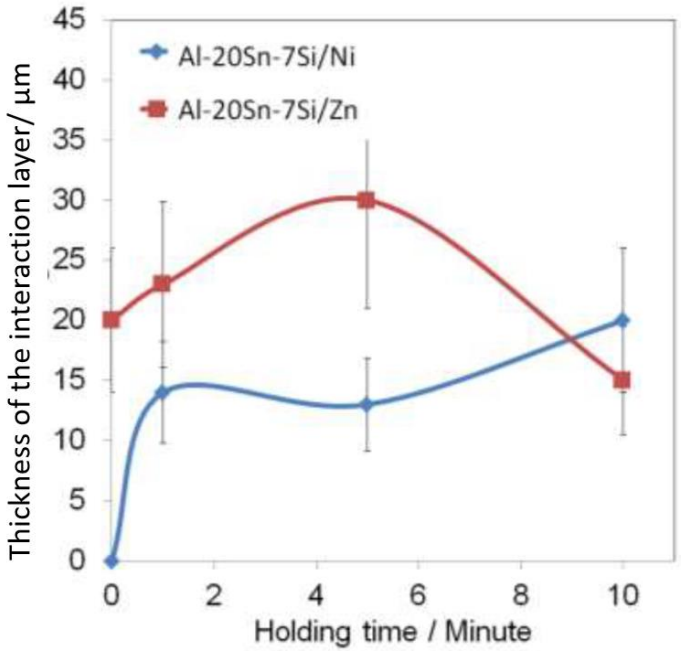

Figure 5-7-Thickness of the interaction layer in overcast Al-20Sn-7Si on nickel coated steel and zinc coated steel prepared by holding the melt at 750 ºC for various time.

Figure 5-8 shows measured bond strength of the overcast Al-20wt%Sn-7wt%Si on nickel coated steel and zinc coated steel that was prepared by holding the melt at 750 ºC for time ranging from 0-10 minutes. The average bond strength of overcast Al-20wt%Sn-7wt%Si on Ni coated steel is found to be higher than that from Zn coated steel. The average bond strength of overcast samples with zinc coated steel ranged from 3MPa to 4MPa, while the average bond strength of overcast samples with Ni coated steel were ranged from 0 and 10MPa, as a function of holding time. This demonstrates that the effect of holding time on the average bond strength of the overcast samples with Ni coated steel is more significant than that with Zn coated steel.

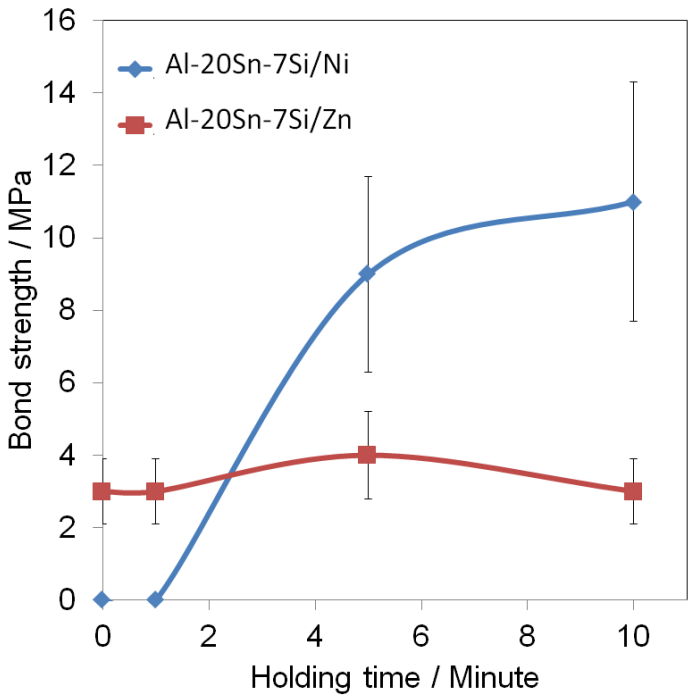

Figure 5-8- Bond strength of the overcast Al-20Sn-7Si onto nickel coated and zinc coated steel prepared by holding at 750°C for various time.

5.5 Joining of steel to Al6060 alloy

Table 3-2 lists the chemical composition of Al6060 that was used in this study. Figure 5-9 shows a typical as-cast microstructure of Al6060.

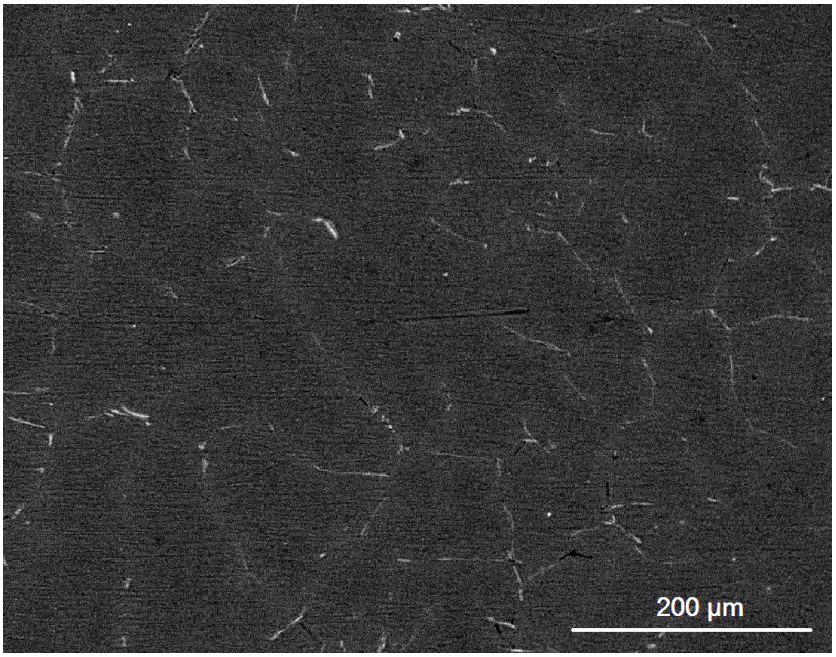

Figure 5-9- SEM micrograph of as-cast Al6060.

IMC layer formed between Al6060/zinc coated steel and Al6060/nickel coated steel and developed between the aluminium alloy and steel. Interaction layer between the coated steels and the aluminium alloy in different holding times shown at Figure 5-10.

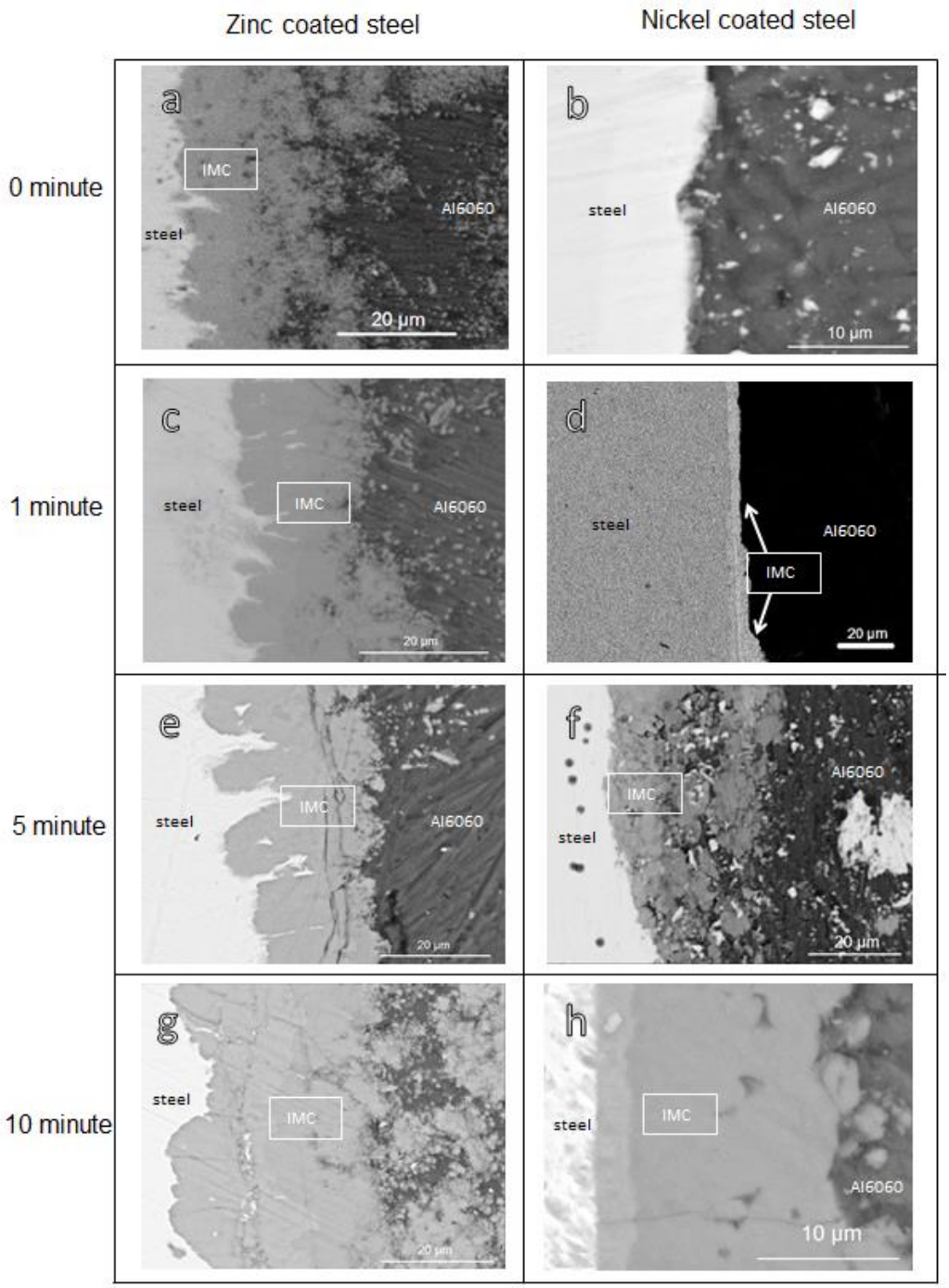

Figure 5-10- Micrograph of interaction between zinc coated and nickel coated steel and 6060 aluminium alloy after holding at 750 ºC for 0, 1, 5 and 10 minutes.

Uniform interaction layer was formed between the Al6060 alloy and zinc coated steel alongside the bond that is visible in Figure 5-11(a). Figure 5-11 (b) is high magnification of the red rectangle of Figure 5-11 (a) that is showing 2 distinctive IMC layers of interaction. A lighter IMC layer next to steel and a darker IMC next to the aluminium alloy detected. Composition of the lighter phase was changed across the bond. However the composition of the darker IMC layer was approximately stable at the EDX line scan, Al(12)Ni(10)Fe(2)Si.

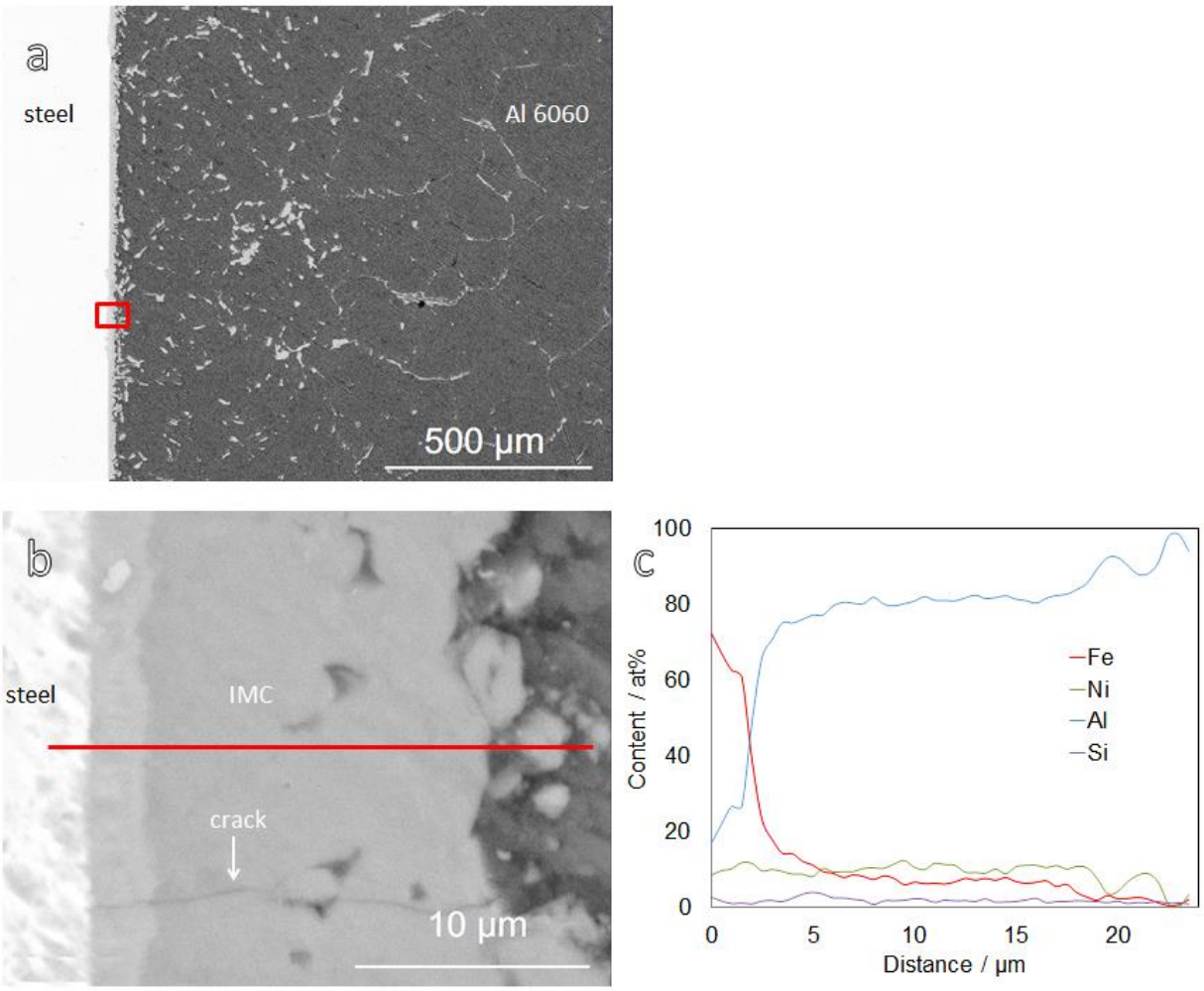

Figure 5-11- (a) SEM micrograph of the cross section of nickel coated steel and 6060 aluminium alloy held at 750 ºC for 10 minutes. (b)High magnification of the red rectangular at a. (c)EDX line scan of the red line at (b).

Bond strength of nickel coated steel/Al6060 was zero in holding at 750 ºC for zero minute however increased to 14 MPa by holding for 1 and 5 minutes. Holding for 10 minutes increased the bond strength to 20 MPa. Bond strength of zinc coated

steel/Al6060 was increased from 20 MPa to 30 MPa by holding at 750 ºC for 5 minutes and then was declined to 14 MPa by holding for 10 minutes. Figure 5-12 shows change of the thickness and Figure 5-13 shows the change of bond strength vs. holding time for Al6060-Zn and Al6060-Zn overcast parts.

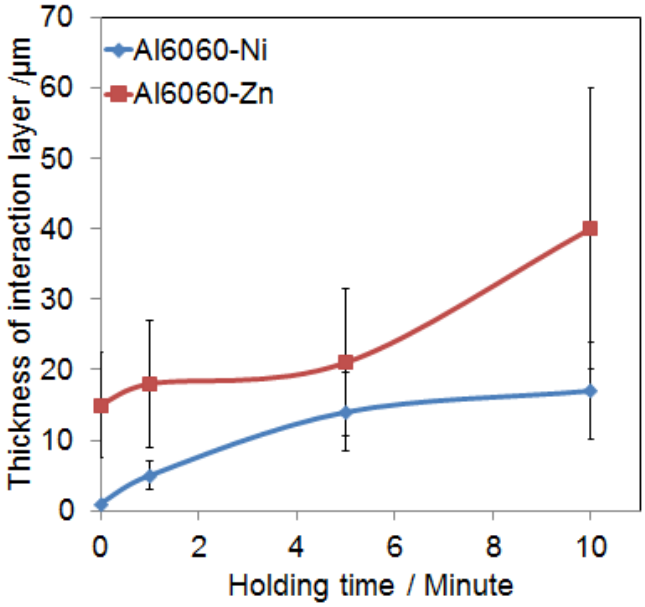

Figure 5-12- Thickness of the reaction layer at Al6060/nickel coated steel and Al6060/zinc coated steel in different holding times at 750 ºC.

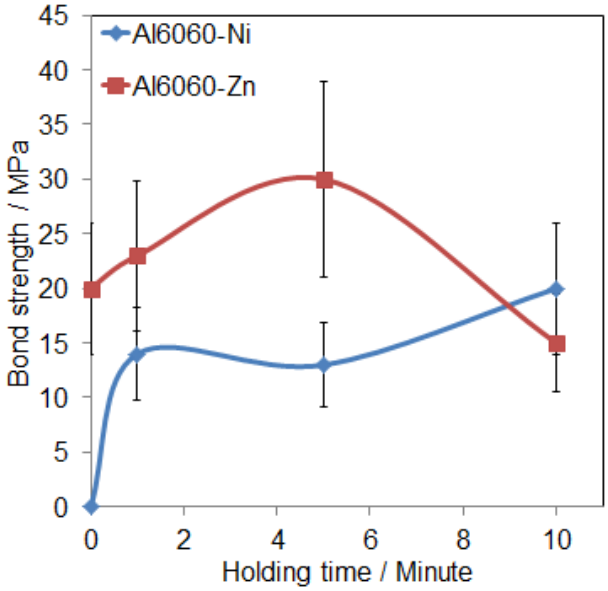

Figure 5-13-Bond strength of Al6060/nickel coated steel and Al6060/zinc coated steel couples in different holding times at 750 ºC.

5.6 Imperfections

Imperfections can influence the bond strength of dissimilar joints. Among different imperfections, cracks are the most important of imperfections, which dramatically deteriorate the mechanical properties of the joint. A clear crack is observed in the interaction layer between nickel coated steel and 6060 aluminium alloy prepared by holding the melt at 750 ºC for 10 minutes (Figure 5-11). The crack was started on the interface between the steel and interaction layer adjacent to steel, which then propagated through the interaction layer and towards the aluminium alloy side. The detailed comparison of cracks characteristics in different aluminium alloys joints will be discussed later at chapter 6.

Porosities can be the preferred nucleation sites for cracks. Also, porosities connect the crack to each other that may finish by failure of a joint.

Figure 5-14 shows the microstructure of interaction layer between Al-20wt%Sn-7wt%Si and Zinc coated steel prepared by holding the melt at 750 ºC for 30 minutes. Kirkendal micro-voids are clearly observed in the microstructure of the interaction region. The pores mostly stretched vertical to the interface of the bimetal, suggests direction of diffusion of the atoms that finally formed the pores. Different sizes of pores detected to maximum of 30 µm length. While, no Kirkendal micro-voids were detected in overcast sample prepared by holding the melt for a period up to 10 minutes (Figure 5-5 and Figure 5-6), many micro-voids are observed in the interaction layer in overcast sample prepared by holding the melt for 30 minutes. This indicates that the Kirkendal effect is not significant in overcast samples processed with holding time of the melt up to 10 minutes. Moreover, the observation of porosities in the steel-side-IMC compare to the aluminium-side-IMC, steel, and aluminium alloy, implying the higher flux of iron atoms to the melt in comparison to the aluminium flux from melt to IMC solid. This may result higher vacancy content of IMC layer, which in turn may lead to the formation of Kirkendal voids inside IMC layer. Basically, Kirkendal effect occurs as a consequence of difference in diffusion rates of the metal atoms [119], so presence of the Kirkendal pores in the IMC, shows that diffusion rate of iron atoms to aluminium was higher than rate of diffusion of aluminium atoms into the steel.

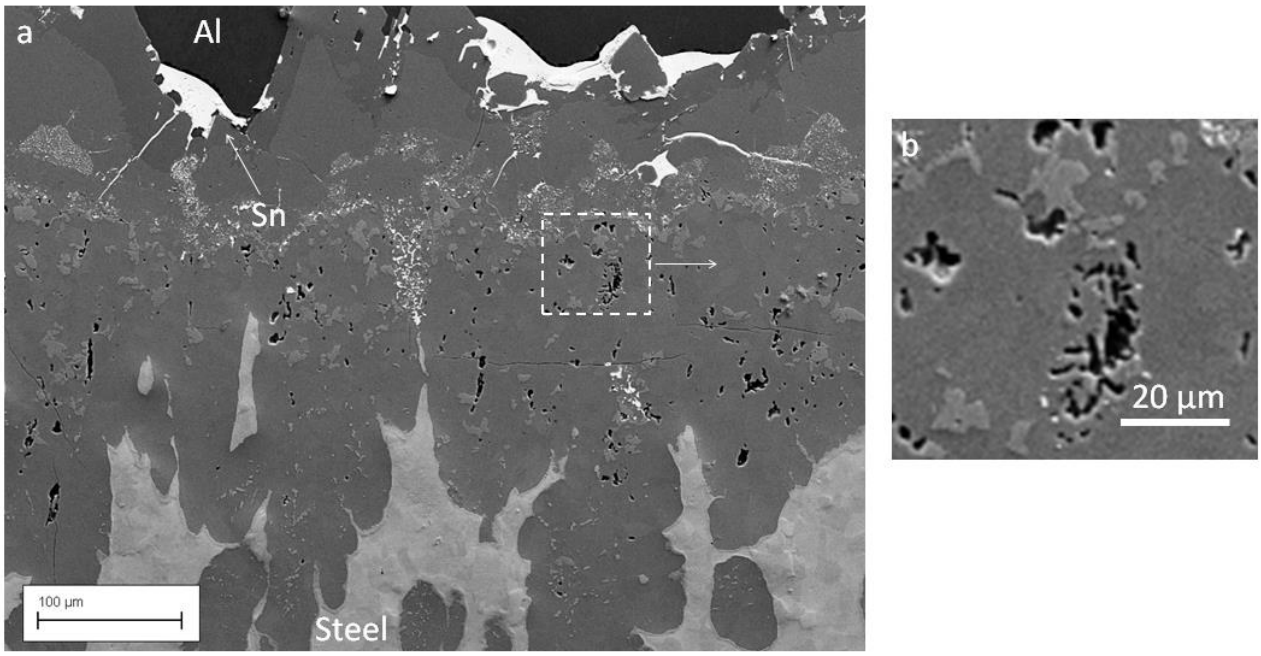

Figure 5-14- (a) Formation of Kirkendal voids at Al-20wt%Sn-7wt%Si overcast on to zinc coated steel prepared by holding the melt at 750 ºC for 30 minutes. (b) High magnification of the white dashed rectangular at a.

Also, occurrence of Kirkendal effect was studied in chapter 4 for pure aluminium/zinc coated steel.

Chapter 6 Discussion

6.1 Effects of processing conditions on microstructure of overcast samples

Based on the results obtained from the studies of interaction between liquid aluminium and solid steel insert during overcasting process in chapter 4, it is believed that when the liquid aluminium touches the surface of the steel insert at 750 °C, the iron starts to dissolve into the molten aluminium up to solubility limit of Fe in liquid aluminium, i.e. 5 wt.%. This leads to an increase in the Fe content in the Al melt near the steel insert and the formation of $Al_{13}Fe_4$ intermetallic phase adjacent to solid steel insert. As the holding time of melt in contact with the steel prior to cooling increases. By increasing the holding time and rising the thickness of interaction layer, the Al_5Fe_2 is formed next to the steel surface due to diffusion of aluminium throughout the $Al_{13}Fe_4$ IMC layer. The fact that Al_5Fe_2 IMC thickness increases as a function of time (Figure 4-9) is verifying that this IMC layer forms mainly by the interdiffusion process rather than solidification.

In the presence of Si in the melt (Al-Si alloys), Al_5Fe_2 and Al_8Fe_2Si IMC phases form next to steel and aluminium alloys, respectively. Similar to pure aluminium/steel joints, solidification and interdiffusion are two major responsible mechanisms for the formation and growth of the IMC layers between liquid Al-Si alloys and steel at 750 °C. As the bonding characteristics of pure aluminium/steel and Al-Si aluminium alloys/steel joints have been studied before, the thickness of these intermediate IMCs could be controlled to achieve the suitable bonding properties of the joints.

Figure 6-1 shows the schematic representation of intermediate layers in aluminium/steel joints prepared through overcasting process. Based on the microstructural micrographs of aluminium alloys/steel joints reported in the chapters 4 and 5, it can be concluded that the interaction layer for overcasting process is not as uniform of other joining processes. This can be attributed to the different growth rate of Al_5Fe_2 phase in different directions. Heumann and Dittrich [117] has been reported the preferentially growth of Al_5Fe_2 intermetallic phase in c-axis and [001] direction during solid state growth. Therefore, grains with c-axis parallel to heat and mass diffusion direction may grow faster than other grains and form finger like feature

IMC/steel interface. As heat sink parallel to diffusion direction are vertical to the interaction layer, mass diffusion is faster along c-axis and growth is preferential towards steel.

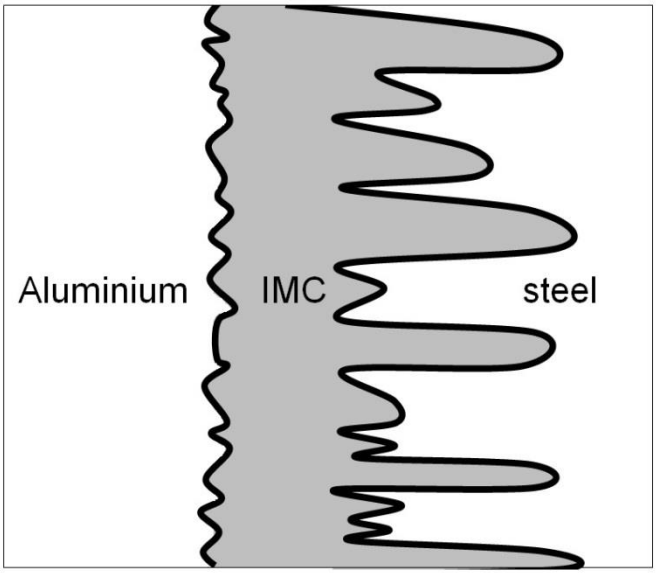

Figure 6-1-Schematic view of the interface of the bond between the steel and the overcast aluminium.

Equilibrium phase diagram of aluminium and iron shows 5 different intermetallic phases of the metals; however, researchers reported presence of only 2 intermetallic phases of Al_5Fe_2 and $Al_{13}Fe_4$. So, according to experimental observations, 3 equilibrium phases missed. This shows that various effects have to be considered in the mechanism of nucleation and growth of intermetallic layers. Type of the formed intermetallic layers and their thicknesses are very important to obtain a joint with optimum performance. So, it is very important to understand development of the intermetallic layers. A better understanding of phase formation and morphology on the interface and the growth mechanisms will provide guidelines to predict and control the reaction on the interface.

The kinetics of formation and growth of the IMC layer of pure aluminium/zinc coated steel was faster than pure aluminium/nickel coated steel because low melting point of the zinc coat facilitated wetting of the solid steel by liquid aluminium. Melting point of zinc is 1035 ºC lower than melting point of nickel.

6.2 Effects of alloy composition and surface coating for steel inserts on the microstructure of overcast samples and bond properties

Figure 6-2 shows changes in the thickness of the IMC layer as a function of melt holding time for different alloy compositions in Al-Si binary system. While the thickness of interaction layer increases with increasing holding time for both nickel and zinc coated steel inserts, the addition of Si in the aluminium melt reduces the growth rate of the interaction layer. This can be seen in Figure 6-3, showing the changes in thickness of interaction layer within the overcast samples formed after holding the melt at 750°C for 10 minutes as a function of Si content. Both steel-side-IMC (Al_5Fe_2 phase) and aluminium-side-IMC ($Al_{13}Fe_4$ phase for Al alloys and Al_8Si_2Fe phase for Al-Si alloys) layers have clearly shown a reduction in thickness with increasing Si content. However, the thickness of Al_5Fe_2 layer decreases more significantly as compared to that of Al_8Fe_2Si layer. The reduction in the thicknesses of intermetallic compound layers can be attributed to the lowering of atomic diffusion and reaction kinetics as a result of silicon addition to the melt.

Decreasing in atomic diffusion by increasing Si content of the Al_5Fe_2 phase has been reported previously [118]. This decline in diffusion rate is described by occupying the structural vacancies of the IMC by Si atoms. The similar change in diffusion rate can be expected for Al_8Fe_2Si phase as a result of changes in Si content. However, the effect of Si on atomic diffusions in Al_8Fe_2Si phase can be a topic of future works. Moreover, Si may decrease the kinetic of solid/liquid reaction and thereby reduce the formation rate of Al_8Fe_2Si phase from Al-Si melts as the Si is also needed to partition to outer IMC layer, during the solidification process.

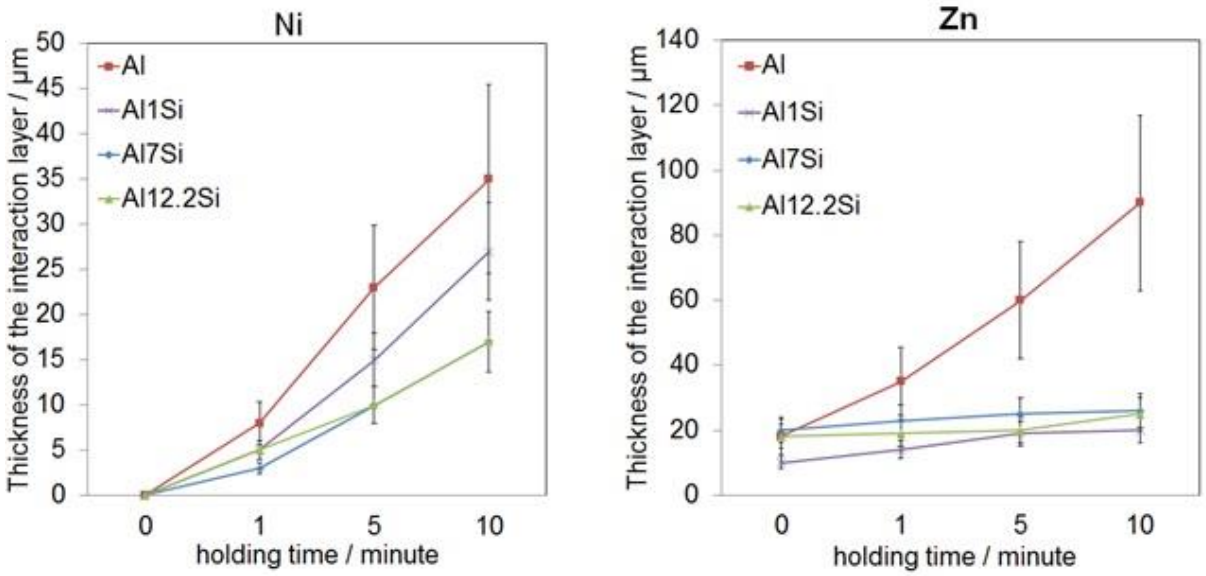

Figure 6-2- Thickness of the interaction layer vs. time for different alloy compositions prepared using nickel coated and zinc coated steel inserts.

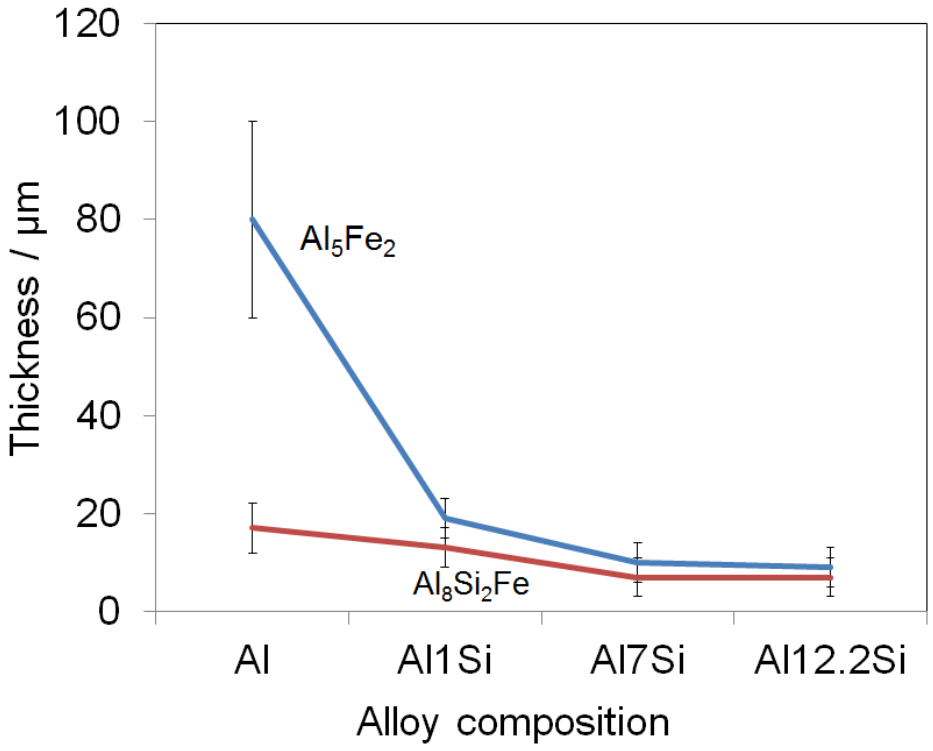

Figure 6-3-Thickness of the Al_5Fe_2 and Al_8Si_2Fe intermetallic layers within samples prepared by overcasting of different Al-Si binary alloys overusing nickel coated steel , using10 minutes holding time at 750 ºC prior to cooling.

To achieve a uniform interaction layer A better understanding of phase aluminium/steel joints, the steel should be coated with a protective layer; it is discussed earlier at chapter 4. These protective layers such as zinc, nickel, or NiZn, protect the steel surface from oxidation and thereby may increase the wettability of the surface by liquid aluminium. In order to compare the effect of zinc and nickel coating on the interaction layer formation kinetics of different aluminium alloys/steel joints, the results of IMC thickness measurements are shown in Figure 6-4.

For all aluminium alloys studied in this project, overcasting process on the zinc coated steel insert shows a higher kinetic of IMC layer formation as compared to other conditions (Uncoated, nickel coated, and NiZn coated steel inserts). The only exceptional result was measured for the Al-1Si/steel joints after holding for 10 minutes at 750 °C, in which the IMC thickness of nickel coated steel is higher than zinc coated steel. This exceptional behaviour can be attributed to the non-uniform nature of overcasting process that may lead to a more scattered result. For all coatings, the IMC thickness increases with increasing holding time of the melt prior to cooling (Figure 4-8). As the melting temperature of nickel is 1035 ºC higher than zinc melting point, dissolving of nickel in aluminium alloy melts are more time-consuming process compared to the zinc. Therefore, no IMC layer was detected for nickel coated steel after overcasting process as well as early stages of holding time. After dissolving of the nickel coating in the aluminium alloy melt, the interaction layer growth rate exhibits almost the similar rate of zinc coated steels.

The growth behaviour of IMC layer in overcast samples using NiZn coated steel insert gives an approximately similar trend as compared to other overcast samples using Ni, Zn coated and uncoated steel inserts. However, the IMC layer thickness for overcast samples prepared using NiZn coated steel inserts for a given holding time always lies between those prepared using either nickel and zinc coated steel inserts.

In general, the coatings of steel play two major roles in controlling the interaction of liquid aluminium and solid steel insert. Firstly, they protect the surface of steel and prevent the steel surface from oxidation before being in contact with liquid aluminium [78]. Furthermore, the coating can also delay the contact of steel surface and

aluminium melt [122].

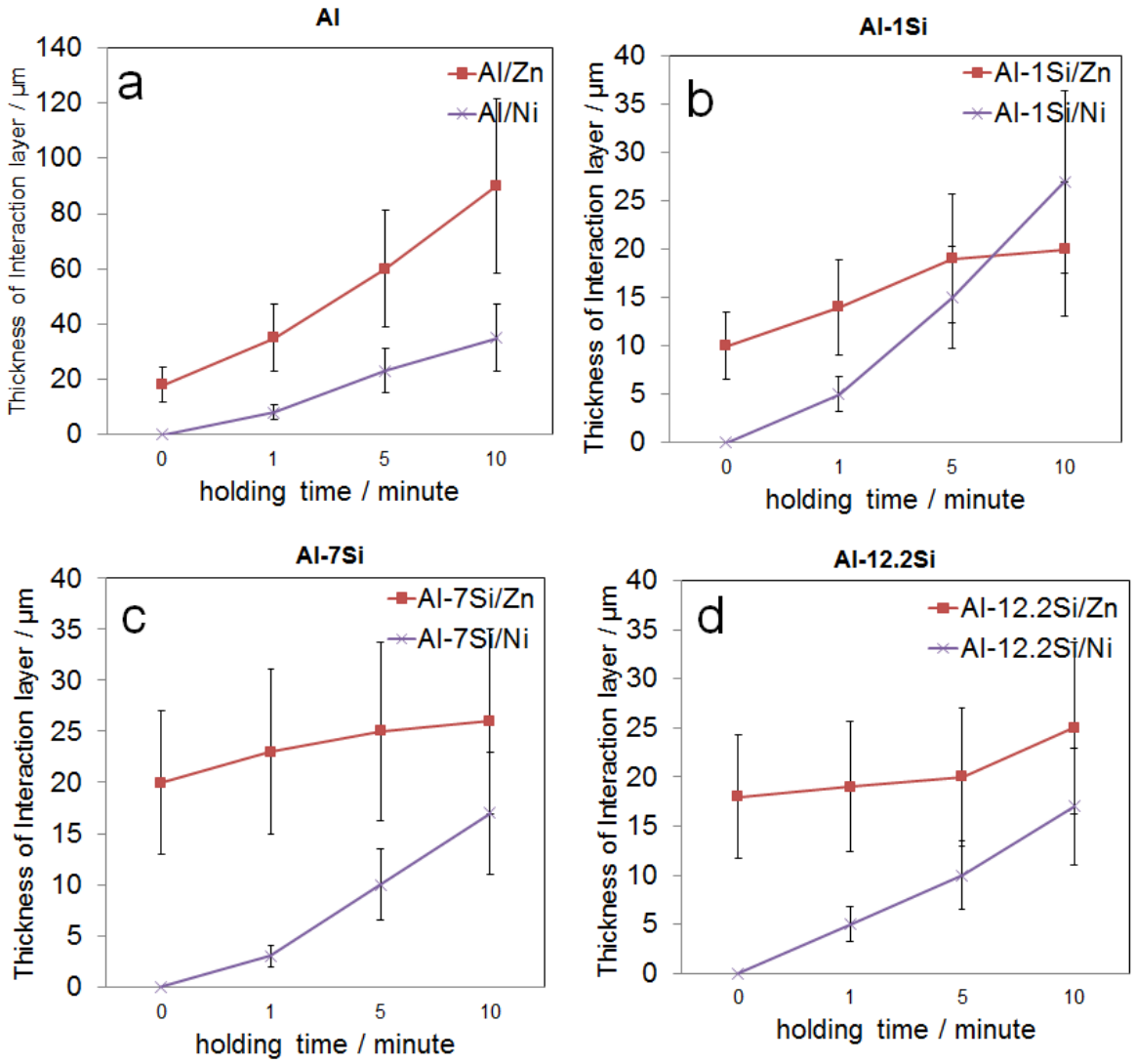

Figure 6-4-Thickness of the interaction layer vs. time for overcast samples prepared using nickel coated and zinc coated steel inserts for various alloy compositions: (a) Pure aluminium, (b) Al-1wt%Si, (C) Al-7wt%Si, and (d) Al-12.2wt%Si.

As it was discussed in previous paragraph, the addition of Si to aluminium alloy decreases the thickness of interaction layer significantly. For diffusion bonding processes, it was claimed that the strength of the bimetallic Al/steel joint declines as the IMC layer exceeded a critical thickness of 10 µm [119]. However, in the current study it was found that the bond strength of overcast sample did not necessarily correlate with the IMC thickness.

Figure 6-5 shows the bond strength for the joints between different aluminium alloys and different coated steels. Generally, it can be seen that the nickel coated steel insert exhibits higher bond strength as compared to uncoated and zinc coated steels at holding time between 5 to 10 minutes. However, the results of bond strength measurement for NiZn coated steel with pure aluminium show that their bond strength is higher than bond strength of Ni coated steel/pure aluminium and Zn coated steel/pure aluminium joints. It seems the NiZn coatings benefits from both higher wettability of zinc coatings and controlled dissolution of the nickel coatings inside aluminium melts. The NiZn coated steel wet by aluminium sooner than nickel coated steel because it formed IMC layer sooner.

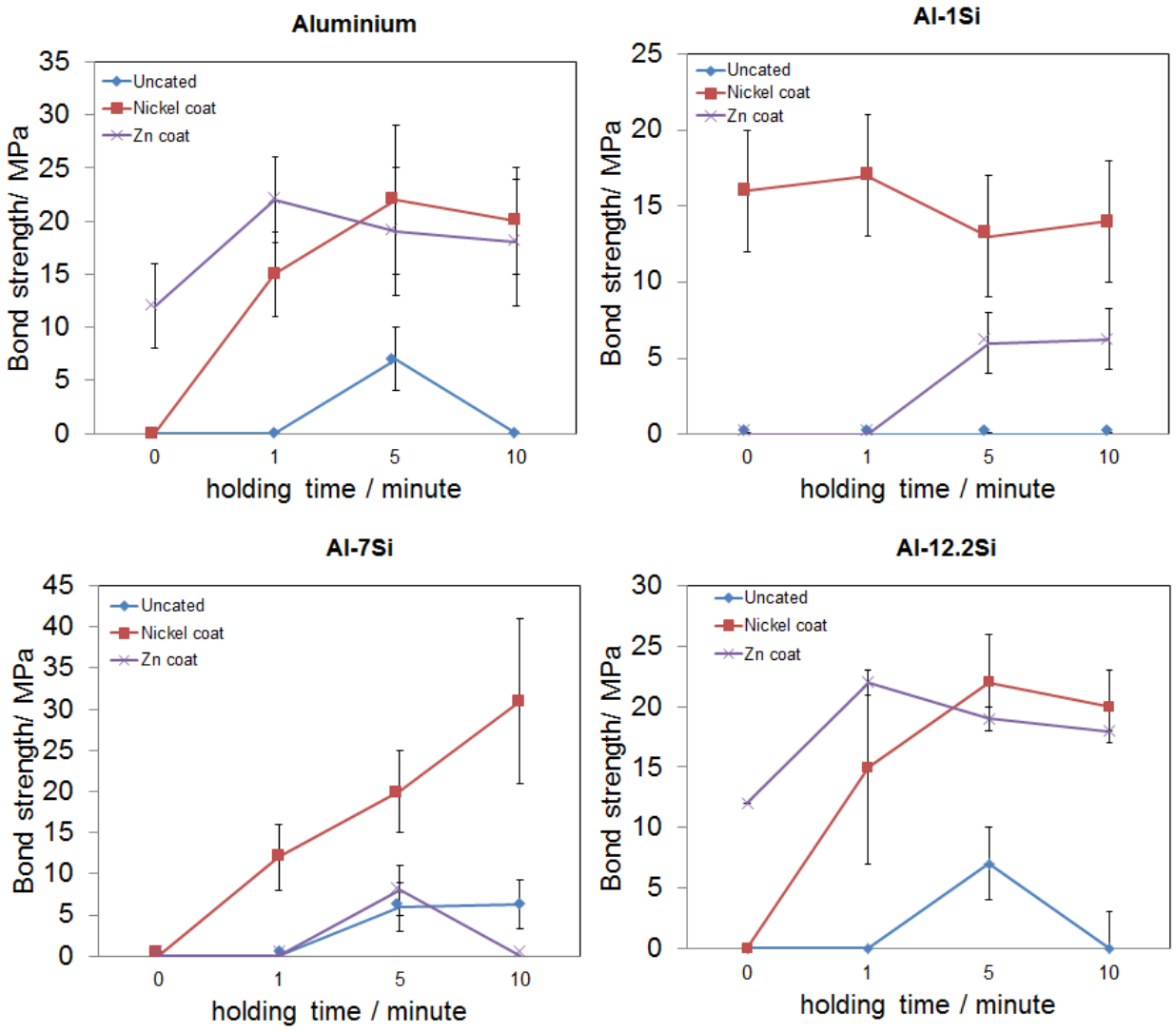

Figure 6-5- Bond strength vs. holding time of melt for overcasting of different Al-Si alloys onto various coated steel inserts.

As the bond strength of different processing conditions in Figure 6-5 does not show a distinguished trend by increasing the holding time, it can be concluded that IMC thickness are not necessarily an effective factor to determine the bond strength of overcasting joints. Similarly, although the Si addition reduces the thickness of IMC layer, the bond strength of different aluminium alloy joints are not considerably influenced by Si contents of the alloys. Moreover, the investigation of the interaction layer between Al-20Sn-7Si alloys and nickel coated steel indicates that the segregation of tin to the IMC/aluminium interface may influence the bond strength more than IMC thickness (Figures 5-5 and 5-7). Segregation of tin to the IMC/aluminium interface leads to the formation of Sn particles in the interaction layer, which act as the imperfections during bond strength test.

Springer et al. reported that tensile strength of steel and pure aluminium is mostly governed by formation of Kirkendal porosities [87]. However, the current research shows that cracks, micro-porosities, and segregation are main imperfections were observed in different aluminium/steel joints. According the fractography studies (Figure 4-13 and Figure 4-14), cracks are mainly responsible for the failure of joints in overcast samples. The cracks usually form in overcast joints as a result of chemical segregation or thermal expansion. For instance, the cracks were found in overcast samples of Al-20wt%Sn-7wt%Si with nickel coated steels inserts. They are believed to be caused by segregation of Sn and Si during the overcasting process.

Moreover, the difference between the thermal expansion coefficients of intermetallic, aluminium and steel layers may lead to cracks formation as observed in overcasting of pure aluminium onto nickel coated steel insert. In comparison to the samples with aluminium-silicon binary alloys, more cracks were detected at the IMC layer of pure aluminium/steel joints. This is attributed to the higher interaction layer thickness in the overcast pure aluminium/ steel joints, leading to possibility of crack formation due to the difference in thermal expansion coefficient.

The micro-porosities were detected at the samples with more 10 minutes holding times. As discussed earlier the formation of these micro-pores are attributed to the Kirkendal effect of aluminium/steel diffusion couple. High rate of diffusion of iron atoms into liquid aluminium and lower rate of diffusion of aluminium into iron can lead to the formation of Kirkendal pores that may decrease the bond strength by facilitation of crack initiation in the bond, leading to the failure of the joint under applied load.

6.3 Kinetics of Fe/Al bimetal interaction layer formation

As discussed earlier at chapter 2, it is possible to use parabolic law to show growth rate of IMC layer. Researchers demonstrated that the kinetics of formation of the intermetallic layer between aluminium and steel is governed mainly by a parabolic law resulted from atomic diffusion mechanism:

$$x^2 = kt \quad \text{Equation (6-1)}$$

x, k and t parameters defined earlier at chapter 2.

However, the results obtained from this project have shown that the kinetics of formation of the intermetallic layer can be affected by the melt composition and the coating for steel insert.

The horizontal axis of the plot at Figure 6-6 is $\sqrt{t}$ while the vertical axis is thickness of the interaction layer. The coloured points at Figure 6-6 show the measured thickness of interaction layer of overcast samples prepared using different alloy composition, coating for steel inserts and holding time at 750 ºC prior to cooling. From the plot, a straight line can be drawn for every processing condition, with a preposition of crossing the line from the point that equation 2 is crossing from.

$$\text{Interaction layer} = \sqrt{t} = 0 \quad \text{Equation (6-2)}$$

Using the above-mentioned method, it is possible with a good approximation to compare the kinetics of IMC formation processed using different conditions. Figure 6-6 shows the highest rate of IMC formation results from the interaction of pure aluminium melt and zinc coated steel and the lowest rate of formation of IMC layer results from the interaction of Al-7wt%Si.

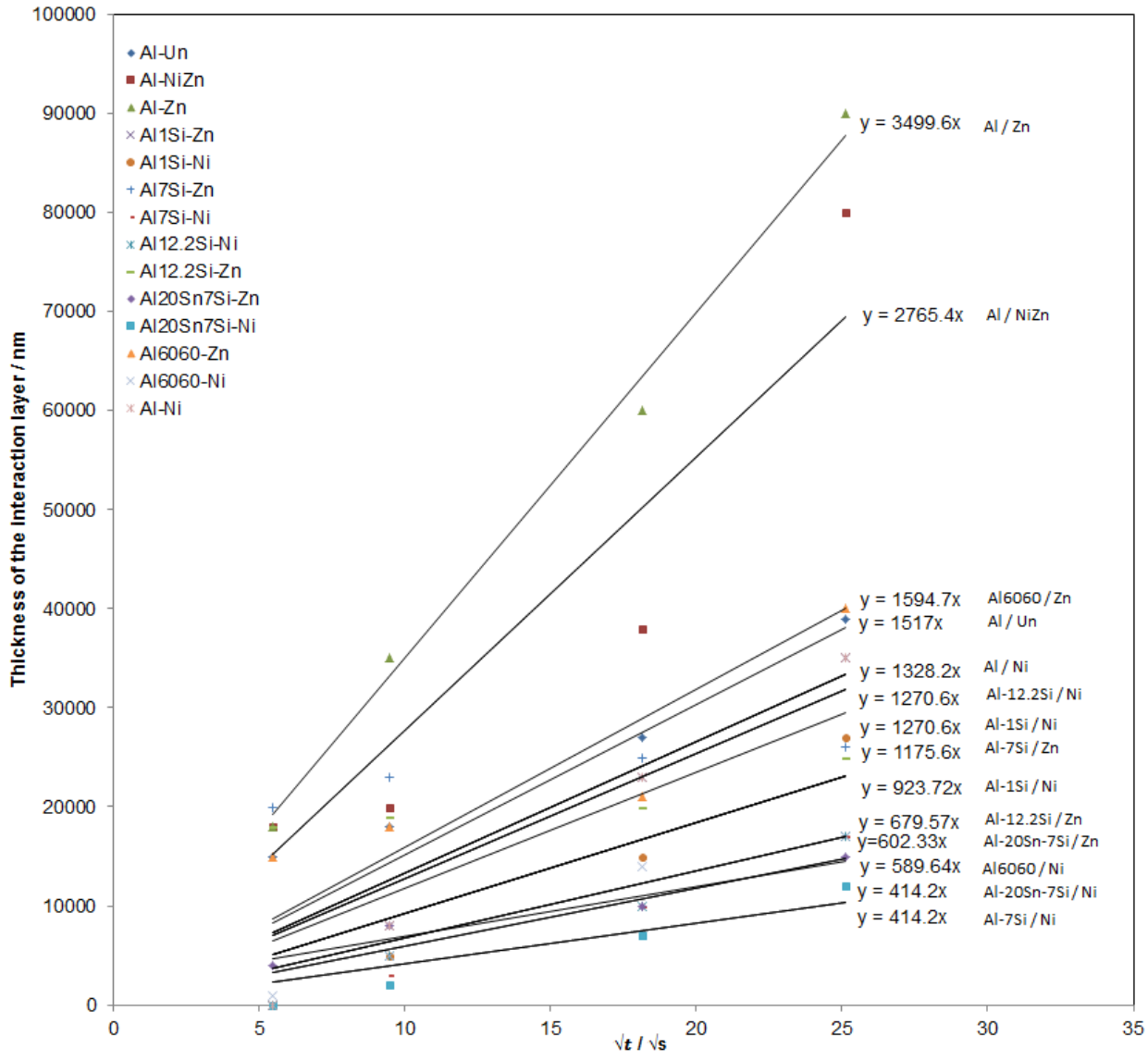

Figure 6-6-Thickness of the interaction layer vs. square root of the time for all overcast samples prepared in this study. The coloured points show the average measured thickness of interaction layer for various processing conditions.

6.4 Bonding area development

Different micrographs of optical microscope and SEM presented microstructures of different processing conditions in the results chapters. The following schematics in this section help to understand the interaction between aluminium and steel in different processing conditions.

Figure 6-7 shows the schematic of interaction between uncoated steel and liquid aluminium. The layer of iron oxide that is forming on top of steel, is forming a non-

uniform layer of intermetallic. Figure 6-7d represents schematic of the microstructure of a sample with similar processing conditions that was shown in Figure 4-1.

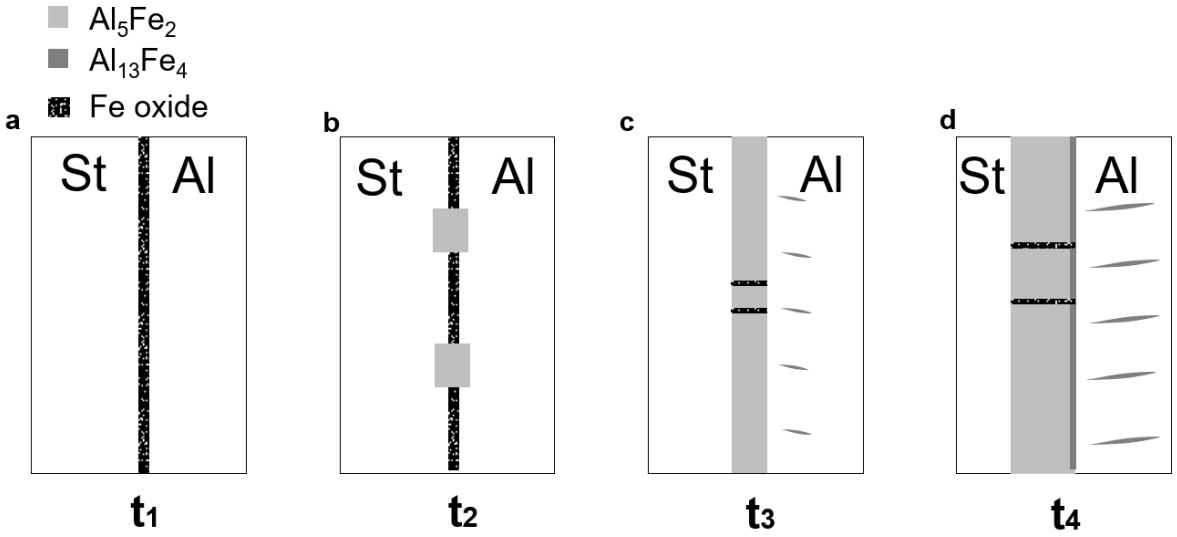

Figure 6-7- Schematic of the growth behaviour of interaction between liquid aluminium and uncoated steel. (a) Liquid aluminium touches the surface of uncoated steel while despite the primary cleaning, there is a layer of iron oxide on the surface (b) after holding at 750 ºC for 1 minute, islands of intermetallic compound form in the interaction layer (c) By holding at 750 ºC for 5 minutes islands of Al_5Fe_2 intermetallic compound growth (d) After holding the joint at 750 ºC for 10 minutes, the Al_5Fe_2 islands growth and touch each other while a thin layer of $Al_{13}Fe_4$ forms between the IMC and aluminium.

Figure 6-8 demonstrates schematic of the interaction between liquid aluminium and solid zinc coated steel in room temperature. Figure 6-8a demonstrates a schematic of the interaction when aluminium and steel interacted, the zinc coat was dissolved in aluminium and a thin layer of Al_5Fe_2 intermetallic was formed on the interface of steel. It should be mentioned that overcasting process, due to the severe turbulence of the liquid aluminium and high temperature of casting, the small amount of zinc coat was dissolves in the liquid aluminium fast and it is not easy to characterise it in the aluminium after solidification. Figure 6-8d demonstrates 10 minutes of interaction between aluminium and zinc coated steel, Figure 4-5b shows the microstructure of a sample with similar processing conditions.

At cooling rate of 0.63 K/s (750/500 ºC) when the liquid aluminium touched the zinc coat, the zinc coat dissolved in the liquid aluminium and Al_5Fe_2 intermetallic phase was formed. Figure 6-8a demonstrates this stage of the interaction. Formation of the Al_5Fe_2 intermetallic layer is uniform across the joint while the thickness is about 8 µm. A finger-like feature of Al_5Fe_2 was formed and grown from the aluminium side into the steel side. The aluminium side of the layer is flatter with small perturbations while on the other side of the intermetallic layer that grows inside steel there are more finger-like feature perturbations. The intermetallic layer formed uniformly across the joint and nowhere was found without formation of intermetallic. At this step, the continuous layer act as a diffusion barrier for aluminium and iron atoms, so diffusion of aluminium/iron is not controlling the interactions any more. Therefore, the concentration gradient was declined across the recently formed intermetallic barrier layer. By increasing the holding time, the mentioned situation of concentration of atoms leads to formation of a second phase of $Al_{13}Fe_4$, with a higher level of aluminium content, between the aluminium and the previously formed Al_5Fe_2 phase.

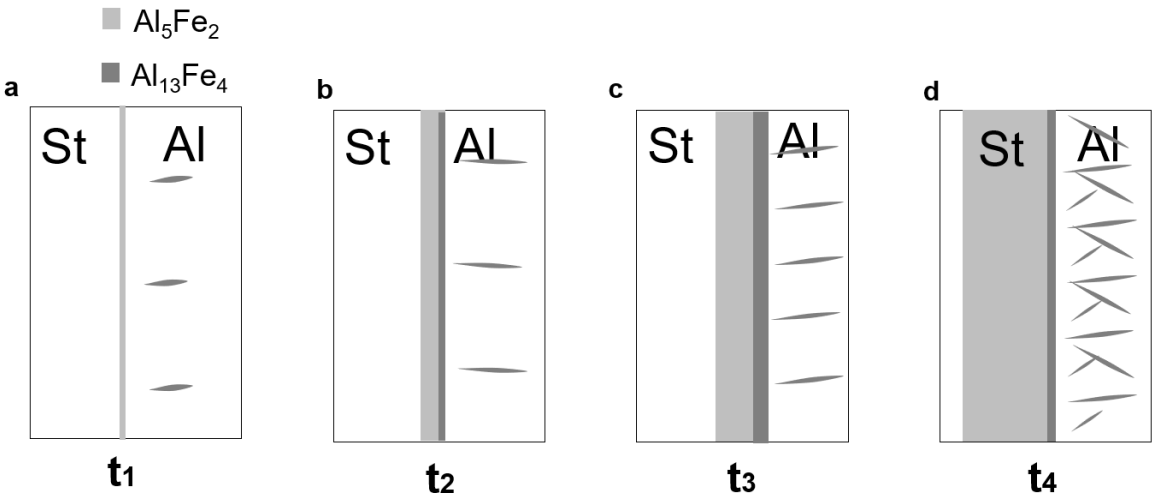

Figure 6-8- Schematic of the growth behaviour of interaction between liquid aluminium and zinc coated steel. (a) Liquid aluminium touches the surface of zinc coated steel, zinc dissolves in aluminium and a layer of Al_5Fe_2 form (b) by holding at 750 ºC for 1 minute thickness of the interaction layer increases and $Al_{13}Fe_4$ IMC form (c) holding at 750 ºC for 5 minutes lead to a thicker IMC layer and more aluminium riched IMC in aluminium (d) After holding the joint at 750 ºC for 10 minutes more IMC in the interface and in aluminium form.

Figure 6-9 demonstrates the schematic of the growth behaviour of the interaction between overcast pure aluminium and nickel coated steel. When pure aluminium was overcast on top of nickel coated steel and cooled to room temperature, no interaction detected between aluminium and steel.

Figure 6-9 demonstrates the schematic of the growth behaviour of the interaction between overcast pure aluminium and nickel coated steel. When pure aluminium was overcast on top of nickel coated steel and cooled to room temperature, no interaction detected between aluminium and steel.

Figure 6-9a demonstrates the schematic of the nickel coated steel and overcast pure aluminium. At this scenario, the overcast aluminium did not affect the nickel coat, so the nickel coat remained un-touched on the surface. However, when the overcast aluminium was remained in touch with liquid aluminium, islands of intermetallic was formed at the joint. Figure 6-9b shows the schematic of the cross section of the nickel coated steel with overcast pure aluminium. An island of intermetallic compound formed and the nickel coat dissolved in the aluminium while 20% of the nickel coat was characterised on surface of the steel. The thickness of the intermetallic islands formed after 1minute holding time was been maximum 10 micron and the lengths where different. Figure 4-16 shows the microstructure of a sample with similar processing conditions.

Figure 6-9c and d show schematic of the cross section of the nickel coated steel and overcast aluminium that was held at 750 ºC for 5 and 10 minutes respectively. The islands of intermetallic were connected to each other and formed a continuous and uniform layer of intermetallic compound. Similar to the previous surface conditions, most of the formed intermetallic layer that is next to steel was Al_5Fe_2. However, morphologies of the grains extension and size were different. The IMC particles in nickel coated steel were shorter and more curved while the grains in zinc coated steel were slimmer, longer and extended inside steel.

Figure 6-10 demonstrates the stages of interaction of nickel-zinc coated steel and overcast aluminium. Developments of the interaction layer in nickel-zinc coated steel demonstrates exactly the steps of zinc coated steel.

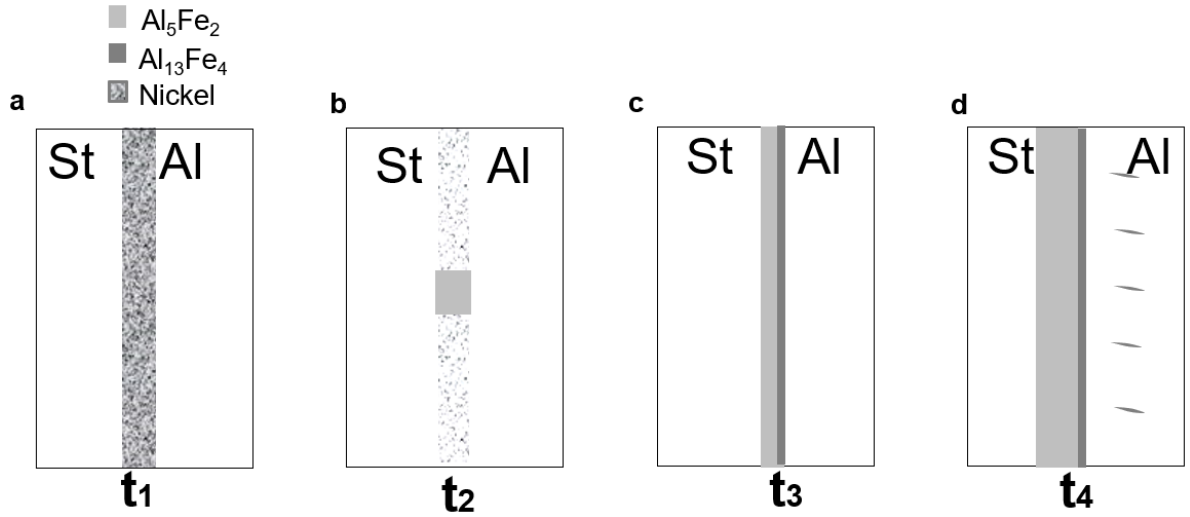

Figure 6-9- Schematic of the interaction between liquid aluminium and nickel coated steel. (a) Liquid aluminium touches the surface of nickel coated steel (b) after holding at 750 ºC for 1 minute, islands of Al_5Fe_2 intermetallic compound were formed (c) By holding the sample at 750 ºC for 5 minutes islands of Al_5Fe_2 intermetallic compound growth. Between Al_5Fe_2 intermetallic phase and aluminium. (d) After holding the joint at 750 ºC for 10 minutes, the Al_5Fe_2 IMC layer was grown, nickel disappear from the interface and a thin layer of $Al_{13}Fe_4$ was formed alongside the bond. Also, aluminium rich IMC particles were detached and moved to the aluminium.

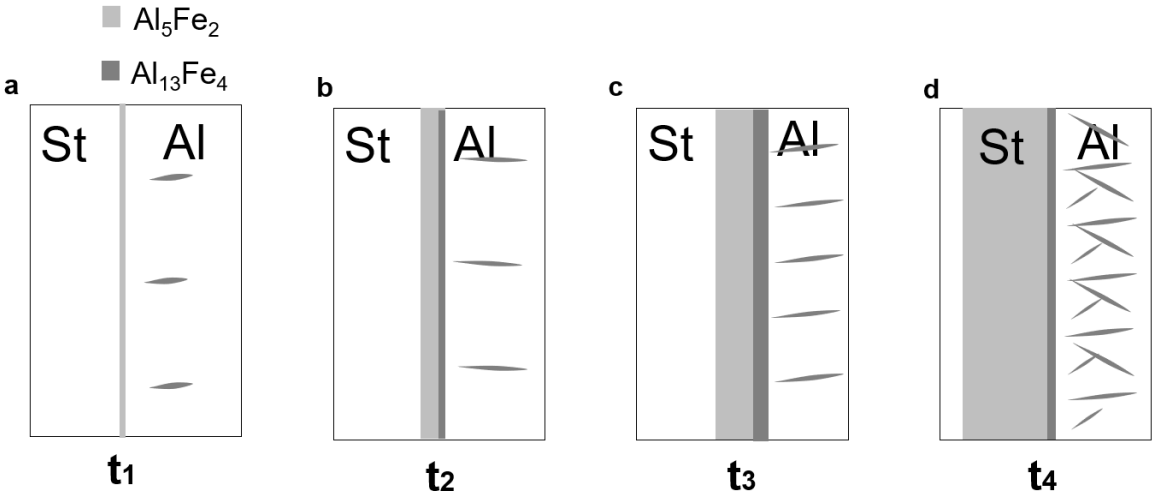

Figure 6-10-Schematic of the growth behaviour of interaction between liquid aluminium and nickel-zinc coated steel. (a) Liquid aluminium was touched the surface of NiZn coated steel, NiZn was dissolved in aluminium and a layer of Al_5Fe_2 was formed (b) by holding at 750 ºC for 1 minute, thickness of the interaction layer was increased and $Al_{13}Fe_4$ IMC was formed (c) holding at 750 ºC for 5 minutes lead to a thicker IMC layer and more aluminium riched IMC in aluminium (d) After holding the joint at 750 ºC for 10 minutes more IMC at the interface and in aluminium was formed.

Figure 6-11 highlights the schematic of formation of IMC on the surface between aluminium and steel, regardless of coating. Study of interaction between liquid aluminium and solid steel proved similar interactions for uncoated steel or steel with different coatings. In all of the surface conditions, the coat was removed by time, however the process of solution of the coat was faster in zinc coat and slower in nickel coat. Following removal of the coating, interaction layer was formed and liquid aluminium was diffused into solid steel and IMC layers were formed. In the next step, iron/aluminium IMCs were dispatch from the steel plate and moved towards aluminium. All of this process was happened in all of the steel plate with different coatings however with different kinetics. Figure 6-11 demonstrates kinetics of interaction between various phase boundaries, liquid aluminium and steel in a stable temperature for 3 different periods of time t1, t2 and t3. The time may vary in different coatings and uncoated surface however they all follow similar process of reactions.

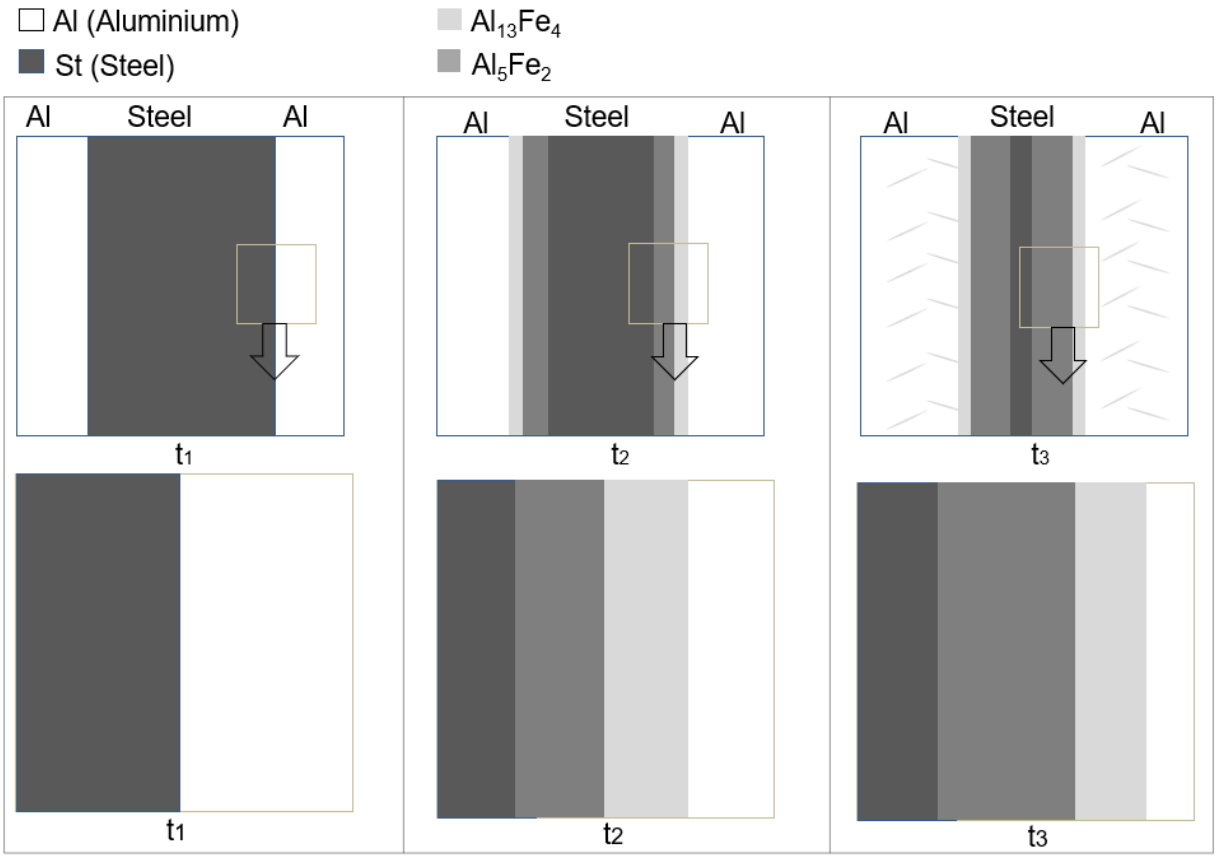

Figure 6-11- Schematic of interaction between liquid aluminium and solid steel in a fixed temperature.

Rezaei et al. suggested a model for interaction of aluminium and uncoated steel at 750 ºC for up to 70 seconds [100], however the main advantage of the their model in comparison with the models presented before is to show the disappearance of steel by time. Rezaei et al. demonstrated that detachment of the IMC controls the interfacial reaction of solid iron and liquid aluminium [100]. However Springer and some other researchers demonstrated the parabolic rate law controls the reaction [87, 97, 114, 115].

Chapter 7 Conclusions

In this project, the effect of processing conditions including melt holding time, coatings for steel insert and aluminium based alloy composition on the interaction between liquid aluminium and solid steel insert was investigated to develop a low-cost overcasting method to fabricate bimetallic joint. It was found that:

The conclusions that were drawn from this research are summarised below:

- At a high cooling rate of 5 K/s (750/500 ºC), no interaction layer was formed between zinc coated steel and pure aluminium at the overcast sample that was cast at 750 °C. However, in a lower cooling rate of 0.63 K/s (750/500 ºC), a finger-like feature interaction layer was formed between zinc coated steel insert and pure aluminium overcast sample that was cast in same temperature. The interaction layer consisted of Al_5Fe_2 phase with a preferential growth along c-axis, leading to the formation of the finger-like feature inside steel. However, $Al_{13}Fe_4$ phase was found within the interaction layer adjacent to the aluminium side of the bimetallic joint.
- The growth rate of Al_5Fe_2 layer was greater than that of $Al_{13}Fe_4$ for pure aluminium that was overcast on top of zinc coated steel.
- TEM characterisation revealed of the interaction layer of pure aluminium/zinc coated steel that held at 750 ºC for 10 minutes, shows formation of a thin layer of Al_6Fe_2 IMC next to steel and $Al_{13}Fe_4$ next to the overcast aluminium side of the interaction layer. SEM and XRD characterisation show formation of Al_5Fe_2 between Al_6Fe_2 and $Al_{13}Fe_4$.
- Coating for steel can play three major roles in the overcasting process. Firstly, it can prevent the surface of steel from oxidation before overcasting. Secondly, it can improve wetting properties of steel surface for a better interaction. Thirdly, the coating can facilitate or reduce the rate of interaction between aluminium and steel. Zinc coat improves wetting and enhances interaction between liquid aluminium and steel insert, leading to thicker interaction layer. Although nickel coating reduces the wettability of coated steel by molten aluminium, nickel coat controls thickness of the intermetallic layer by deaccelerating the interaction between molten aluminium and steel.

- Growth of the IMC layer follows a parabolic relationship between layer thickness and melt holding time prior to cooling. The rate of formation of the interaction was the highest for overcast samples prepared from overcasting of aluminium on top of Zn coated steel insert. However, interaction of liquid aluminium with other NiZn and Ni coated steel inserts was found to be slower than overcast samples using Zn coated steel inserts. For a given holding time and casting alloy composition, the order of interaction layer thickness ranging from highest to lowest values was found in overcast samples using Zn, NiZn, Ni coated steel and uncoated steel insert, respectively.
- The overcast samples produced from Al-xSi binary casting alloys and steel inserts were found to consist of Al_5Fe_2 IMC layer adjacent to the steel and Al_8Fe_2Si layer adjacent to the aluminium alloy. It was found that the thickness of the interaction layer reduced with increasing silicon content. The result repeated in different holding times and different coatings.
- Generally, three types of imperfections detected at samples with different processing conditions, crack, micro-porosity and chemical segregation. This research project shows that imperfections such as micro-porosities, cracks, and chemical segregation are the main source of weakness for the bonding of aluminium to steel prepared by overcasting process.
- Based on parabolic law, a method introduced to compare the kinetics of IMC formation in different conditions by a good approximation. The method demonstrated that pure aluminium/zinc coated steel has the highest kinetics of interaction while Al-7wt.%Si / Nickel coated steel has the lowest kinetics of interactions.
- Based on the results, I suggest to use nickel coated steel to bond aluminium to steel by using optimised overcasting process parameters.

Future works

- Using different types of pressure in overcasting process to improve the bond strength. For example, exploit automatic die casting method or squeeze casting for overcasting process to reduce the variability of joint quality in terms of

microstructure and strength, caused by manual casting approach and to increase the sample complexity and productivity of dissimilar joint fabrication.

- More detailed microstructural investigation using TEM, especially to quantify the proportion and type of intermetallic phases within the interaction layers to understand reaction between casting alloy and steel insert with and without coatings.
- To apply other testing methods such as bond strength in elevated temperatures or fatigue test to study the bond strength of overcast samples

References

[1] Ian C.stone, “Report on TSB project Hi-TINAL: Advanced High-Tin Aluminium Plain Bearing Alloys Produced by Intensive Melt Shearing Technology,” 2014.

[2] A. E. Mironov, I. S. Gershman, and E. I. Gershman, “Influence of Tin on the Tribotechnical Properties of Complex Antifriction Aluminum Alloys,” *J. Frict. Wear*, vol. 39, no. 5, pp. 394–399, Sep. 2018, doi: 10.3103/S1068366618050100.

[3] M. Stephen and I. Kimber, “Bearing arrangement,” EP 1 267 076 A2, 2002.

[4] A. R. Valizadeh, A. R. Kiani-Rashid, M. H. Avazkonandeh-Gharavol, and E. Z. Karimi, “The Influence of Cooling Rate on the Microstructure and Microsegregation in Al–30Sn Binary Alloy,” *Metallogr. Microstruct. Anal.*, vol. 2, no. 2, pp. 107–112, Apr. 2013, doi: 10.1007/s13632-013-0064-x.

[5] K. Zhang, X. Bian, Y. Li, Y. Liu, and C. Yang, “New evidence for the formation and growth mechanism of the intermetallic phase formed at the Al/Fe interface,” *J. Mater. Res.*, vol. 95, pp. 3279–3287, 2015, doi: 10.1557/jmr.2013.345.

[6] F. C. Yin, M. X. Zhao, Y. X. Liu, W. Han, and Z. Li, “Effect of Si on growth kinetics of intermetallic compounds during reaction between solid iron and molten aluminum,” *Trans. Nonferrous Met. Soc. China (English Ed.*, vol. 23, no. 2, pp. 556–561, 2013, doi: 10.1016/S1003-6326(13)62499-1.

[7] H. R. Shahverdi, M. R. Ghomashchi, S. Shabestari, and J. Hejazi, “Microstructural analysis of interfacial reaction between molten aluminium and

solid iron," *J. Mater. Process. Technol.*, 2002, doi: 10.1016/S0924-0136(02)00225-X.

[8] H. Springer, A. Kostka, E. J. Payton, D. Raabe, A. Kaysser-Pyzalla, and G. Eggeler, "On the formation and growth of intermetallic phases during interdiffusion between low-carbon steel and aluminum alloys," *Acta Mater.*, 2011, doi: 10.1016/j.actamat.2010.11.023.

[9] M. Zhe, O. Dezellus, B. Gardiola, M. Braccini, and J. C. Viala, "Chemical changes at the interface between low carbon steel and an Al-Si alloy during solution heat treatment," *J. Phase Equilibria Diffus.*, 2011, doi: 10.1007/s11669-011-9949-z.

[10] M.KleinerS.ChattiA.Klaus, "Metal forming techniques for lightweight construction," 2007, doi: https://doi.org/10.1016/j.jmatprotec.2006.04.085.

[11] A. I. Taub, P. E. Krajewski, A. A. Luo, and J. N. Owens, "The evolution of technology for materials processing over the last 50 years: The automotive example," *JOM*, vol. 59, no. 2, pp. 48–57, Feb. 2007, doi: 10.1007/s11837-007-0022-7.

[12] J. L. Song, S. B. Lin, C. L. Yang, C. L. Fan, and G. C. Ma, "Analysis of intermetallic layer in dissimilar TIG welding–brazing butt joint of aluminium alloy to stainless steel," *Sci. Technol. Weld. Join.*, vol. 15, no. 3, pp. 213–218, 2010, doi: 10.1179/136217110X12665048207610.

[13] X. HAN *et al.*, "Microstructure and properties at bonding interface of AA4045/AA3003 aluminum alloy cladding billet prepared by semi-continuous casting," *Trans. Nonferrous Met. Soc. China (English Ed.*, vol. 26, no. 3, pp. 658–664, 2016, doi: 10.1016/S1003-6326(16)64155-9.

[14] Z. Sun and R. Karppi, "The application of electron beam welding for the joining of dissimilar metals: an overview," *J. Mater. Process. Technol.*, vol. 59, no. 3, pp. 257–267, May 1996, doi: 10.1016/0924-0136(95)02150-7.

[15] S. K. Dinda, J. Kar, S. Jana, G. Gopal Roy, and P. Srirangam, "Effect of beam oscillation on porosity and intermetallics of electron beam welded DP600-steel to Al 5754-alloy," *J. Mater. Process. Technol.*, vol. 265, pp. 191–200, Mar. 2019,

doi: 10.1016/j.jmatprotec.2018.10.026.

[16] P. . Roberts, *Introduction to Brazing Technology*. CRC Press: Boca Raton, FL, USA, 2016.

[17] G. Filliard, M. El Mansori, M. De Metz-Noblat, C. Bremont, A. Reullier, and L. Tirado, “Influence of process parameters on thermal cycle and intermetallic compounds formation in high speed laser weld-brazing of aluminium-steel angle joints,” *Procedia Manuf.*, vol. 26, pp. 690–699, 2018, doi: 10.1016/j.promfg.2018.07.079.

[18] V. Nguyen, Q. Nguyen, and S.-C. Huang, “Microstructure and Mechanical Properties of Butt Joints between Stainless Steel SUS304L and Aluminum Alloy A6061-T6 by TIG Welding,” *Materials (Basel).*, vol. 11, no. 7, p. 1136, Jul. 2018, doi: 10.3390/ma11071136.

[19] P. Wang, X. Chen, Q. Pan, B. Madigan, and J. Long, “Laser welding dissimilar materials of aluminum to steel: an overview,” *Int. J. Adv. Manuf. Technol.*, vol. 87, no. 9–12, pp. 3081–3090, 2016, doi: 10.1007/s00170-016-8725-y.

[20] G. H. S. F. L. Carvalho, I. Galvão, R. Mendes, R. M. Leal, and A. Loureiro, “Explosive welding of aluminium to stainless steel,” *J. Mater. Process. Technol.*, vol. 262, pp. 340–349, Dec. 2018, doi: 10.1016/j.jmatprotec.2018.06.042.

[21] T. Kovacs-Coskun, B. Volgyi, and I. Sikari-Nagl, “Investigation of aluminum-steel joint formed by explosion welding,” *J. Phys. Conf. Ser.*, vol. 602, p. 012026, 2015, doi: 10.1088/1742-6596/602/1/012026.

[22] T. Wang, Y. Zhang, X. Li, B. Zhang, and J. Feng, “Influence of beam current on microstructures and mechanical properties of electron beam welding-brazed aluminum-steel joints with an Al5Si filler wire,” *Vacuum*, vol. 141, pp. 281–287, Jul. 2017, doi: 10.1016/j.vacuum.2017.04.029.

[23] K. Devendranath Ramkumar *et al.*, “Investigations on the structure – Property relationships of electron beam welded Inconel 625 and UNS 32205,” *Mater. Des.*, vol. 68, pp. 158–166, 2015, doi: 10.1016/j.matdes.2014.12.032.

[24] M. Sun, S. T. Niknejad, G. Zhang, M. K. Lee, L. Wu, and Y. Zhou, “Microstructure and mechanical properties of resistance spot welded AZ31/AA5754 using a

nickel interlayer," *Mater. Des.*, vol. 87, pp. 905–913, 2015, doi: 10.1016/j.matdes.2015.08.097.

[25] M. R. R. Arghavani, M. Movahedi, and A. H. H. Kokabi, "Role of zinc layer in resistance spot welding of aluminium to steel," *Mater. Des.*, vol. 102, pp. 106–114, 2016, doi: 10.1016/j.matdes.2016.04.033.

[26] A. M. Milani, M. Paidar, A. Khodabandeh, and S. Nategh, "Influence of filler wire and wire feed speed on metallurgical and mechanical properties of MIG welding–brazing of automotive galvanized steel/5754 aluminum alloy in a lap joint configuration," *Int. J. Adv. Manuf. Technol.*, vol. 82, no. 9–12, pp. 1495–1506, 2016, doi: 10.1007/s00170-015-7505-4.

[27] H. Wang, L. Liu, and F. Liu, "The characterization investigation of laser-arc-adhesive hybrid welding of Mg to Al joint using Ni interlayer," *Mater. Des.*, vol. 50, pp. 463–466, 2013, doi: 10.1016/j.matdes.2013.02.085.

[28] C. Thomy, F. Wagner, A. Wirth, M. Kreimeyer, and F. Vollertsen, "Laser-MIG-Hybridfügen von Alu - minium-Stahl Leichtbaustrukturen," no. 4, pp. 36–40, 2007.

[29] F. W. Bach, A. Beniyash, K. Lau, and R. Versemann, "Joining of Steel-Aluminium Hybrid Structures with Electron Beam on Atmosphere," *Adv. Mater. Res.*, vol. 6–8, pp. 143–150, 2005, doi: 10.4028/www.scientific.net/AMR.6-8.143.

[30] G. Casalino, P. Leo, M. Mortello, P. Perulli, and A. Varone, "Effects of Laser Offset and Hybrid Welding on Microstructure and IMC in Fe–Al Dissimilar Welding," *Metals (Basel).*, vol. 7, no. 8, p. 282, 2017, doi: 10.3390/met7080282.

[31] H. Zhang, Y. Chen, and A. A. Luo, "Improved Interfacial Bonding in Magnesium/Aluminum Overcasting Systems by Aluminum Surface Treatments," *Metall. Mater. Trans. B Process Metall. Mater. Process. Sci.*, vol. 45, no. 6, pp. 2495–2503, 2014, doi: 10.1007/s11663-014-0140-x.

[32] C. Koerner, M. Schwankl, and D. Himmler, "Aluminum-aluminum compound castings by electroless deposited zinc layers," *J. Mater. Process. Technol.*, 2014, doi: 10.1016/j.jmatprotec.2013.12.014.

[33] “High pressure squeeze casting of stainless steel wire reinforced aluminium matrix composites i : ..,” vol. 19, no. 5, pp. 393–399, 1988.

[34] J. Feng *et al.*, “Bonding of Aluminum Alloys in Compound Casting,” *Metall. Mater. Trans. A Phys. Metall. Mater. Sci.*, vol. 48, no. 10, pp. 4632–4644, 2017, doi: 10.1007/s11661-017-4252-1.

[35] H. Zhang, Y. Chen, and A. A. Luo, “A novel aluminum surface treatment for improved bonding in magnesium/aluminum bimetallic castings,” *Scr. Mater.*, vol. 86, pp. 52–55, 2014, doi: 10.1016/j.scriptamat.2014.05.007.

[36] J. Pan, M. Yoshida, G. Sasaki, H. Fukunaga, H. Fujimura, and M. Matsuura, “Ultrasonic insert casting of aluminum alloy,” *Scr. Mater.*, 2000, doi: 10.1016/S1359-6462(00)00385-7.

[37] B. N. Sarada, P. L. S. Murthy, and G. Ugrasen, “Hardness and Wear Characteristics of Hybrid Aluminium Metal Matrix Composites Produced by Stir Casting Technique,” *Mater. Today Proc.*, vol. 2, no. 4–5, pp. 2878–2885, 2015, doi: 10.1016/j.matpr.2015.07.305.

[38] T. Liu, Q. G. Q. D. Wang, P. Liu, J. W. Sun, X. L. Yin, and Q. G. Q. D. Wang, “Microstructure and mechanical properties of overcast aluminum joints,” *Trans. Nonferrous Met. Soc. China (English Ed.*, vol. 25, no. 4, pp. 1064–1072, 2015, doi: 10.1016/S1003-6326(15)63699-8.

[39] AWS, *Brazing Handbook*. American Welding Society (AWS), 2007.

[40] U. Reisgen, C. Otten, and J. Schönberger, “Investigations about the influence of the time-temperature curve on the formation of intermetallic phases during electron beam welding of steel-aluminium material combinations,” *Weld. World*, vol. 58, no. 4, pp. 443–454, 2014, doi: 10.1007/s40194-014-0128-9.

[41] G. Eggeler, W. Auer, and H. Kaesche, “On the influence of silicon on the growth of the alloy layer during hot dip aluminizing,” *J. Mater. Sci.*, vol. 21, no. 9, pp. 3348–3350, 1986, doi: 10.1007/BF00553379.

[42] B. Lemmens, H. Springer, I. De Graeve, J. De Strycker, D. Raabe, and K. Verbeken, “Effect of silicon on the microstructure and growth kinetics of intermetallic phases formed during hot-dip aluminizing of ferritic steel,” *Surf.*

Coatings Technol., vol. 319, pp. 104–109, 2017, doi: 10.1016/j.surfcoat.2017.03.040.

[43] W. J. Cheng and C. J. Wang, “Microstructural evolution of intermetallic layer in hot-dipped aluminide mild steel with silicon addition,” *Surf. Coatings Technol.*, vol. 205, no. 19, pp. 4726–4731, 2011, doi: 10.1016/j.surfcoat.2011.04.061.

[44] H. Umeshita, “Effects of Alloying Copper and Silicon on the Bondability of Dissimilar Metal Joints of Aluminum Alloys to Steel ∗,” pp. 187–191, 2009.

[45] S. Kang, K. Han, K. Kim, Y. Kang, K. Son, and D. Kim, “Formation Behavior of an Intermetallic Compound Layer during the Hot Dip Aluminizing of Cast Iron,” *ISIJ Int.*, vol. 52, no. 7, pp. 1342–1347, 2012, doi: 10.2355/isijinternational.52.1342.

[46] S.-H. Hwang, J.-H. Song, and Y.-S. Kim, “Effects of carbon content of carbon steel on its dissolution into a molten aluminum alloy,” *Mater. Sci. Eng. A*, vol. 390, no. 1–2, pp. 437–443, Jan. 2005, doi: 10.1016/j.msea.2004.08.062.

[47] L. Sun, C. A. Li, J. W. Tu, and M. C. Peng, “Effect of surface treatment to inserted ring on Al-Fe bonding layer of aluminium piston with reinforced cast iron ring,” *J. Cent. South Univ.*, vol. 21, no. 8, pp. 3037–3042, 2014, doi: 10.1007/s11771-014-2273-0.

[48] K. H. Choe *et al.*, “Study of the Interface between Steel Insert and Aluminum Casting in EPC,” *J. Mater. Sci. Technol*, vol. 24, no. 1, pp. 60–64, 2008.

[49] F. Haddadi, D. Strong, and P. B. Prangnell, “Effect of zinc coatings on joint properties and interfacial reactions in aluminum to steel ultrasonic spot welding,” *Jom*, vol. 64, no. 3, pp. 407–413, 2012, doi: 10.1007/s11837-012-0265-9.

[50] L. Jia, J. Shichun, S. Yan, N. Cong, C. Junke, and H. Genzhe, “Effects of zinc on the laser welding of an aluminum alloy and galvanized steel,” *J. Mater. Process. Technol.*, vol. 224, pp. 49–59, 2015, doi: 10.1016/j.jmatprotec.2015.04.017.

[51] H. He, S. Lin, C. Yang, C. Fan, and Z. Chen, “Combination effects of nocolok flux with Ni powder on properties and microstructures of aluminum-stainless steel TIG welding-brazing joint,” *J. Mater. Eng. Perform.*, vol. 22, no. 11, pp.

3315–3323, 2013, doi: 10.1007/s11665-013-0615-y.

[52] T. Sakiyama *et al.*, “Growth of Fe 2 Al 5 Phase on Pure Iron Hot-Dipped in Al – Mg – Si Alloy Melt with Fe in Solution,” *Mater. Sci. Eng. A*, vol. 23, no. 1–2, pp. 1455–1460, 2008, doi: 10.1016/S0921-5093(03)00469-6.

[53] T. Hattori, S. Sakai, A. Sakamoto, and C. Fujiwara, “Brazeability of aluminum in vacuum-nitrogen partial-pressure atmosphere brazing ,” *Welding Journal (Miami, Fla)* , vol. 73, no. 10. pp. 2335–2405, 1994, [Online]. Available: http://brunel.summon.serialssolutions.com/2.0.0/link/0/eLvHCXMwtV1LS8NAEB6UelBEtL7qo-xBvJRITJOWHDxYsRRUPLTiMWxeEm2T0iYq_fXO7ObVQEEPXpawIUuy3-7MZGfmG4C6dqUqFZmwXAowr45a9P0rsNiH0FKi7B_AzQfFDrxGiLFFkLH9Fcy9GV94kmtb-Mo5CpuAotuDsPXJnSSZKLhpZ9EbxWLR83ysiNhX4TiI.

[54] H. W. Liu, C. Guo, Y. Cheng, X. F. Liu, and G. J. Shao, “Interfacial strength and structure of stainless steel–semi-solid aluminum alloy clad metal,” *Mater. Lett.*, vol. 60, no. 2, pp. 180–184, Jan. 2006, doi: 10.1016/j.matlet.2005.08.015.

[55] G. Durrant, M. Gallerneault, and B. Cantor, “Squeeze cast aluminium reinforced with mild steel inserts,” *J. Mater. Sci.*, vol. 31, no. 3, pp. 589–602, 1996, doi: 10.1007/BF00367873 U6 - http://dx.doi.org/10.1007/BF00367873 M4 - Citavi.

[56] M. Şimşir, L. C. Kumruoğlu, and A. Özer, “An investigation into stainless-steel/structural-alloy-steel bimetal produced by shell mould casting,” *Mater. Des.*, vol. 30, no. 2, pp. 264–270, Feb. 2009, doi: 10.1016/j.matdes.2008.04.074.

[57] M. Divandari and A. R. Vahid Golpayegani, “Study of Al/Cu rich phases formed in A356 alloy by inserting Cu wire in pattern in LFC process,” *Mater. Des.*, vol. 30, no. 8, pp. 3279–3285, Sep. 2009, doi: 10.1016/j.matdes.2009.01.008.

[58] Y. Tanaka, M. Kajihara, and Y. Watanabe, “Growth behavior of compound layers during reactive diffusion between solid Cu and liquid Al,” *Mater. Sci. Eng. A*, vol. 445–446, pp. 355–363, Feb. 2007, doi: 10.1016/j.msea.2006.09.047.

[59] G. Xu, A. A. Luo, Y. Chen, and A. K. Sachdev, “Interfacial phenomena in magnesium/aluminum bi-metallic castings,” *Mater. Sci. Eng. A*, vol. 595, pp.

154–158, Feb. 2014, doi: 10.1016/j.msea.2013.11.093.

[60] B. Xiong, C. Cai, H. Wan, and B. Lu, “Fabrication of high chromium cast iron and medium carbon steel bimetal by liquid–solid casting in electromagnetic induction field,” *Mater. Des.*, vol. 32, no. 5, pp. 2978–2982, May 2011, doi: 10.1016/j.matdes.2011.01.006.

[61] T. P. D. Rajan, R. M. Pillai, and B. C. Pai, “Reinforcement coatings and interfaces in aluminium metal matrix composites,” *J. Mater. Sci.*, vol. 33, pp. 3491–3503, 1998, doi: 10.1023/A:1004674822751.

[62] C. H. E., Carl Swartz, “Method of bonding dissimilar metals,” 1938.

[63] J. C. Viala, M. Peronnet, F. Barbeau, F. Bosselet, and J. Bouix, “Interface chemistry in aluminium alloy castings reinforced with iron base inserts,” 2002, doi: 10.1016/S1359-835X(02)00158-6.

[64] M. Çöla, F. G. Koça, H. Öktemb, and D. Kır, “The role of boron content in high alloy white cast iron (Ni-Hard 4) on microstructure, mechanical properties and wear resistance.”

[65] AWS C3 Committee on Brazing and Soldering, *Brazing Handbook (5th Edition)*. American Welding Society (AWS), 2007.

[66] A. S. M. International and H. E. Kottcamp, *ASM METALS HANDBOOK VOLUME 3 Alloy Phase Diagrams*. 1992.

[67] S. Kobayashi and T. Yakou, “Control of intermetallic compound layers at interface between steel and aluminum by diffusion-treatment,” *Mater. Sci. Eng. A*, 2002, doi: 10.1016/S0921-5093(02)00053-9.

[68] D. Naoi and M. Kajihara, “Growth behavior of Fe2Al5 during reactive diffusion between Fe and Al at solid-state temperatures,” *Mater. Sci. Eng. A*, vol. 459, no. 1–2, pp. 375–382, 2007, doi: 10.1016/j.msea.2007.01.099.

[69] K. Bouché, F. Barbier, and A. Coulet, “Intermetallic compound layer growth between solid iron and molten aluminium,” *Mater. Sci. Eng. A*, vol. 249, no. 1–2, pp. 167–175, 1998, doi: 10.1016/S0921-5093(98)00573-5.

[70] H. Springer, A. Szczepaniak, and D. Raabe, “On the role of zinc on the formation

and growth of intermetallic phases during interdiffusion between steel and aluminium alloys," *Acta Mater.*, vol. 96, pp. 203–211, 2015, doi: 10.1016/j.actamat.2015.06.028.

[71] E. Pocheć, S. Jóźwiak, K. Karczewski, and Z. Bojar, "Maps of Fe–Al phases formation kinetics parameters during isothermal sintering," *Thermochim. Acta*, vol. 545, pp. 14–19, Oct. 2012, doi: 10.1016/j.tca.2012.06.015.

[72] P. J. Black, "The structure of FeAl3. II," *Acta Crystallogr.*, vol. 8, no. 3, pp. 175–182, Mar. 1955, doi: 10.1107/S0365110X55000637.

[73] U. Burkhardt, Y. Grin, M. Ellner, and K. Peters, "Structure refinement of the iron–aluminium phase with the approximate composition Fe2Al5," *Acta Crystallogr. Sect. B*, vol. 50, no. 3, pp. 313–316, 1994, doi: 10.1107/S0108768193013989.

[74] W. Jiang, Z. Fan, and C. Li, "Improved steel/aluminum bonding in bimetallic castings by a compound casting process," *J. Mater. Process. Tech.*, vol. 226, pp. 25–31, 2015, doi: 10.1016/j.jmatprotec.2015.06.032.

[75] R. Asthana, *Solidification Processing of Reinforced Metals*. 1997.

[76] H. Dong, W. Hu, Y. Duan, X. Wang, and C. Dong, "Dissimilar metal joining of aluminum alloy to galvanized steel with Al-Si, Al-Cu, Al-Si-Cu and Zn-Al filler wires," *J. Mater. Process. Technol.*, vol. 212, no. 2, pp. 458–464, 2012, doi: 10.1016/j.jmatprotec.2011.10.009.

[77] A. R. Valizadeh, A. R. Kiani-Rashid, M. H. Avazkonandeh-Gharavol, and E. Z. Karimi, "The Influence of Cooling Rate on the Microstructure and Microsegregation in Al-30Sn Binary Alloy," *Metallogr. Microstruct. Anal.*, vol. 2, no. 2, pp. 107–112, 2013, doi: 10.1007/s13632-013-0064-x.

[78] Z. W. Chen and S. Yazdanian, "Microstructures in interface region and mechanical behaviours of friction stir lap Al6060 to Ti–6Al–4V welds," *Mater. Sci. Eng. A*, vol. 634, pp. 37–45, May 2015, doi: 10.1016/j.msea.2015.03.017.

[79] C. H. Muralimohan, V. Muthupandi, and K. Sivaprasad, "Properties of Friction Welding Titanium-stainless Steel Joints with a Nickel Interlayer," *Procedia Mater. Sci.*, vol. 5, pp. 1120–1129, 2014, doi: 10.1016/j.mspro.2014.07.406.

[80] C. A. Rodopoulos, *Metal Matrix Composites*. 2004.

[81] M. R. Arghavani, M. Movahedi, and A. H. Kokabi, “Role of zinc layer in resistance spot welding of aluminium to steel,” *Mater. Des.*, vol. 102, pp. 106–114, Jul. 2016, doi: 10.1016/j.matdes.2016.04.033.

[82] H. Laukant *et al.*, “Fluxless laser beam joining of aluminium with zinc coated steel,” *Sci. Technol. Weld. Join.*, vol. 10, no. 2, pp. 219–226, 2005, doi: 10.1179/174329305X37051.

[83] A. A. Shirzadi, G. Saindrenan, and E. R. Wallach, “Flux-Free Diffusion Brazing of Aluminium-Based Materials Using Gallium (Patent Application: UK 0128623.6),” *Mater. Sci. Forum*, vol. 396–402, pp. 1579–1584, 2002, doi: 10.4028/www.scientific.net/MSF.396-402.1579.

[84] H. R. Pakzaman, M. Divandari, and A. R. Khavandi, “Effect of nickel coating on steel wire reinforcement on mechanical properties of aluminum matrix composites produced via lost foam casting,” *Arak , I . R . Iran*, 2012.

[85] G. Sierra, P. Peyre, F. Deschaux Beaume, D. Stuart, and G. Fras, “Galvanised steel to aluminium joining by laser and GTAW processes,” *Mater. Charact.*, 2008, doi: 10.1016/j.matchar.2008.03.016.

[86] Y. Liu *et al.*, “Interfacial microstructures and properties of aluminum alloys/galvanized low-carbon steel under high-pressure torsion,” *Mater. Des.*, vol. 64, pp. 287–293, 2014, doi: 10.1016/j.matdes.2014.07.053.

[87] C. Tan, L. Li, Y. Chen, and W. Guo, “Laser-tungsten inert gas hybrid welding of dissimilar metals AZ31B Mg alloys to Zn coated steel,” *Mater. Des.*, vol. 49, pp. 766–773, 2013, doi: 10.1016/j.matdes.2013.02.049.

[88] N. Eustathopoulos, F. Hodaj, and O. Kozlova, *The wetting process in brazing*. Woodhead Publishing Limited, 2013.

[89] V. Raghavan, “Al-Si-Zn (Aluminum-Silicon-Zinc),” *J. Phase Equilibria Diffus.*, vol. 197, no. 28, 2007.

[90] P. K. Choi, N. Takahashi, and M. Takahashi, “Gallium penetration into aluminum alloys detected using laser-generated Rayleigh waves,” *Mater. Sci. Eng. A*, vol. 442, no. 1-2 SPEC. ISS., pp. 187–190, 2006, doi: 10.1016/j.msea.2006.01.154.

[91] Q. Han, “A Modified Cast-on Method for the Reinforcement of Aluminum

Castings with Dissimilar Metals," *Metall. Mater. Trans. B*, vol. 47, no. 6, pp. 3266–3273, Dec. 2016, doi: 10.1007/s11663-016-0612-2.

[92] C. Hoppe *et al.*, "Influence of the Surface and Heat Treatment on the Bond Strength of Galvanized Steel/Aluminum Composites Joined by Plastic Deformation," *Adv. Eng. Mater.*, vol. 18, no. 8, pp. 1371–1380, Aug. 2016, doi: 10.1002/adem.201600085.

[93] S. Mrowec and A. Stokłosa, "Calculations of parabolic rate constants for metal oxidation," *Oxid. Met.*, vol. 8, no. 6, pp. 379–391, Dec. 1974, doi: 10.1007/BF00603388.

[94] J. J. Tomán, G. Schmitz, and Z. Erdélyi, "Linear-parabolic transition in reactive diffusion – A concept of kinetic modelling," *Comput. Mater. Sci.*, vol. 138, pp. 183–191, Oct. 2017, doi: 10.1016/j.commatsci.2017.06.009.

[95] H. J. Springer, "Fundamental Research into the role intermetallic phases in Joining Aluminium alloys to steel," 2011.

[96] L. A. Jacome, "Influence of Alloying Elements on the Microstructure and Mechanical Properties of Steel-Aluminium-Joints Produced by Metal Arc Joining with Special Focus on the Intermetallic Phase Seam," p. 94, 2008.

[97] H. Meifeng, L. Lei, W. Yating, Z. Cheng, H. Wenbin, and P. Deng, "Kinetics and mechanism of multilayer Mg-Al intermetallic compound coating formation of magnesium alloy by AlCl3-NaCl molten salt bath treatment," *J. Alloys Compd.*, vol. 551, pp. 389–398, 2013, doi: 10.1016/j.jallcom.2012.11.005.

[98] Carl Soderhjelm, "Multi-Material Metal Casting: Metallurgically Bonding Aluminum to Ferrous Inserts," Worcester Polytechnic Institute, 2017.

[99] A. Ul-Hamid, *A Beginners' Guide to Scanning Electron Microscopy*. Cham: Springer International Publishing, 2018.

[100] H. Rezaei, M. R. Akbarpour, and H. R. Shahverdi, "Effects of interfacial layers fracture on the dissolution mechanism of solid fe in liquid Al," *Jom*, vol. 67, no. 7, pp. 1443–1450, 2015, doi: 10.1007/s11837-015-1435-3.

[101] N. Tang, Y. P. Li, S. Kurosu, Y. Koizumi, H. Matsumoto, and A. Chiba, "Interfacial reactions of solid Co and solid Fe with liquid Al," vol. 60, pp. 32–37,

2012, doi: 10.1016/j.corsci.2012.04.015.

[102] M. Windmann, A. Röttger, and W. Theisen, “Phase formation at the interface between a boron alloyed steel substrate and an Al-rich coating,” *Surf. Coatings Technol.*, vol. 226, pp. 130–139, Jul. 2013, doi: 10.1016/j.surfcoat.2013.03.045.

[103] N. Takata, M. Nishimoto, S. Kobayashi, and M. Takeyama, “Crystallography of Fe2Al5 phase at the interface between solid Fe and liquid Al,” *Intermetallics*, vol. 67, no. August, pp. 1–11, 2015, doi: 10.1016/j.intermet.2015.07.011.

[104] W. J. Cheng and C. J. Wang, “Study of microstructure and phase evolution of hot-dipped aluminide mild steel during high-temperature diffusion using electron backscatter diffraction,” *Appl. Surf. Sci.*, vol. 257, no. 10, pp. 4663–4668, 2011, doi: 10.1016/j.apsusc.2010.12.118.

[105] J. Rong, Z. Kang, S. Chen, D. Yang, J. Huang, and J. Yang, “Growth kinetics and thickness prediction of interfacial intermetallic compounds between solid steel and molten aluminum based on thermophysical simulation in a few seconds,” *Mater. Charact.*, vol. 132, pp. 413–421, Oct. 2017, doi: 10.1016/j.matchar.2017.09.012.

[106] K. Saito, K. Sugiyama, and K. Hiraga, “Al13M4-type structures and atomic models of their twins,” *Mater. Sci. Eng. A*, vol. 294–296, pp. 279–282, Dec. 2000, doi: 10.1016/S0921-5093(00)01213-2.

[107] C.E.Albright, “The Fracture Toughness of Steel-Aluminum Deformation Welds,” *Weld. J.*, 1981, doi: https://app.aws.org/wj/supplement/WJ_1981_11_s207.pdf.

[108] E. Ferchaud *et al.*, “Gallium Distribution in Gallium-Coated Aluminum for Brazing Application,” *Defect Diffus. Forum*, vol. 309–310, pp. 255–260, 2011, doi: 10.4028/www.scientific.net/DDF.309-310.255.

[109] A. A. Shirzadi and E. R. Wallach, “Novel method for diffusion bonding superalloys and aluminium alloys (USA patent 6,669,534 B2, European patent pending),” *New Front. Process. Eng. Adv. Mater.*, vol. 502, pp. 431–435, 2005, doi: 10.4028/0-87849-980-6.431.

[110] M. Kajihara, “Quantitative Evaluation of Interdiffusion in Fe₂Al₅ during Reactive Diffusion in the Binary

Fe–Al System," *Mater. Trans.*, vol. 47, no. 6, pp. 1480–1484, 2006, doi: 10.2320/matertrans.47.1480.

[111] N. Masahashi, S. Watanabe, N. Nomura, S. Semboshi, and S. Hanada, "Laminates based on an iron aluminide intermetallic alloy and a CrMo steel," *Intermetallics*, vol. 13, no. 7, pp. 717–726, Jul. 2005, doi: 10.1016/j.intermet.2004.12.017.

[112] A. Śmiglewicz and M. Jabłońska, "Thermal Expansion of Alloys from the Al-Fe System," *Defect Diffus. Forum*, vol. 326–328, pp. 587–592, Apr. 2012, doi: 10.4028/www.scientific.net/DDF.326-328.587.

[113] F. Seitz, "On the theory of diffusion in metals," *Acta Crystallogr.*, vol. 3, no. 5, pp. 355–363, Sep. 1950, doi: 10.1107/S0365110X50000999.

[114] N. Rangaraju, T. Raghuram, B. V. Krishna, K. P. Rao, and P. Venugopal, "Effect of cryo-rolling and annealing on microstructure and properties of commercially pure aluminium," *Mater. Sci. Eng. A*, vol. 398, no. 1–2, pp. 246–251, May 2005, doi: 10.1016/j.msea.2005.03.026.

[115] D. H. Shin, B. C. Kim, Y.-S. Kim, and K.-T. Park, "Microstructural evolution in a commercial low carbon steel by equal channel angular pressing," *Acta Mater.*, vol. 48, no. 9, pp. 2247–2255, May 2000, doi: 10.1016/S1359-6454(00)00028-8.

[116] M. Yılmaz, M. Çöl, and M. Acet, "Interface properties of aluminum/steel friction-welded components," *Mater. Charact.*, vol. 49, no. 5, pp. 421–429, Dec. 2002, doi: 10.1016/S1044-5803(03)00051-2.

[117] N. D. T Heumann, "Structure character of the Fe2Al5 intermetallics compound in hot dip aluminizing process," *Z Met.*, 1959.

[118] J. E. Nicholls, "HOT-DIPPED ALUMINIUM," 1964.

[119] L. H. Shah and M. Ishak, "Review of research progress on aluminum-steel dissimilar welding," *Mater. Manuf. Process.*, vol. 29, no. 8, pp. 928–933, 2014, doi: 10.1080/10426914.2014.880461.

[120] J. An, Y. B. Liu, M. Z. Zhang, and B. Yang, "Effect of Si on the interfacial bonding strength of Al – Pb alloy strips and hot-dip aluminized steel sheets by hot rolling,"

J. Mater. Process. Tech., vol. 120, pp. 30–36, 2002.

[121] H. R. Shahverdi, M. R. Ghomashchi, S. Shabestari, and J. Hejazi, “Kinetics of interfacial reaction between,” *J. Mater. Sci.*, vol. 37, pp. 1061–1066, 2002, doi: Pii S0924-0136(02)00225-XDoi 10.1016/S0924-0136(02)00225-X.